Chemical and Neural Regulation of Embryonic Branching Morphogenesis

Thesis by

Danielle V. Bower

In Partial Fulfillment of the Requirements

for the Degree of

Doctor of Philosophy

California Institute of Technology

Pasadena, California

2013

(Defended April 29th, 2013)

Acknowledgements

I have many people to acknowledge who assisted me on this exciting expedition to summit a remote alpine peak. The success of this journey was made possible by the expert guidance of my expedition leader, Scott Fraser. His keen insight was critical to the safe navigation of corniced cliffs, and multiple times the expedition may have become mired in steep rocky sections if it weren't for his experienced judgment to anticipate and navigate around them. His optimism was infectious and gave me the strength to believe in our success even when we were blinded by a blizzard.

Co-captains Edwin Jesudason, David Warburton, and Kai Zinn ensured that we stayed on route and did not get lost in the wrong valley or become cut off from the ridge we needed to gain to the summit. Their guidance was essential for interpreting icy conditions and impending changes in weather. I am ever grateful for being able to learn from such skilled masters and for their patience as I learned. I was encouraged to press onwards knowing they were checking my rope work and anchors.

Expedition advisors Paul Patterson and Michael Elowitz provided essential knowledge from previous expeditions that guided our choice of route. With their advice, we were prepared with the proper equipment for a river crossing and were able to navigate a path that skirted a dangerous avalanche chute.

Rusty Lansford ensured that I started out on solid footing running proper experimental controls. He also helped me keep the journey in perspective and I appreciated his reminders that sometimes it's necessary to set down the load and go have fun skiing a few laps on a nearby powder slope.

I acknowledge the support of my labmates who helped me learn the essential skills of glacier travel and crevasse rescue. Thank you to Thai Truong for your expert assistance troubleshooting laser ablation and nuances of microscopy; Le Trinh for your knowledgeable guidance in zebrafish experiments; Peter Lee for patiently instructing me in the art of fly work and throwing me a rope on a few slippery slopes to help speed my ascent; David Koos and David Huss for helping me assemble equipment with any tools we had to hand and teaching me basic skills like tissue sectioning; Aura Keeter and other staff for keeping the lab running. I appreciate the collaborative lab atmosphere created by all my colleagues. We had many engaging discussions and bonded during long days holed up in tents waiting for storms to pass.

I also appreciate the contributions of my colleagues Sonia Navarro and Nick Lansdale to the SERCA study in helping me carry gear up to high camp for the attack on the summit. Alon Lazarus kindly shared some work he had completed and contributed an image for the nerve ablation study.

I enjoyed socializing and climbing and skiing expeditions from base camp with many close friends—the Kelbers, Harrisons, Matzens, Chapmans, June Wicks and JD Bagert, Nick Stadie, Patrick Sanan, and Pratyush Tiwary—to name just a few. We've made great memories together along our travels at Caltech.

I am indebted to my family for their unwavering support of everything I do. Their encouragement and meticulous planning from basecamp set me up for success and ensured our safe return. I could also always count on my brother to crack a joke over the radio and lighten the mood when we'd be huddled on a snow shelf waiting for the weather to turn.

Finally, I am forever grateful for my pragmatic climbing partner, Dan Bower, who committed to undertaking this journey with me. He never failed to help me through challenging times when I was tired and struggling, pulling me out of a few crevasses I fell into along the way. Thank you for obliging my curiosity and taking some detours off route with me to go see the view from the next ridge.

The panorama from the summit was spectacular and worth the trials to get there. I learned much along the way and look forward to new adventures to come.

Abstract

Lung development is a complex process orchestrated by as many as 40 different types of cells and many signaling and regulatory factors. The spatial sequence of branching of bronchial epithelial tubes is known to be stereotyped. However, it remains unknown how the timing of branch formation is encoded and whether this branching clock function is unique for different tissue types or is conserved across species and lineages that undergo iterative branching. Investigations of the function of the sarcoplasmic-endoplasmic reticulum calcium ATP-ase (SERCA) reveal that protein kinase C (PKC)-modulated SERCA activity controls branch formation across tissues and species.

SERCA pumps calcium from the cytoplasm into the endoplasmic reticulum (ER), where it is stored for release back into the cytoplasm by the binding of inositol trisphosphate (IP3) to the IP3 receptor in the ER. PKC modulates the amount of IP3 present, and the balance between PKC and SERCA activity establishes various patterns of calcium dynamics in the cell.

SERCA controls intersomitic blood vessel sprouting and branching in zebrafish embryos. The rate of outgrowth of vessels is controlled by SERCA activity in a dose-dependent manner as revealed by graded inhibition of the pump. Vessel sprouting

recovers upon removal of inhibition and restoration of pump activity. SERCA controls the rate of vessel growth and budding by regulating endothelial cell motility.

During *Drosophila* embryonic development, SERCA activity is required for the proper formation of the network of tracheal tubules that deliver oxygen to tissues during larval stages of development. In the embryo, this system forms entirely by migration of epithelial cells following cessation of cell proliferation. SERCA blockade results in breaks in the tracheal structure. Removal of inhibitor partially rescues the defects, while simultaneous treatment with both SERCA inhibitor and PKC activator remarkably rescues tracheal structure. Thus, SERCA governs branch formation in a system that is entirely independent of cell proliferation, and PKC activation can largely compensate for SERCA inhibition.

Similarly, SERCA activity is necessary for *Drosophila* embryonic central nervous system development as revealed by the formation of the longitudinal axon fascicles. Disruption of SERCA activity generates breaks, displaced axons, and abnormal mergings of the axon tracts which are consistent with perturbed cell migration and guidance. The proper neural structure is partially restored by removal of inhibition, and the defects are again rescued by ectopic PKC activation alongside SERCA blockade.

Dynamic imaging of *Drosophila* embryonic tracheal morphogenesis demonstrates that SERCA's principal function is to govern cell migration. The breaks in the tracheal network that are observed following SERCA inhibition result from failed migration of tracheal cells to their destined locations within the embryo.

Together, these finding reveal that SERCA regulates cell migration, and this serves

as a conserved mechanism that governs branch formation in various cell types and species during development. A general mechanism directing cell migration simplifies the control of branch formation and obviates the need for individual morphogenes to specify formation of each branch of an iteratively branching tissue.

On the other hand, morphogens are important for specifying lung fate and coordinating the various cell types and behaviors necessary to grow and mature a complex, specialized organ such as the lung. Signaling between the bronchial epithelium, mesenchyme, endothelium, the basement membrane matrix, and other players directs the growth of the ramified structure that must form before the lung can become functional. Nerves are also known to be present from the early stages of lung branching. Yet a role for nerves in modulating epithelial branching remains to be discerned. Denervation of embryonic mouse lung explants reveals that lung branching requires nerves. Targeted neural ablation, but not inhibition of acetylcholine receptors, halts lung branching and causes a reduction in endothelial cells and epithelial and mesenchymal proliferation. Likewise, ablation of nerves in *Drosophila* embryos derails tracheal morphogenesis. Therefore, nerves play a conserved role in enabling epithelial airway branching.

These studies expand our understanding of the basic elements regulating the development of complex branched organs, such as the mammalian lung, zebrafish vasculature, and *Drosophila* tracheal and neural networks. Harnessing this knowledge may open the door to new interventions in congenital disorders or tumor angiogenesis.

Contents

List of Figures

List of Tables

Part I

PKC-modulated SERCA governs branching morphogenesis by regulating cell migration

Chapter 1

Introduction

1.1 Lung branching is stereotyped

The lung originates as a bud from the foregut endoderm and forms by periodic, iterative branching. The branching programs of mammalian lung and *Drosophila* tracheal development are known to be highly stereotyped (*Metzger et al.*, 2008). Three patterns of bud elaboration give rise to the three-dimensional structure of the lung. These are: (1) domain branching, where buds form sequentially off a pre-existing tubule; (2) planar bifurcation, where a tip bifurcates into two; and (3) orthogonal bifurcation, which is planar bifurcation but with a 90 degree rotation between bifurcation events. The sequence of these budding events is nearly identical from one individual to the next. While the spatial patterning of the lung is thus understood, what serves as the clock that regulates the timing of branch formation remains unknown.

1.2 SERCA in periodic muscle contraction

Conversely, cardiac muscle contractility is known to be regulated by calcium dynamics. The highly periodic contractions of the heart depend on cycles of calcium influx into the cell cytoplasm to drive muscle contraction followed by rapid sequestration of calcium in the sarcoplasmic reticulum to repolarize the cell for a subsequent contraction. These cycles of calcium release and calcium clearance depend on a core group of proteins that modulate calcium dynamics (see Figure 1.1). Phospholipase C cleaves phosphatidylinositol 4,5-bisphosphate (PIP2) in the membrane to release diacyl glycerol (DAG) and inositol 1,4,5-trisphosphate (IP3) (*Berridge*, 1993). IP3 binds an IP3 receptor (IP3R) in the membrane of the endoplasmic reticulum, and this induces release of calcium from its store in the endoplasmic reticulum (or sarcoplasmic reticulum in muscle) (*Jacob*, 1990). Calcium is pumped from the cytoplasm back into the endoplasmic reticulum by the sarcoplasmic-endoplasmic reticulum calcium ATPase, or SERCA (*Berridge et al.*, 2003).

This enables iterative cycles of calcium release and permits such behaviors as muscle relaxation (*Berridge and Galione*, 1988). SERCA binds two calcium molecules at a time and hydrolyzes ATP to pump calcium into the endoplasmic reticulum against a concentration gradient to remove calcium from the cytosol in preparation for the next release of calcium (*East*, 2000; *Misquitta et al.*, 1999). Protein kinase C (PKC) can bind to DAG and inhibit PLC, which results in less production of IP3 (*Nishizuka*, 1988). Thus, the interplay between PKC-regulated PLC and SERCA establishes a calcium dynamic in the cell. Computational modeling and *in vitro* studies

have demonstrated that different levels of these regulatory proteins can establish a range of calcium dynamics from stable levels to oscillations to spiking patterns with varying frequencies (*Bobe et al.*, 2011; *Dolmetsch et al.*, 1998; *Kang and Othmer*, 2007; *Schuster et al.*, 2002). Thus, calcium can serve as a tunable medium for regulating cell behaviors.

In cardiac muscle, resting polarization of the membrane potential leads to activation of a slowly depolarizing sodium-potassium current which activates a voltage-gated calcium current influx and calcium-induced-calcium release of additional calcium from the sarcoplasmic reticulum into the cytoplasm to drive muscle contraction (*Berridge et al.*, 1999; *DiFrancesco*, 2006; *Nerbonne and Kass*, 2005; *DiFrancesco*, 1985; *Bers*, 2000). The calcium is cleared and potassium efluxes from the cell to repolarize. The SERCA pump is critical for this periodic contractility by removing cytosolic calcium (*Bers*, 2000; *Sanyal et al.*, 2006; *Periasamy et al.*, 1999).Without sequestration of calcium by SERCA, high levels of calcium in the cardiac cell inactivate voltage-gated calcium and potassium channels, and periodic contractions cease (*Sanyal et al.*, 2005).

In skeletal muscle activation, SERCA serves a similarly important role in regulating and maintaining repeated muscle contraction. SERCA expression in motor nerve terminals is necessary for synaptic plasticity and controls the quantal size of neurotransmitter release (*Freeman et al.*, 2010). In skeletal muscle, SERCA is essential to sequester calcium following action potential-induced contraction to enable muscle relaxation and prepare for subsequent stimulation. Loss of SERCA activity

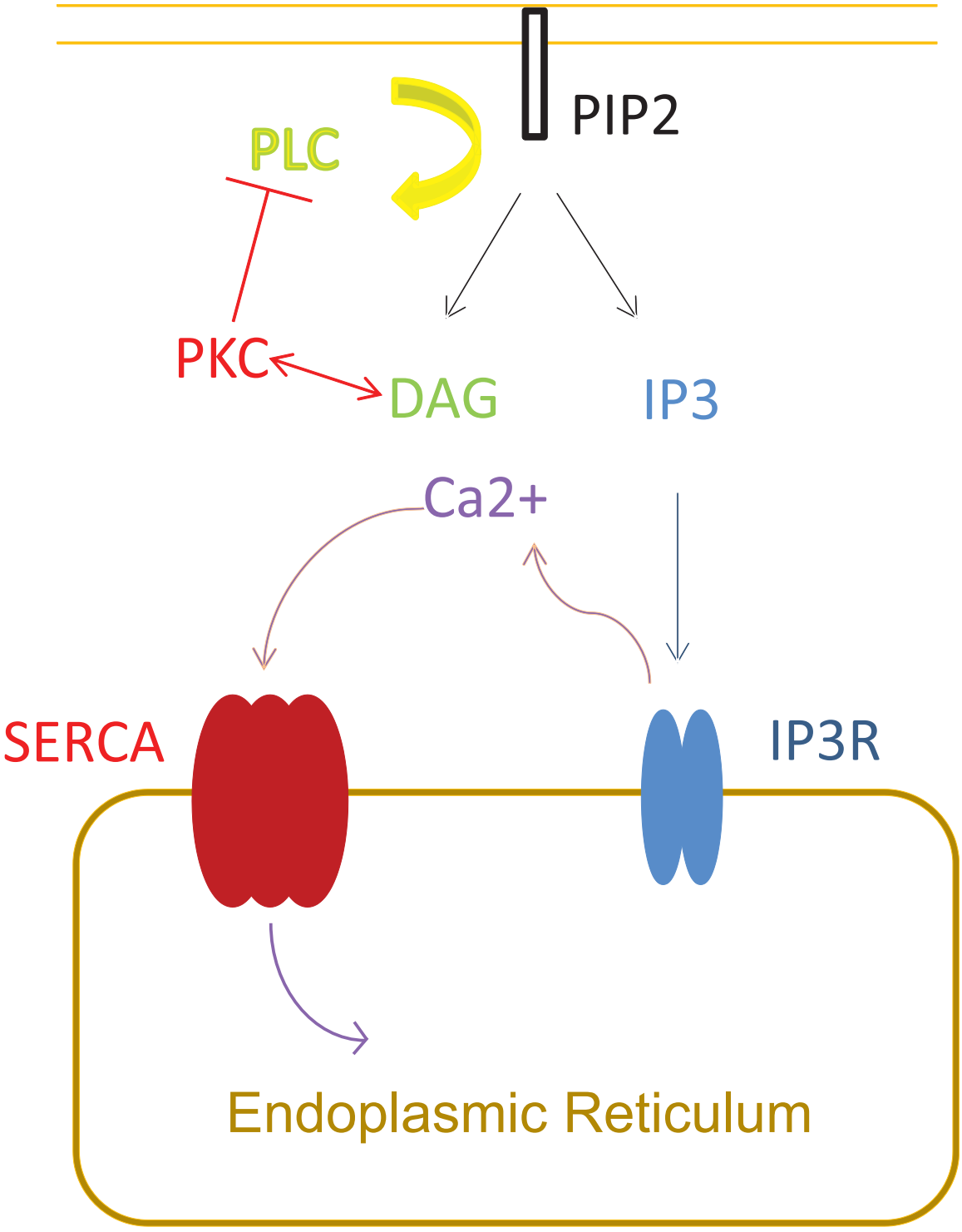

Figure 1.1: The balance between PKC-regulated release of calcium and SERCA returning cytosolic calcium to the endoplasmic reticulum (ER) determines intracellular calcium dynamics. PKC-regulated PLC generates IP3 which stimulates release of stored calcium, and SERCA enables repeated release of calcium by pumping it back into the ER to replenish the store. The relative activities of these opposing operations can result in different patterns and frequencies of calcium flux.

results in contracted muscle paralysis that is dependent on nerve-induced stimulation (*Sanyal et al.*, 2005). Thus, SERCA is a critical modulator of calcium dynamics that underpin periodic muscle contractility, yet its function is not limited to muscle.

1.3 SERCA expression and disease associations

In mammals, SERCA pumps are encoded by three genes, and different splice isoforms of these genes are expressed in different tissues (*East*, 2000). SERCA1a is expressed in fast-twitch skeletal muscle, 1b in neonatal muscle, 2a in cardiac muscle, 2b in all cell types for housekeeping functions, and isoform 3 is expressed in various subsets of cells, including endothelial cells and secretory tissues (*Misquitta et al.*, 1999; *East*, 2000; *Berridge et al.*, 1999). *Drosophila* possess only one SERCA gene, and zebrafish possess three (*Sanyal et al.*, 2005; *Magyar et al.*, 1995; *Gleason et al.*, 2004; *Strausberg et al.*, 2002). Mutations in SERCA genes result in cardiac dysfunction (*Sanyal et al.*, 2006; *Periasamy et al.*, 1999; *Qi et al.*, 1997) and skeletal muscle paralysis (*Sanyal et al.*, 2005). SERCA dysfunction is associated with a range of disorders resulting in cell stress, tissue remodeling, inflammation, and apoptosis, including cystic fibrosis, lung fibrosis, asthma, lung cancer, and diabetes (*Ahmad et al.*, 2009; *Korfei et al.*, 2008; *Lawson et al.*, 2011; *Tanjore et al.*, 2012; *Cantero-Recasens et al.*, 2010; *Mahn et al.*, 2009; *Korosec et al.*, 2006; *Schröedl et al.*, 2009; *Kono et al.*, 2012; *Ravier et al.*, 2011; *Takada et al.*, 2012; *Zherebitskaya et al.*, 2012). SERCA function therefore underlies the normal basal activity of many cell types and is important for proper tissue function.

1.4 SERCA regulates fungal hyphal tip growth

Regulation of intracellular calcium levels has been shown to direct cell polarization, growth, and branching in fungi (*Brand et al.*, 2007; *Virag and Griffiths*, 2004; *Jackson and Heath*, 1993; *Robson et al.*, 1991a). Indeed, maintenance of a steep calcium gradient at the tip of growing hypae is essential for hyphal projection and cytoskeletal rearrangement (*Levina et al.*, 1995; *Robson et al.*, 1991b; *Virag and Griffiths*, 2004). Intracellular calcium sequestration in the endoplasmic reticulum by the SERCA pump is responsible for establishing this tip calcium gradient, and inhibition of SERCA abolishes this calcium gradient, disrupts the hyphal cytoskeletal actin network, and prevents hyphal outgrowth (*Silverman-Gavrila and Lew*, 2001). Hyphal extension activates other calcium modulators to reinforce the tip growth (*Silverman-Gavrila and Lew*, 2003). Transient release of calcium into the cytosol results in cytoskeletal contraction and initiation of a new hyphal branch (*Grinberg and Heath*, 1997; *Regalado*, 1998; *Robson et al.*, 1991b). This intrinsic role of calcium in fungal branching suggests that calcium dynamics may also feature in the regulation of branching in other organisms.

1.5 Periodic peristalsis during lung development

During embryonic lung development, mammalian and avian lungs undergo spontaneous peristaltic contractions that commence after the first few rounds of branching and increase in frequency near term (*Lewis*, 1924; *Schopper*, 1935; *Jesudason et al.*,

2006; *Wilson et al.*, 2007). These contractions propel lumenal fluid through the bronchial tubules and induce stretch at distended tubule tips (*McCray and Joseph*, 1993; *Schittny et al.*, 2000). Mechanical distension is necessary for lung growth and morphogenesis, as manifest by resulting hypoplastic lungs following drainage of lumenal fluid or demuscularization, compared with accelerated growth and maturation of lungs with increased distension from tracheal occlusion (*Harding and Hooper*, 1996; *Carmel et al.*, 1965; *Agostoni*, 1959; *Tseng et al.*, 2000; *Wilson et al.*, 1993). Mechanical stretch can result in cell signaling and modulation of the cytoskeleton (*Liu et al.*, 1996). Furthermore, inhibiting the peristaltic lung contractions *in vitro* by blocking voltage-gated calcium channels results in lungs with reduced volume but the same number of buds (*Roman*, 1995; *Jesudason et al.*, 2005; *Jesudason*, 2007). This block in lung growth is not rescued by additional FGF10 growth factor (*Jesudason et al.*, 2005). Thus, an influx of extracellular calcium is necessary for cell proliferation to increase total lung volume but is not necessary for continued lung branching.

However, *Featherstone et al.* (2005) demonstrated that spontaneous calcium waves propagating through bronchial airway smooth muscle connected by gap junctions precede and drive these spontaneous contractions. Furthermore, extracellular calcium entry is required to maintain intracellular calcium stores, and calcium release from the sarcoplasmic reticulum raises cytosolic calcium levels and generates the propagating calcium waves. Without these calcium waves traveling through electrically linked airway smooth muscle, peristalsis ceases. Finally, blocking the activity of the SERCA pump abolishes the peristaltic contractions as baseline cytosolic calcium levels rise,

resulting in tonic airway contraction. Upon removal of the SERCA inhibitor, the paralysis relaxes and calcium waves followed by peristaltic airway contractions resume (*Featherstone et al.*, 2005). Importantly, during this block in peristalsis from SERCA inhibition, airway branching halts completely and resumes upon reinitiation of airway peristalsis (*Jesudason*, 2007). Therefore, calcium dynamics underlie the peristaltic activity of developing embryonic lungs and play a role in regulating lung branching.

1.6 SERCA in mammalian lung peristalsis

The importance of lung peristalsis for proper lung growth and maturation prompted further investigation of the role of calcium dynamics for branching during development. Effects on mammalian lung branching were measured for varying levels of inhibition of SERCA activity. The fungal toxin cyclopiazonic acid (CPA) is a highly specific inhibitor of all forms of SERCA protein but does not inhibit mitochondrial F1, sodium-potassium, or other cellular ATPases (*Seidler et al.*, 1989). In lungs explanted from embryonic day 13 (E13) rat embryos, lungs cultured with varying doses of CPA or no CPA show a dose-dependent reduction in the rate of branching with increasing doses of CPA (Fig. 1.2A) (*Lansdale et al.*, 2010). In parallel, lung peristalsis is reduced with increasing concentrations of CPA (Fig. 1.2B). At the same dose of CPA that halts branching, peristalsis is abolished. Upon removal of SERCA inhibition, peristalsis resumes. Lung peristalsis and branching are regulated in parallel by SERCA activity.

Recovery of peristalsis following removal of SERCA inhibition suggests that lung branching might also resume. In E13 rat lungs cultured for three days with CPA,

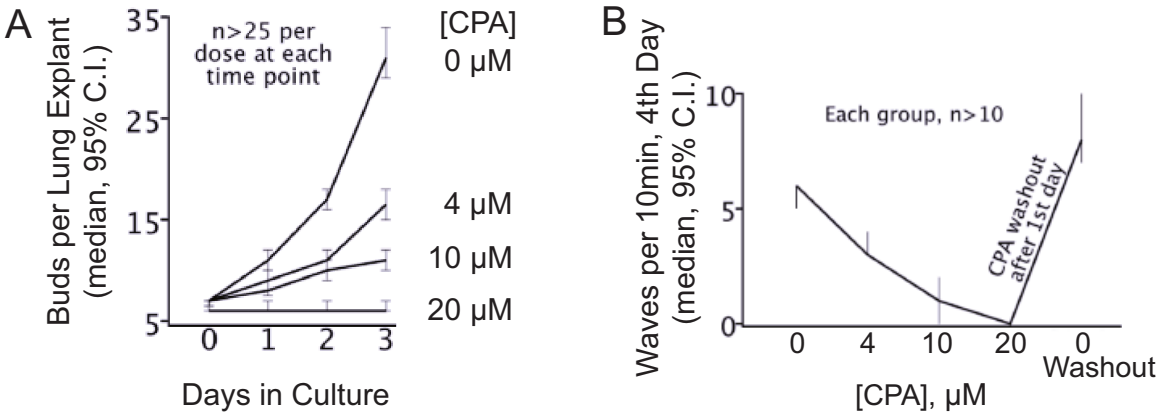

Figure 1.2: Mammalian lung branching depends on SERCA activity in a dose-dependent manner. (A) Explanted rat lung buds are cultured with varying doses of SERCA inhibitor CPA, or without CPA, and the number of buds counted each day for 3 days of culture. The rate of lung branching decreases in a dose-dependent manner with increasing concentration of CPA. At a concentration of 20μM CPA, branching is halted completely. (B) Explanted lungs are cultured with increasing doses of CPA for four days, or lungs are cultured with 20μM CPA for one day followed by three more days of culture without CPA, and on the fourth day the number of peristalses per minute are quantified. Lung peristalsis decreases dose-dependently with an increase in SERCA inhibition, and peristalsis rebounds following removal of inhibition. Error bars represent 95% confidence intervals.

branching remains suppressed. However, when CPA is removed after one or two days and the lungs are cultured without SERCA inhibition for the duration of the three days, branching is restored at approximately the same rate as in lungs cultured without inhibitor (Fig. 1.3A) (*Lansdale et al.*, 2010). Furthermore, branching resumes at the point it was halted in the stereotyped budding sequence. In E13 rat lungs explanted with the same initial number of buds, for each day of SERCA inhibition, the next bud due to form is delayed by one day (Fig. 1.3B). Thus, blockade of branching by SERCA inhibition is reversible, and the onset and rate of branching are controlled by SERCA activity.

These studies of SERCA function in mammalian lung branching demonstrate that

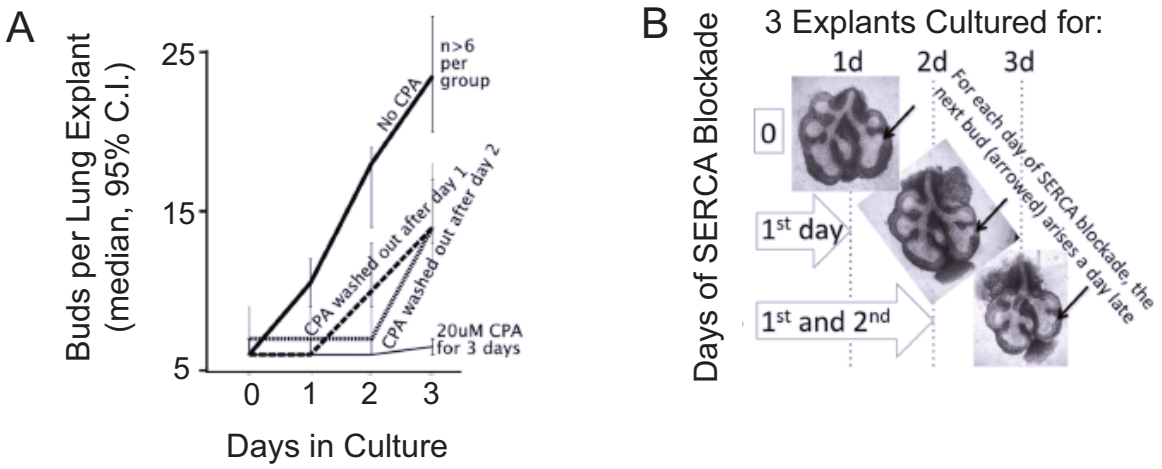

Figure 1.3: Lung branching resumes at the normal rate where it left off in the budding sequence when SERCA inhibition is removed. (A) E13 rat lungs are cultured for three days with the SERCA inhibitor, CPA, for 0, 1, 2, or 3 days. No branching occurs while CPA is present, but upon washout of CPA after 1 or 2 days, lung budding resumes at approximately the same rate as in uninhibited controls lungs. (B) E13 rat lungs are explanted with the same number of buds and cultured for 3 days with different durations of SERCA inhibition. With no inhibition, the next bud to form elaborates after one day, and for each day of SERCA inhibition, that same bud forms a day later.

cellular calcium dynamics regulated by SERCA activity govern both lung peristaltic activity that is important for lung growth and maturation and the rate and onset of lung branching. The continuation of branching that is seen with blockade of extracellular calcium influx (*Roman*, 1995) can be explained by the persistence of SERCA activity and demonstrates that intracellular calcium dynamics involving regulation of calcium stores in the endoplasmic reticulum govern the onset and rate of branching. Budding is independent of extracellular calcium, although total lung volume depends on extracellular calcium, at least *in vitro*.

The finding that the SERCA pump, which regulates intracellular calcium levels and sequestration in the endoplasmic reticulum, directs lung branching raises the question of whether SERCA might serve to regulate branching *in vivo* and across

different species and tissue types. To determine whether SERCA's regulation of calcium dynamics is a generalized mechanism conserved through evolution to regulate budding or bifurcation decisions, I undertook a comparative analysis of SERCA function in different organisms and tissues.

Using *Drosophila* tracheal and neural development and zebrafish intersomitic vascularization, I investigated the importance of SERCA function for budding decisions *in vivo* in processes that depend differently on cell shape changes, cell migration, and proliferation to determine whether SERCA activity serves as a general mechanism that regulates budding decisions and to determine which cellular behaviors SERCA regulates.

1.7 *Drosophila* tracheal development

The tracheal system is a bilaterally symmetric network of epithelial tubules in *Drosophila melanogaster* that delivers oxygen to all body tissues (*Wigglesworth*, 1972). This respiratory network forms in the embryo by initial proliferation of progenitor cells at thoracic and abdominal segments (from T2 to A8), forming paired clusters of cells on both lateral sides of the embryo (*Samakovlis et al.*, 1996a; *Manning and Krasnow*, 1993). These approximately 80 cells per hemisegment form a sac that invaginates but remains attached to the epithelial surface for air entry (*Samakovlis et al.*, 1996a; *Affolter and Caussinus*, 2008). The cells cease to divide and migrate to form a stereotyped segmental structure with 6 primary branches, including the spiracular branch that projects to the epidermal surface. FGF/FGFR signaling directs this cell

migration to generate the branched tracheal network (*Sutherland et al.*, 1996; *Klämbt et al.*, 1992; *Glazer and Shilo*, 1991; *Lee et al.*, 1996).

Cells forming the dorsal and lateral trunks migrate and fuse with partner cells in the adjacent tracheal segments (*Tanaka-Matakatsu et al.*, 1996; *Samakovlis et al.*, 1996a,b). Intercellular junctions connect the cells of the dorsal trunk, where pairs of cells connect to form the circumference of the tube. Cell intercalation results in smaller branches like the lateral trunk, where a single cell forms the circumference of the tube (*Ribeiro et al.*, 2004). These cells have an intracellular junction with themselves. Secondary branches form at the ends of primary branches, and these are made of unicellular tubes. The terminal branches that extend to all tissues of the embryo to deliver oxygen consist of cellular projections without junctions that lumenize for oxygen transport. A chitin matrix is secreted to stabilize and support the tracheal lumen, and then lumenal proteins must be cleared for air transport (*Araújo et al.*, 2005; *Tsarouhas et al.*, 2007; *Wang et al.*, 2006; *Devine et al.*, 2005).

The resulting structure of the tracheal system is highly stereotyped, with bilateral fused dorsal and lateral trunks, dorsal branches, transverse connectives, spiracular branches, visceral branches, and ganglionic branches (see Figure 1.4). Dorsal branches from each side of the embryo fuse to connect the left and right side networks. Through *Drosophila* metamorphosis the tracheal system is remodeled to form the series of tubules and air sacs for respiration in the adult fly. Studying formation of the embryonic *Drosophila* tracheal system enables *in vivo* analysis of processes that depend on cell shape changes and cell migration without proliferation. The tracheal

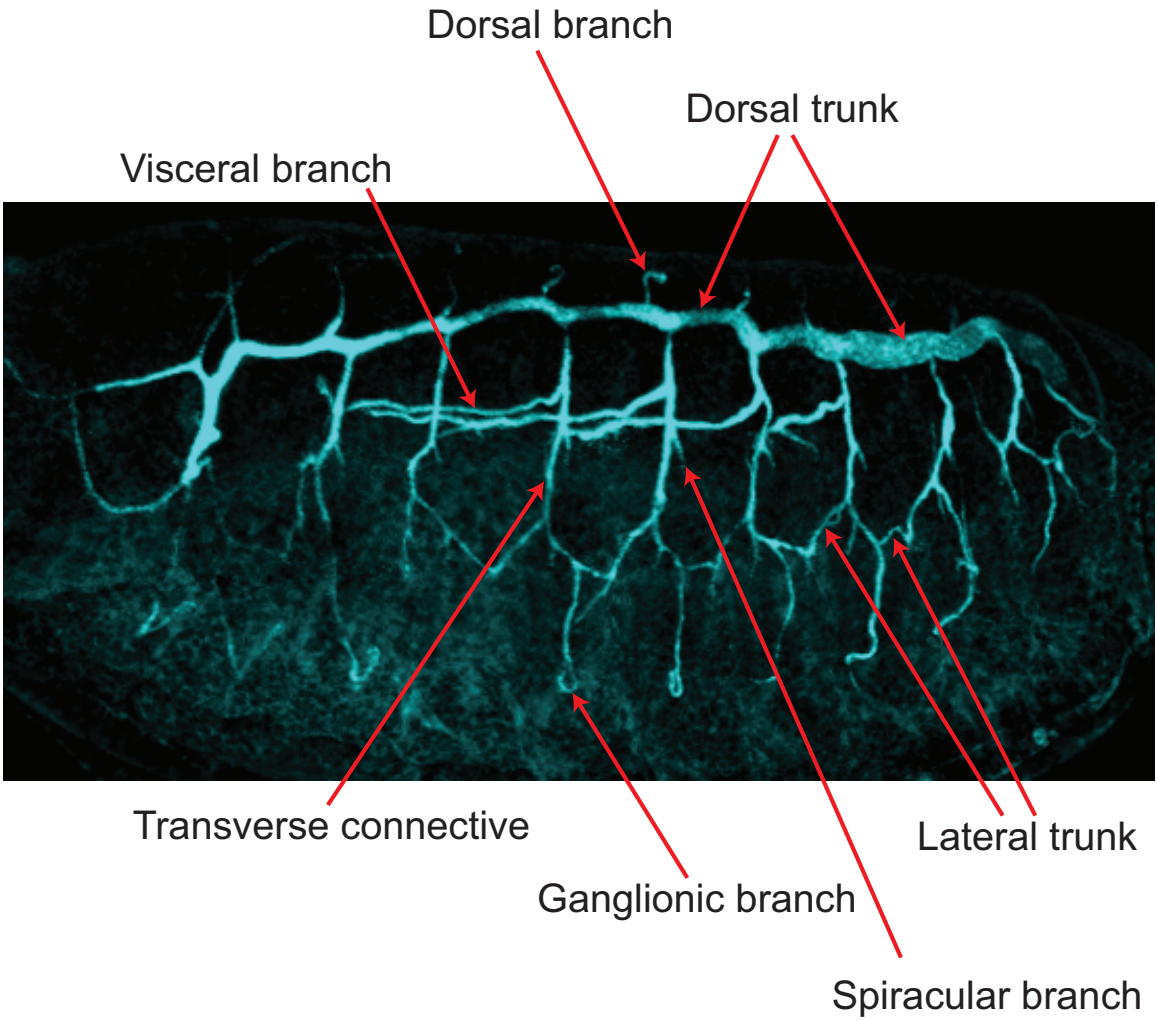

Figure 1.4: The stereotyped structure of embryonic *Drosophila* trachea. The diagram indicates the primary branches that form the stereotyped structure of embryonic *Drosophila* tracheal tubules. Anterior to the left, dorsal up.

system is also homologous to the mammalian lungs, but the less complicated genetics simplifies studies.

1.8 *Drosophila* neural development

Nervous system development in *Drosophila* is highly stereotyped, with approximately 100 neural lineages, each of which arises from a single neuroblast and innervates

specific targets (*Spindler and Hartenstein*, 2010). The ventral nerve cord of the insect is like the vertebrate spinal cord and consists of cell bodies and structured nerve tracts along which axons travel (*Nambu et al.*, 1993; *Arendt and Nübler-Jung*, 1999). Early in the neuroectoderm, glial cells position in distinct locations and serve as a scaffold for the formation of neural tracts (*Hidalgo et al.*, 1995; *Hidalgo and Booth*, 2000; *Jacobs and Goodman*, 1989; *Klämbt and Goodman*, 1991; *Hartenstein and Campos-Ortega*, 1984). Specific nerve cells along the ventral neuroectoderm activate expression of Fasciclin II (FasII), an adhesion molecule homologous to vertebrate N-CAM (*Nassif et al.*, 1998). These cell bodies form a substratum that outlines where the axon tracts of the nerve cord will travel. These FasII-positive neurons extend pioneer axons which also express FasII, adhere to, and are guided by the cell bodies and glial cells to form the innermost of the three FasII bundles of the longitudinal tracts of the nerve cord that form on either side of the midline (*Nassif et al.*, 1998; *Kuzina et al.*, 2011). Follower axons are guided along these tracts by FasII expression and other adhesion molecules (*Sánchez-Soriano et al.*, 2007).

Guidance of axons across the midline at specific commissures is governed by attractive and repulsive signals such as netrins from the midline (*Bhat*, 2005; *Harris et al.*, 1996; *Therianos et al.*, 1995; *Kennedy et al.*, 1994; *Klämbt et al.*, 1991; *Mitchell et al.*, 1996; *Sun et al.*, 2000). Growth cones of nerves that express the *commissureless* gene decrease expression of Robo receptors and are not repelled by midline Slit ligand until they cross the midline, turn off *commissureless*, and activate Robo, which prevents re-crossing (*Keleman et al.*, 2002; *Kidd et al.*, 1998; *Parsons et al.*, 2003;

Sánchez-Soriano et al., 2007; *Tear et al.*, 1996; *Thomas*, 1998). Certain cell axons do not express *commissureless* and thus remain ipsilateral due to Robo responding to Slit and negating attractive signals from the midline (*Bhat*, 2005; *Seeger et al.*, 1993). The combination of Robos and Robo receptors expressed determines which of the three lateral tracts the axons follow (*Bhat*, 2005; *Simpson et al.*, 2000; *Rajagopalan et al.*, 2000).

The tracts and commissures give rise to the ladder-like ventral nerve cord, and bilateral segmental and intersegmental motor nerves extend axons to the periphery (refer to Figure 1.5). Axons of other neural lineages use the FasII tracts for guidance to their respective targets (*Sánchez-Soriano and Prokop*, 2005; *Lin et al.*, 1994). Complex migration and guidance decisions are required to orchestrate nervous system development in *Drosophila*. Regulation of calcium dynamics may impact the elaboration of axon tracts and projections.

1.9 Zebrafish vascular development

In zebrafish embryos, endothelial progenitor cells arise from the lateral plate mesoderm (*Weinstein*, 2002; *Zhong et al.*, 2001). Migration of cells to the midline forms the dorsal aorta and posterior cardinal vein, where the endothelial cells continue to proliferate (*Chittenden et al.*, 2006). Beginning around 20 hours post-fertilization, the bilateral intersomitic blood vessels form sequentially in an anterior-to-posterior direction by individual endothelial cells migrating from the dorsal aorta and posterior cardinal vein, alternating artery and vein at each division between somites (*Siekmann*

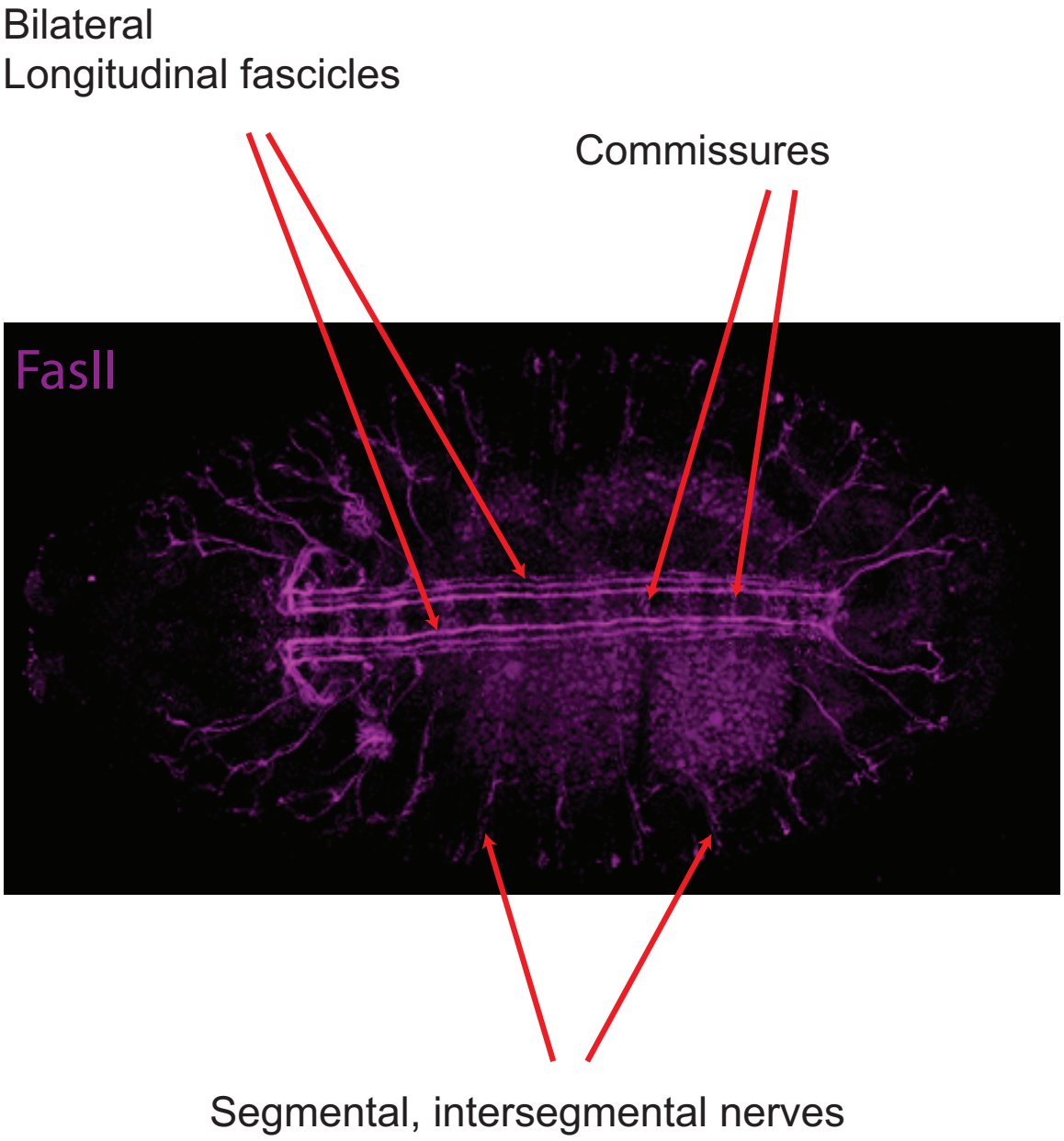

Figure 1.5: The Fasciclin II (FasII) CNS tracts and peripheral nerves. The diagram illustrates the parallel, bilateral triplets of FasII labeled neural tracts that extend through the ventral nerve cord, with commissural connections between them. FasII-positive segmental and intersegmental nerve axons project to peripheral targets.

and Lawson, 2007). On both sides of the embryo, three or more cells migrate in succession between adjacent somites and then form intercellular junctions between them (*Siekmann and Lawson*, 2007; *Childs et al.*, 2002). The endothelial cells lumenize by exocytosis and merging of vacuoles between overlapping endothelial cells to form a continuous tube that joins to larger vessels (*Kamei et al.*, 2006; *Blum et al.*, 2008). The tip cell at the most distal reach of the vessel extends projections and contacts tip cells from adjacent intersomitic vessels on the same lateral side of the embryo. These tip cells fuse to form the longitudinal anastomotic vessel that runs dorsal to the somites (*Isogai et al.*, 2001). See Figure 1.6 for a simplified diagram of zebrafish vasculature at the stage of interest.

Cell division may, or may not, occur in a non-stereotyped manner during individual intersomitic vessel outgrowth, but cell migration plays an invariant and prominent role in formation of the zebrafish intersomitic vasculature (*Siekmann and Lawson*, 2007; *Blum et al.*, 2008; *Childs et al.*, 2002). Zebrafish intersomitic vascular development permits characterization of the *in vivo* role of SERCA function in a non-epithelial tissue where predominantly migration, and some dispersed proliferation, generate a branched structure.

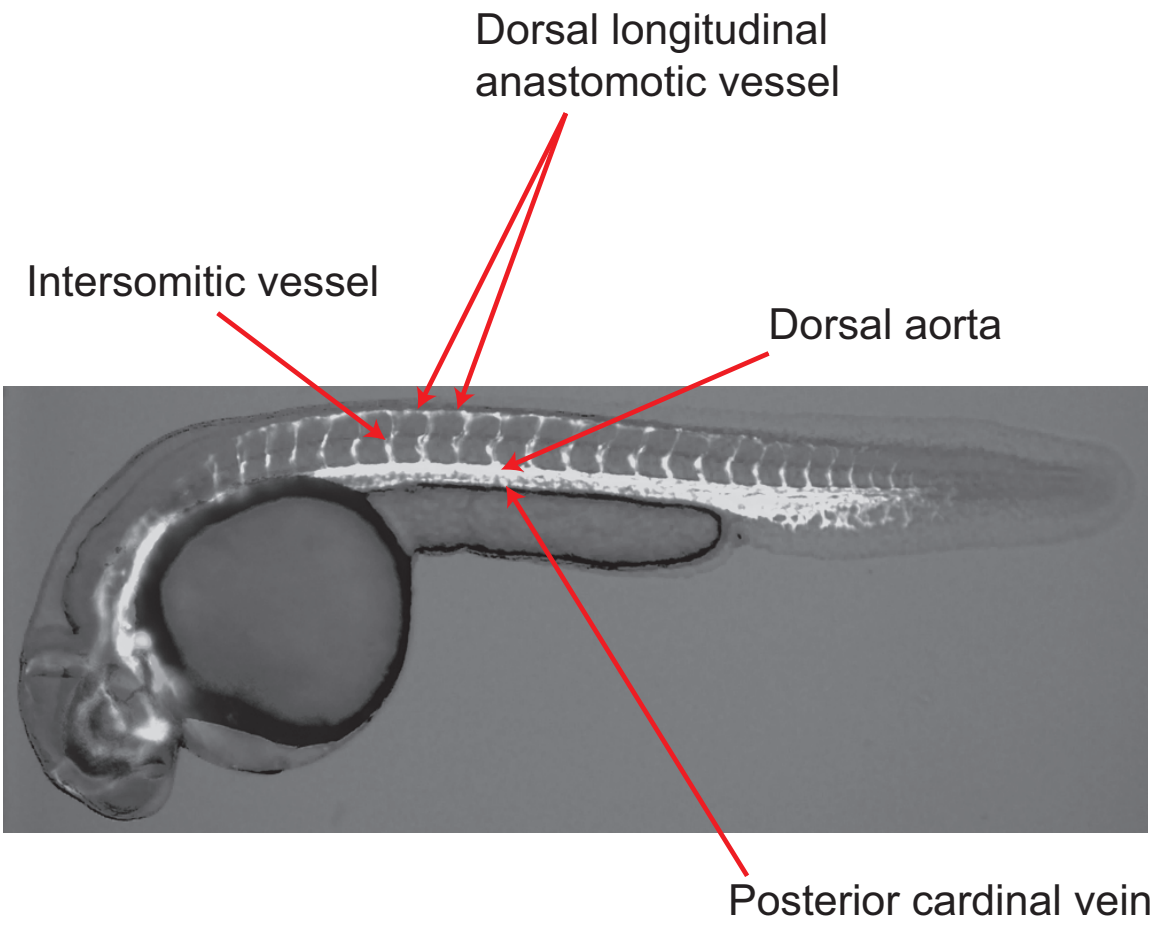

Figure 1.6: The vascular structure of the 28 hour post-fertilization (hpf) zebrafish embryo. The diagram shows the wild type structure of the intersomitic and trunk vasculature of the 28 hpf zebrafish embryo.

Chapter 2

Methods

2.1 Zebrafish intersomitic vasculature studies

Transgenic Tg(kdrl:eGFP) zebrafish with the VEGF receptor promoter driving eGFP expression express eGFP in endothelial cells. These fish were crossed with wild type fish and embryos were collected and incubated until 21 hours post-fertilization (hpf). eGFP positive embryos were sorted and dechorionated. Embryos were incubated with cyclopiazonic acid (CPA) (Sigma 1530) or DMSO from 22 hpf until 28 hpf in 1.5 mL of egg water. CPA was applied at concentrations of 1.25μM, 5μM, 10μM, or 20μM. For drug washout studies, embryos were incubated in 10μM or 20μM CPA for 2 hours, then rinsed 3 times in egg water and incubated for the remaining 4 hours without drug. After 6 hours of incubation, embryos were rinsed 3 times in egg water and fixed overnight at 4 degrees C in 4% PFA. To collect widefield images, embryos were positioned on top of methylcellulose. For confocal imaging, embryos were mounted on coverslip-bottomed imaging dishes in 1% agarose molds and covered with 1% low-melting point agarose. Imaging was performed with a Zeiss LSM 510 meta microscope.

Tiled z-stacks were collected with the following image collection parameters: 488nm laser excitation, 2μm pinhole, 2μm z-step interval. Z-stacks were assembled, and Imaris software (Bitplane) was used to generate 3D images and measure intersomitic vessel branches, lengths, and height in three dimensions to quantify the effects of CPA on intersomitic vessel growth and branching.

Data plots for vessel count, height, length, and branching were generated using python code (courtesy of Daniel J. Bower). Graphs for the rate of branching and cell migration were produced using MATLAB.

2.2 *Drosophila* embryo collection and drug treatment

Drosophila embryos were collected in egg-laying chambers for three hours. Fly lines used are listed in Table 2.1. Embryos were dechorionated in 50% bleach for 2 minutes and rinsed in tap water. Embryos were then transferred to nylon cell strainers (BD Falcon 2360) and permeabilized with permeabilization solvent (90% D-limonene, 5% cocamide DEA, 5% ethoxylated alcohol) as previously described (*Rand et al.*, 2010). This embryo permeabilization solvent (EPS) was diluted 1:10 into modified basic incubation medium (MBIM) for treatment of the embryos as described by *Strecker et al.* (1994); *Rand et al.* (2010) except that the malic acid was not added to the solution (see Table 2.2. Embryos were permeabilized for 30 seconds, washed 4 times in PBS and twice in PBS+0.05% Tween20 and distributed onto nylon cell strainers

Table 2.1: Genotypes of fly lines used.

Description	Genotype
Wild type	w
Tracheal actin-eGFP, nuclear dsRed	w; Btl:Gal4, UAS-dsRed-nuclear localization signal, UAS-actin-eGFP
Tracheal GCamp3	Btl:Gal4, UAS-GCamp3/CyO

Table 2.2: Composition of modified basic incubation medium (MBIM) (1 liter in milli-Q water). pH adjusted to 6.8 with NaOH and KOH and sterile filtered.

Component	(grams)
$MgCl_2$ $6H_2O$	2.2
$MgSO_4$ $7H_2O$	2.97
NaH_2PO_4	0.42
Glutamic Acid	12.1
Glycine	6.05
Sodium Acetate	0.027
Glucose	2.2
$CaCl_2$ $2H_2O$	0.99

or Whatman paper for incubation. Embryos were incubated on cell strainers or Whatman paper in 6 well dishes in contact with drug (20μM CPA, 100nM PMA) or DMSO diluted in MBIM until they reached stages 13 to 16 by gut morphology. For washout experiments, the drug solution was removed at stage 12 and the embryos were rinsed and then incubated for the remainder of the time in MBIM without drug.

2.3 *Drosophila* embryo fixation

For whole mount preparation, when embryos reached stages 13 to 16, they were transferred to glass vials and treated with heptane and 5% PFA in PBS for 15 minutes at room temperature to fix. The PFA was removed and 100% methanol was added, and the embryos were shaken to remove the vitelline membrane. The heptane was aspirated and the embryos were incrementally rehydrated through 70%, 50%, 30%,

0% methanol in PBS and then transferred to PBT (PBS + 0.05% TritonX-100 + 0.1% BSA).

2.4 *Drosophila* embryo antibody staining

For antibody staining, embryos were blocked for 1 hour at room temperature in 5% normal goat serum (NGS) then incubated with primary antibodies in PBT + 2% NGS overnight at 4 degrees C. Embryos were washed 6 times for 30 minutes at room temperature in PBT then blocked for 20 minutes in 5% NGS. Secondary antibodies (Invitrogen) were used at 1:500 in PBT + 2% NGS overnight at 4 degrees C. Embryos were washed 6 times for 30 minutes at room temperature and transferred to PBT/14% glycerol then mounted on glass slides with permafluor and coverslipped for imaging.

Fillet preparations were performed as previously described (*Lee*, 2009). Briefly, following drug treatment embryos were spread on glass slides with guts removed and a wax line drawn around them on the slide. They were fixed in 5% PFA for 30 minutes at room temperature and washed 4 times for 5 minutes in PBS and again in PBT on the slides. Blocking was performed for 30 minutes in 5% NGS, and fillets were incubated with primary antibodies as above at 4 degrees overnight. Fillets were washed 6 times for 10-30 minutes and incubated with secondary antibodies as above at 4 degrees overnight, then washed again 6 times for 10 minutes. Coverslips were mounted and sealed with nail polish. Confocal and two-photon tiled z-stacks were collected with a Zeiss LSM 510 meta microscope with a 2μm pinhole (for confocal) and 1.5μm z-step interval. Images were assembled using Fiji stitching plugins (*Preibisch*

Table 2.3: Antibodies used to stain *Drosophila* embryos. (DSHB) Developmental Studies Hybridoma Bank.

Target	Dilution	Host Animal and Isotype	Manufacturer	Catalog #
Tracheal lumen	1:2	Mouse IgM	DSHB	2A12
Fasciclin II	1:3	Mouse IgG1	DSHB	1D4
eGFP	1:1000	Rabbit IgG	Abcam	AB290

et al., 2009) and viewed in 3D using Imaris software (Bitplane).

2.5 Dynamic imaging of *Drosophila* embryos

Drosophila embryos from the transgenic line w; Btl:Gal4, UAS-dsRed-NLS, UAS-actinGFP were collected and permeabilized as described above. Embryos were treated with DMSO (control) or 20μM CPA and screened for fluorescence around gut stage 12 to 13. Fluorescent embryos were mounted lateral side down either on glass coverslips with heptane glue and imaged with the incubation medium serving as the objective immersion fluid, or they were mounted in coverslip-bottomed dishes in 1% agarose molds. The latter were covered with 1% low-melting point agarose and incubation medium and imaged through the coverslip with water immersion fluid to minimize refractive index mismatch. A high-numerical aperture, long-working-distance water immersion objective (LD-C-Apochromat 40X/1.1W Korr UV-VIS-IR) was used. Direct contact imaging requires thoroughly cleaning the objective of all traces of immersion oil. The embryos were imaged on a Zeiss LSM 510 meta or Zeiss LSM 5 Exciter confocal microscope with 488 nm and either 543 or 561 nm lasers. 318x318x64μm z-stacks were collected with 0.62x0.62x2μm^3 voxel size, and a stack was collected every 3 to 3.5 minutes.

2.6 Processing of dynamic imaging datasets

Datasets were compiled and registered using Imaris 7.6 (Bitplane). Individual cells of the tracheal lateral trunk that are destined to migrate to connect the trunk between segments were manually tracked in 3D from stage 14 to early stage 16. Positions of the tracked cells over the timecourse were exported to MATLAB. The separation between pairs of cells in adjacent segments that should migrate together to form the trunk were measured at the start and end to determine the relative convergence of the pair of cells, for DMSO-treated and CPA-treated embryos. Similarly, the overall direction of movement of one cell in the pair relative to the other was calculated and plotted to collectively visualize the directional migration of all pairs for each treatment.

Chapter 3

SERCA governs zebrafish vascular development by regulating cell migration

To determine the role of SERCA activity in the outgrowth and branching of zebrafish vasculature, zebrafish embryos were exposed to SERCA inhibitor during intersomitic vessel development. From 22 to 28 hours post-fertilization (hpf), after the first approximately four vessels had begun to form, embryos were incubated with increasing doses of the highly specific, pan-SERCA inhibitor, cyclopiazonic acid (CPA). Widefield images of embryos reveal that the overall morphology of the embryo is affected with CPA treatment (Fig. 3.1). The DMSO-treated control displays wild type morphology with a planar body alignment and straight dorsal aorta (vasculature indicated in green) (Fig. 3.1A). The embryos treated with CPA have more limited tail growth and exhibit a curved and twisted body (Fig. 3.1B,D). Increasing doses of CPA increases the severity of kinks in the dorsal aorta and posterior cardinal vein. Individual intersomitic vessels also appear stunted. Removal of CPA after 2 hours and incubation for the remaining time without the SERCA inhibitor broadly

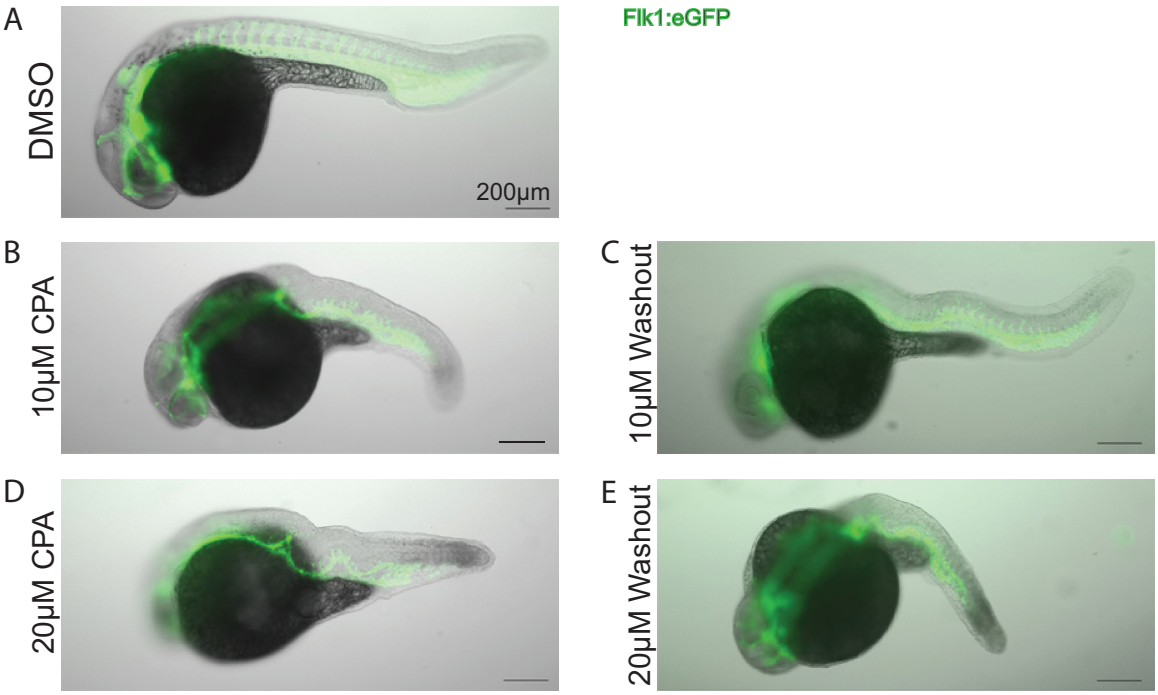

Figure 3.1: CPA affects zebrafish embryo morphogenesis but not eGFP expression. Zebrafish embryos were treated with specific SERCA inhibitor, CPA, during intersomitic vessel development. Overall morphology is normal in (A) DMSO-treated embryos (control). Increasing doses of CPA causes progressive twisting of the body axis, kinking of the dorsal aorta, and stunting of intersomitic vessel outgrowth in (B) 10μM and (D) 20μM. (C and E) Washout of the drug 2 hours into the incubation improves tail and blood vessel morphology. eGFP expression (green) is not affected by drug treatment. (CPA, cyclopiazonic acid)

improves intersomitic vessel outgrowth and tail structure, particularly for the lower dosage of CPA (Fig. 3.1C,E). Importantly, comparable eGFP fluorescence is seen throughout the head vasculature and dorsal aorta, indicating that GFP expression itself is not affected by SERCA inhibition, and therefore the rudimentary appearance of the intersomitic vessels is due to stunted outgrowth rather than lack of GFP expression. Thus, application of a SERCA inhibitor affects embryo development, and the effects on the intersomitic vasculature can be quantified.

To quantitatively investigate the effects of SERCA inhibition on vascular devel-

opment, Flk1:eGFP transgenic embryos expressing eGFP in all endothelial cells were imaged with confocal microscopy, and the tail and intersomitic vasculature were reconstructed in 3D. Figure 3.2A shows a widefield image of a wild type embryo and outlines the region of interest of vessels that formed during the incubation period with or without SERCA inhibitor. This region was imaged at higher resolution and reconstructed. In control DMSO-treated embryos, parallel intersomitic vessels project from a straight dorsal aorta and posterior cardinal vein (Fig. 3.2B). Cell nuclei are visible along the length of vessels with increased density of eGFP localization. At the tips of the intersomitic vessels, cells have extended longitudinal projections towards adjacent vessels to fuse and form the longitudinal anastomotic vessel dorsal to the somites. Younger, more posterior vessels (towards the right) have not yet grown to full length, and cell nuclei have not yet reached the tip of the vessel. Increasing doses of SERCA inhibitor from 1.25μM to 20μM (Fig. 3.2C-E,G) induces increasingly severe curvature of the dorsal aorta and posterior cardinal vein and truncated intersomitic sprouts. While the vessels look relatively normal with 1.25μM CPA (Fig. 3.2C), and the dorsal aorta is only a bit curved with 5μM CPA, the tail and vascular structure are contorted with higher doses (Fig. 3.2E,G). Removal of 10μM CPA after 2 hours of the incubation period ameliorates vascular development (Fig. 3.2F). The tail vasculature is less kinked, and the intersomitic sprouts are longer and greater in number. There are no gaps or 'skipped' intersomitic sprouts, indicating that upon removal of the inhibitor, growth resumes from the stage it was at and proceeds in the normal anterior-to-posterior direction. Thus, inhibition of SERCA slows the rate

of growth such that fewer vessels have formed compared with controls during a fixed amount of time. But this inhibition is reversible, and vascular development proceeds normally with inhibitor washout. Quantitation is necessary to determine the dose dependence. Washout of the 20μM CPA results in less obvious recovery of vascular development that also requires quantitation to identify (Fig. 3.2H).

The 13th through 16th, 19th, and 20th sprouts from the anterior end were compared across treatment with DMSO (control), increasing doses of SERCA inhibitor, and washout of inhibitor after 2 hours. Figure 3.3A shows an overview of the intersomitic vasculature formed during the incubation period and the locations of the individual sprouts 14-15 and 20 depicted in the paired images in B-H. Figure 3.3B displays the typical height and morphology of sprouts in DMSO-treated controls. Three to four cells comprise each of the more mature sprouts, and a cell nucleus is frequently positioned at the distal tip, as indicated by the red arrow. At the end of the incubation period, the 20th sprout is still forming, but cytoplasmic projections extend the sprout to a considerable height.

With increasing concentrations of SERCA inhibitor, the intersomitic sprouts that formed during the middle of the incubation period (sprouts 14-15) and near the end of the incubation period (sprout 20) are shorter and less branched (Fig. 3.3C-E,G). The red arrow in Fig. 3.3E indicates the position of the nucleus of the cell that has migrated the furthest along the vessel. It is situated in the middle of the sprout rather than at the tip. When the SERCA inhibitor is removed after 2 hours and the embryos incubated without drug for the remainder of the time, growth and branching

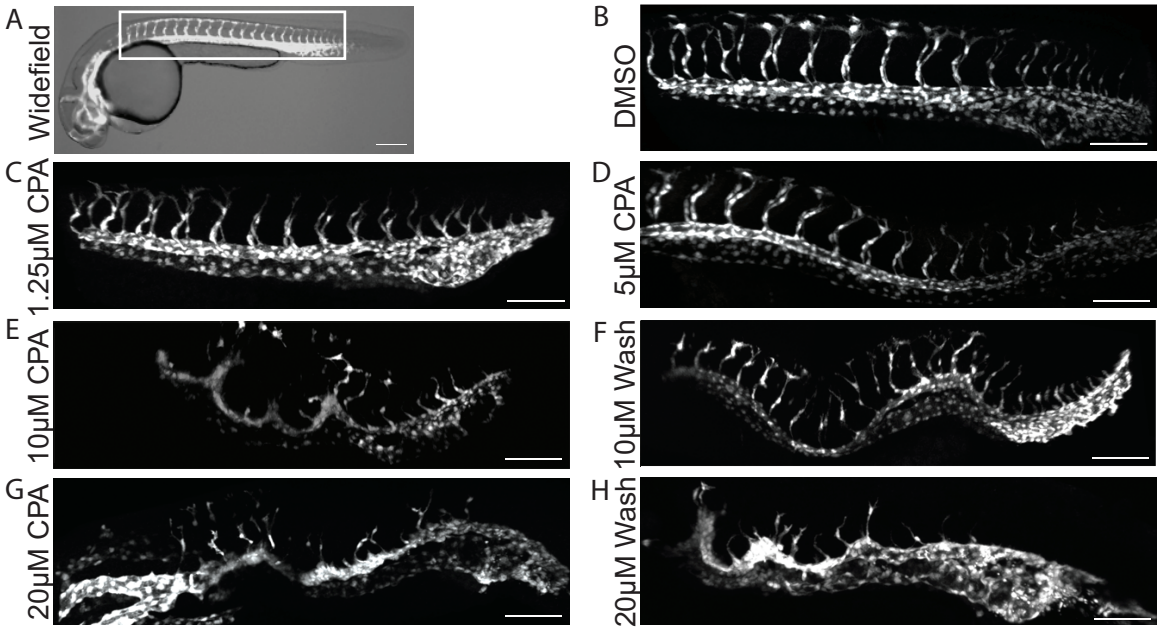

Figure 3.2: SERCA inhibition affects tail vessel morphology and outgrowth. The intersomitic vessels that formed during SERCA inhibition in Flk1:eGFP transgenic embryos were imaged with confocal microscopy and reconstructed in 3D to visualize the impacts on vascular development. (A) The widefield image of wild type embryo shows the vessels formed during the incubation period (scale bar=200μm). Panels B-H show 3D reconstructions of confocal images of intersomitic vasculature from embryos treated with (B) DMSO (control), (C) 1.25μM, (D) 5μM, (E) 10μM, (G) 20μM CPA, or CPA washed out 2 hours into the incubation (F) 10μM washout, (H) 20μM washout (B-H, scale bars=100μm). In controls, the intersomitic vessels extend to the tips of the somites where the vessels branch to fuse with their neighbors. Increasing the dose of SERCA inhibitor increases the severity of dorsal aorta contortion and progressively stunts the outgrowth and branching of the intersomitic vessels. Washout of the inhibitor lessens the severity of the phenotype, and growth resumes from the point it was at when inhibition is released, rather than skipping sprouts.

resume. The sprouts depicted in Fig 3.3F and H are longer with more buds than their counterparts in Fig. 3.3E and G which were exposed to drug for the duration of the six hours. This resumption of growth following release of SERCA inhibition indicates that vascular sprouting and elongation are reversibly on hold when the SERCA pump is blocked. Quantification of outgrowth and branching reveals the extent of growth inhibition and recovery.

The growth dimensions and number of branches were measured for individual intersomitic sprouts formed during the incubation period to quantify the growth and branching effects of SERCA inhibition. The composite length of all branches per sprout, radial height of the sprout from the dorsal aorta, number of branches per sprout, and total number of sprouts that formed per embryo were measured in three dimensions for zebrafish embryos incubated with DMSO, increasing doses of SERCA inhibitor, or embryos with drug washed out after 2 hours. Figure 3.4A shows the total number of intersomitic vessels that formed per embryo for each of the treatment groups. Red lines indicate the median value. Typically 23 or 24 vessels form by 28hpf in control embryos treated with DMSO, and the number decreases as SERCA inhibition increases. Approximately 15 vessels form in embryos treated with 20μM CPA. Following washout of inhibitor, vessel outgrowth increases, albeit only slightly for the 20μM CPA washout embryos. This level of inhibition may be severe enough that it takes longer for sprouting activity to recover, and the recovery is slow. In contrast, in embryos treated with 10μM CPA washed out after 2 hours, an equal number of intersomitic sprouts form by the end of the incubation period as in

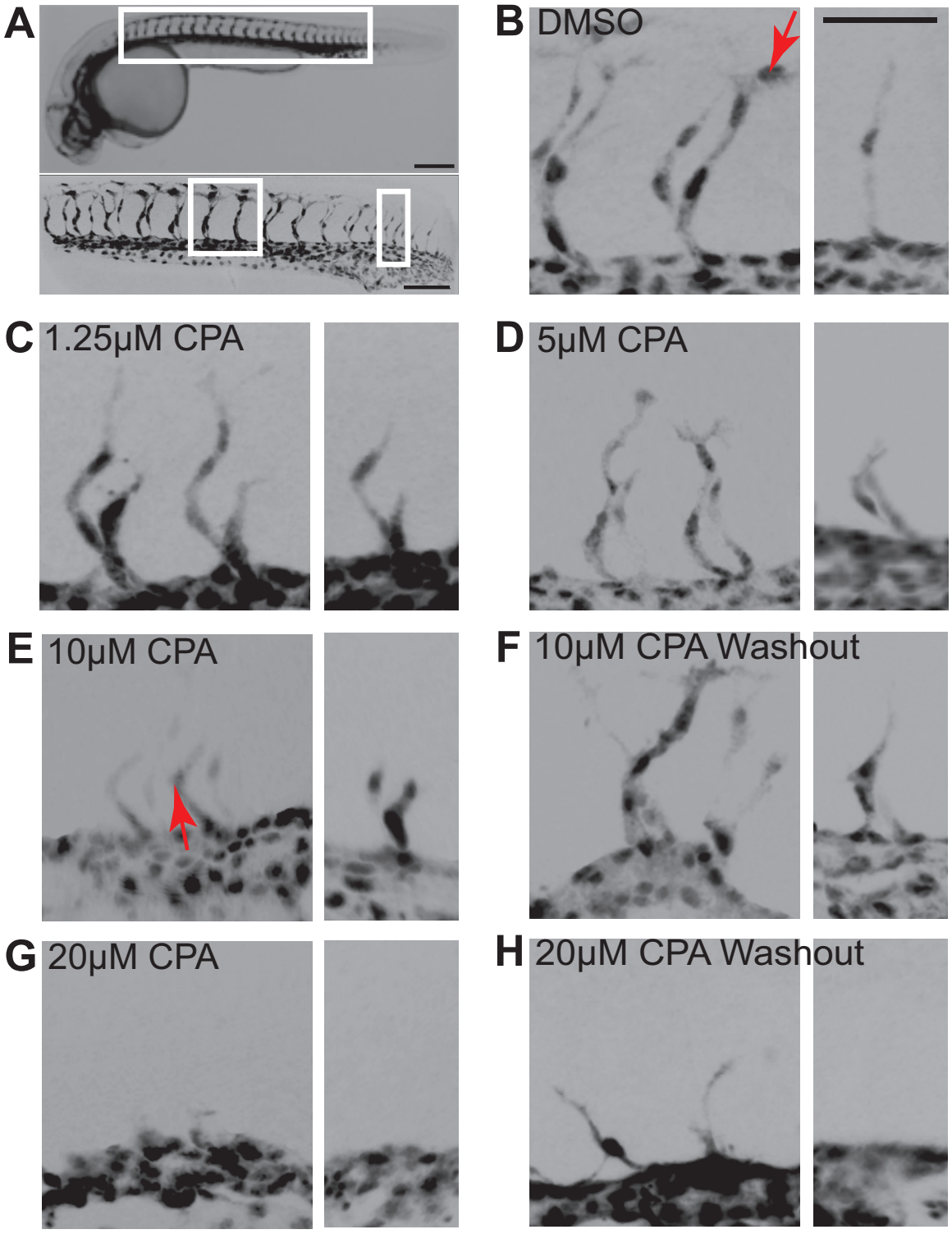

Figure 3.3: Caption next page.

Figure 3.3: Individual intersomitic sprout outgrowth and branching is affected by SERCA inhibition in a dose-dependent manner. The panels in (A) outline the specific sprouts detailed in paired panels that form during the middle and end of the incubation period. Scale bars=200μm (widefield), 100μm (inset). Embryos are incubated from 22 to 28 hpf in the presence of (B) DMSO, (C) 1.25μM, (D) 5μM, (E) 10μM, (G) 20μM CPA, or CPA washed out 2 hours into the incubation (F) 10μM washout, (H) 20μM washout. SERCA inhibition results in a dose-dependent reduction in the growth and branching of vessels that form during the middle and near the end of the incubation period. The extent that individual cell soma have migrated along the length of the vessel is apparent by increased expression in the nucleus. Red arrows indicate a cell that has migrated to the tip of the branch in (B), while in E, the most distally migrated cell is still in the center of the vessel. (F and H) Growth and branching resume following washout of the inhibitor. Scale bars in B-H = 50μm.

controls treated only with DMSO. Embryos treated for the duration with 10μM CPA form approximately 3 fewer vessels than controls. Thus, the rate of vessel outgrowth following removal of SERCA inhibitor must be greater than the wild type rate for some duration of time in order to catch up with the uninhibited embryos. Effects of SERCA inhibition at lower doses are more subtle by measurement of the number of vessels formed, but the inhibitory effects are clear when considering the dimensions and number of buds per vessel.

Figure 3.4B plots the cumulative number of branches, or buds, present on intersomitic vessels 13 through 16 for embryos in each treatment group. These vessels form during the middle of the incubation period after the drug has equilibrated and should exhibit the full effects of SERCA inhibition. Since the panels in Figure 3.3 show that vessels are shorter with increasing SERCA inhibition, the vessels would also be expected to have fewer buds. Endothelial cells of the vessels extend cytoplasmic projections to form the longitudinal anastomotic vessel connecting their tips and a parachordal vessel midway between the dorsal aorta and dorsal longitudinal.

Intersomitic vessels that have not attained their full length would be expected to have few buds. Indeed, the number of buds that have formed on these vessels decreases with increasing SERCA inhibition (Fig. 3.4B). Washout of CPA permits increased budding concomitant with increased vessel length.

To investigate how SERCA inhibition affects the early stages of vessel development, the height, length, and number of buds per vessel were quantified for the 19th and 20th vessels, which form near the end of the incubation period in control embryos and thus are at a younger phase of outgrowth. Figure 3.5A-C plot these measures for each treatment group for the 19th intersomitic vessel, and Figure 3.5D-F plot the values for the 20th vessel. Consistent with the data from sprouts 13 to 16, the individual vessel budding (Fig. 3.5A,D), length (Fig. 3.5B,E), and height (Fig. 3.5C,F) are reduced dose-dependently with SERCA inhibition and partially rescued with washout of inhibitor. At a concentration of 20μM CPA, the 19th and 20th vessels have not yet formed. The median lengths and heights of the 20th vessels in the 10μM CPA washout group are nearly equivalent to the controls. At the point when these vessels are forming, the drug has been absent for several hours, and the results suggest that by the formation of the 20th intersomitic vessel, these embryos have "caught up" with controls in terms of vessel outgrowth. The data also suggest that the initial stages of outgrowth to form an intersomitic vessel proceed more normally than budding following CPA washout because there are fewer buds on the 20th vessel of the 10μM washout embryos compared with controls. The 19th vessels also still have a deficit in height, length, and branching compared with the equivalent vessels

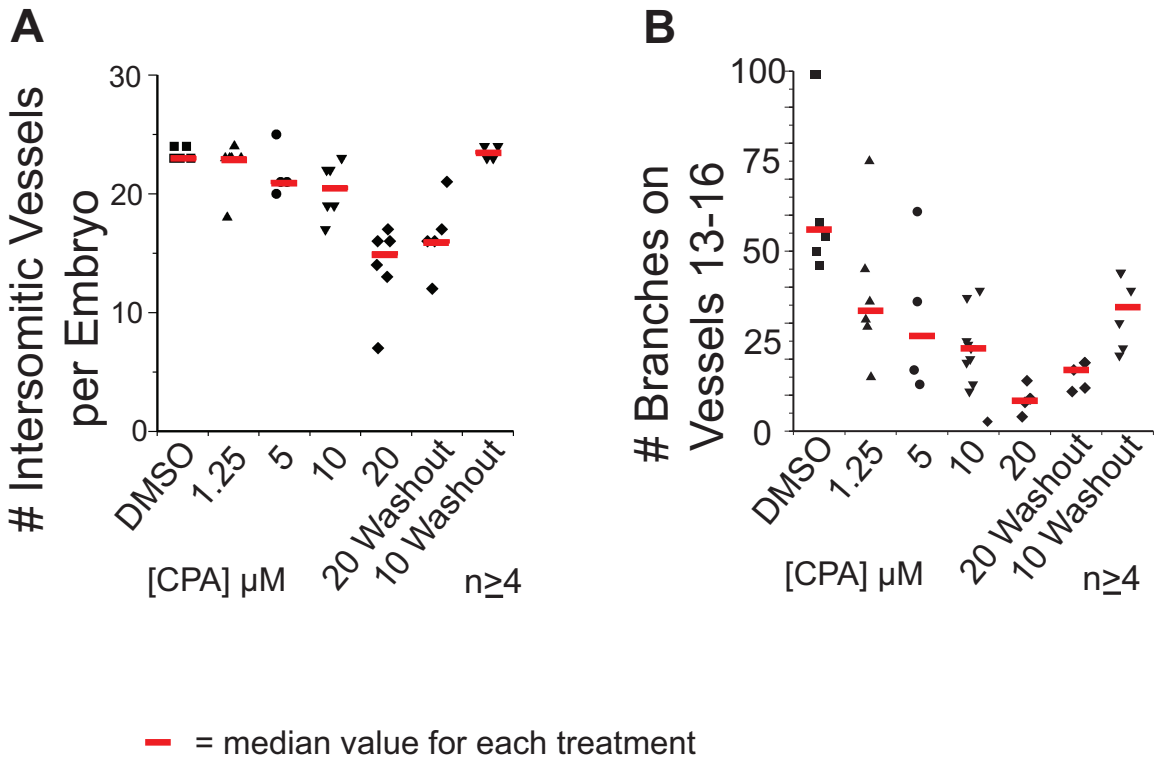

Figure 3.4: The total number of intersomitic vessels and the number of buds on vessels formed during the middle of the incubation period are reduced dose-dependently with SERCA inhibition. (A) The number of intersomitic vessels formed per embryo by 28hpf is plotted for each treatment group. Each symbol represents a measurement from one embryo and the red lines indicate the median values. SERCA inhibition reversibly reduces the number of branches in a dose-dependent manner. Washout of 20μM CPA produces a slight recovery in sprout formation, but washout of 10μM CPA results in complete rescue of the total number of intersomitic vessels that have begun to form by 28hpf. (B) The collective number of branches or buds on intersomitic vessels 13 through 16, which form during the middle of the incubation period, are plotted. The dose-dependent reduction in branching of these vessels with increasing SERCA inhibition is partially rescued by washout of the inhibitor 2 hours into the incubation.

in controls despite the 20th vessels having comparable height and length relative to controls. So the initiation of migration to form the vessel may be fully recovered but later migratory activity and cytoplasmic budding may lag behind.

To further investigate the role of SERCA activity in regulating cytoplasmic extensions, or branching, the rate of branching over time was considered. Since the vessels form in an anterior-to-posterior wave, the more anterior ones have had more development time since their initiation than more posterior ones. A comparison between treatment groups of the number of branches on sequential vessels reflects the rate of branching with time, where higher number vessels are younger. A graph of the number of branches on the 13th, 16th, and 19th intersomitic vessels for each treatment group demonstrates a dose-dependent rate of branching with SERCA inhibition (Fig. 3.6). It also shows that inhibition of the SERCA pump more severely affects the rate of branching during early stages of vessel formation as the slope of the line connecting the younger vessels 19 and 16 is reduced with inhibition of SERCA. The rate of budding at later stages (represented by the line between the 16th and 13th vessels) is similar across treatment groups, although the total number of branches is reduced with SERCA inhibition. Thus, cells may be more sensitive to SERCA inhibition when they are trying to initiate the extension of cytoplasmic projections. Alternatively, all cellular behaviors are most affected by SERCA inhibition early in the process of vessel outgrowth, and so most of the delay in migration and branching occurs then.

Because the intersomitic vessels form by migration of 3 or 4 individual endothelial

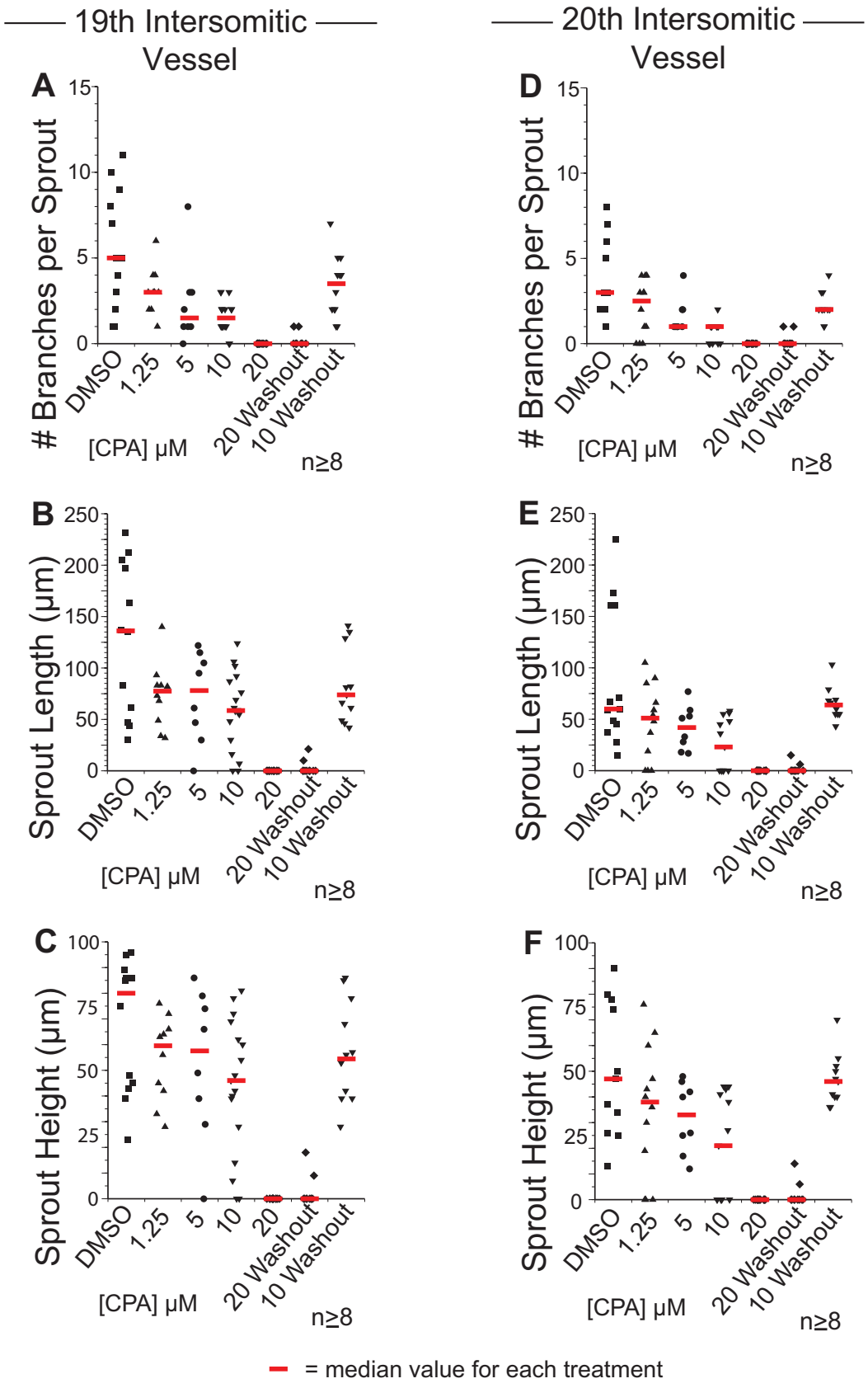

Figure 3.5: Caption next page.

Figure 3.5: The height, length, and number of branches on intersomitic vessels formed near the end of the incubation period are reduced in a dose-dependent manner with SERCA inhibition. (A-C) show plots of the number of branches per vessel, the composite length, and the radial height, respectively, for the 19th intersomitic vessels on embryos from each treatment group. (D-F) plot the same measurements for the 20th intersomitic vessels. Median values for each treatment group are indicated by red lines. All metrics decrease in a dose-dependent manner with increasing SERCA inhibition. For the 19th intersomitic vessel (A-C), washout of the inhibitor results in a partial rescue. Washout of the 10μM CPA results in a complete rescue of vessel outgrowth measured by height and length for the 20th intersomitic vessel, but an incomplete rescue of budding. Initiation of cell migration to form the vessel may be mostly normal while initiation of cytoplasmic projections may be delayed.

cells from the dorsal aorta or posterior cardinal vein, the positions of nuclei along the length of the vessel were quantified as a direct measure of cell migration. For the 12th through 14th intersomitic vessels, Figure 3.7 plots the percentage that possess a cell nucleus at the distal tip of the vessel (refer to Fig. 3.3 for images of cell nucleus positioning along the vessels). In the DMSO-treated controls, the distal-most cell has migrated to the tip of the vessel in 66% of the intersomitic vessels. This percentage declines to 14% in the 20μM CPA-treated embryos and recovers to 47% in the 10μM CPA washout group with statistical significance less than 0.05 by Chi-squared analysis. The graph of the different treatment groups mirrors those for the height, length, branching, and number of intersomitic vessels. Additionally, the reductions in vessel dimensions are not a result of fewer cells constituting the vessels but rather result from the positions of the cells within the vessel. This finding indicates that a defect in endothelial cell migration as a result of inhibition of the SERCA pump accounts for the observed perturbations in intersomitic vessel growth and branching. The behaviors of migration of the cell soma and protrusion of cytoplasmic buds are likely independent, and there may be nuances in the extent to which SERCA regulates

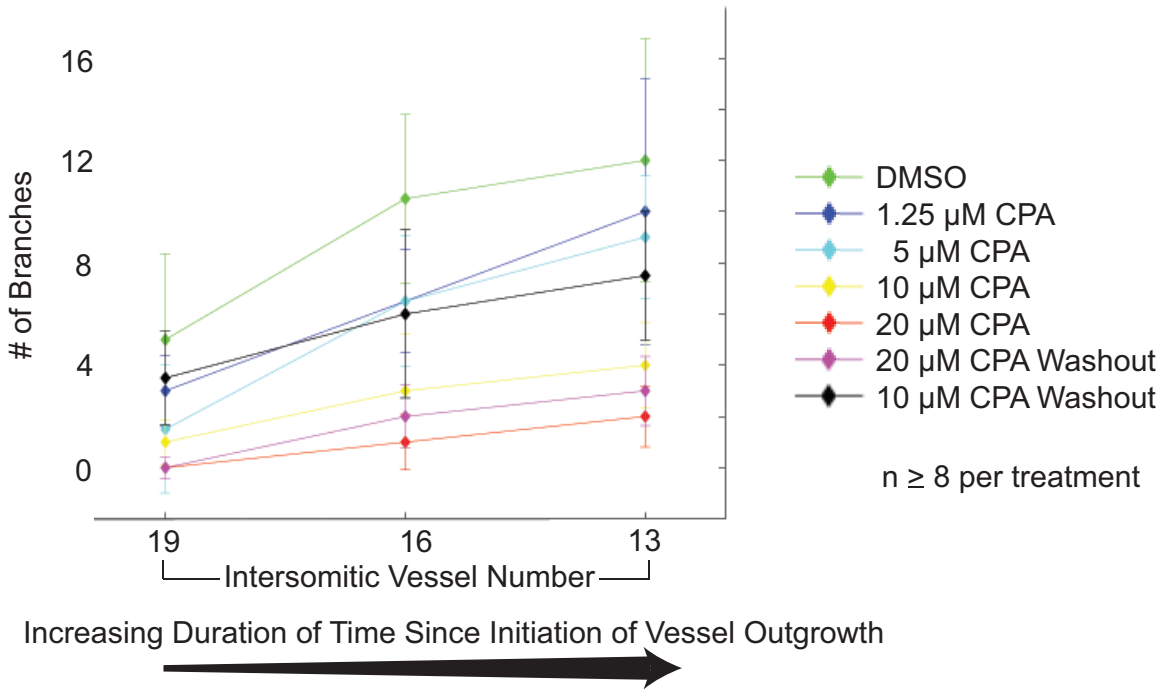

Figure 3.6: Early stages of vessel growth are more sensitive to SERCA inhibition in terms of the rate of initiating branches. The intersomitic vessel number is used as a surrogate for the amount of time a vessel has spent developing since they form in an anterior-to-posterior sequence. Vessels of higher number are younger. The graph shows that the rate of branching is more severely reduced by SERCA inhibition early on in the process of vessel outgrowth: with SERCA inhibition, the slopes of the lines connecting vessels 19 and 16 are less than those at the later developmental age between vessels 16 and 13.

each. However, at a basic level, SERCA's regulation of cell motility explains the dose-dependent defects in intersomitic vessel growth and budding observed with SERCA inhibition.

Calcium's regulation of cell behaviors may depend on dynamic patterns of calcium flux, and the dynamics are governed by the interplay between SERCA activity to store calcium and IP3-driven release of calcium into the cytoplasm. Because protein kinase C (PKC) inhibits phospholipase C (PLC) and thus IP3 production, we asked whether activating PKC in the background of SERCA inhibition could balance the impaired pumping of calcium to the ER and serve as a partial rescue of intersomitic vessel growth and branching. A phorbol ester was used to activate PKC and thus reduce the release of calcium into the cytoplasm by IP3. Addition of PKC activator alone had an inhibitory effect on intersomitic vessel outgrowth and branching. The combinatorial treatment of PKC activation plus SERCA inhibition produced results that were either similar to the SERCA inhibition alone or showed an additive effect (see data in appendix A).

There are several isoforms of PKC performing many activities in a cell, and it may be that inhibition of a select one of them would be necessary to rescue the SERCA inhibition. However, indiscriminate inhibition of multiple isoforms could perturb many different cell behaviors and result in impaired cell motility, which could be dependent on or independent of calcium. Specific inhibition of individual isoforms of PKC would be necessary to determine whether PKC activation and IP3 reduction could partially rescue SERCA inhibition. Alternatively, endothelial cell

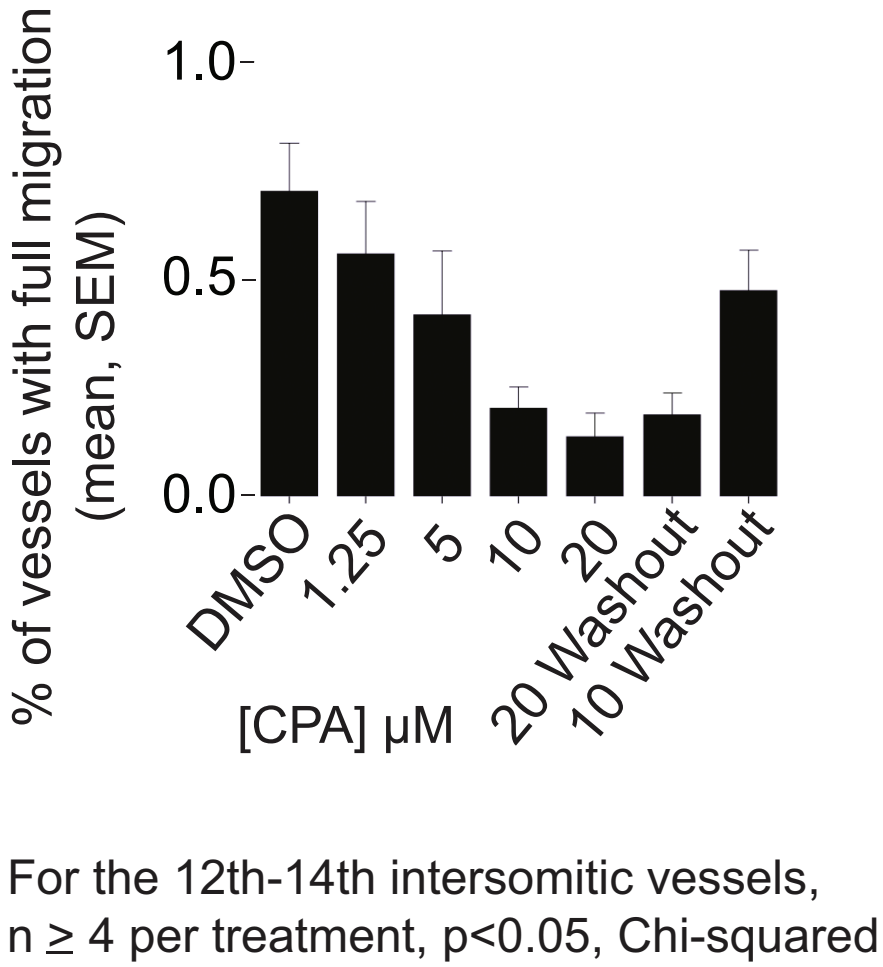

Figure 3.7: SERCA-dependent defects in endothelial cell migration account for the observed impairments in intersomitic vessel outgrowth and branching. Cell migration was measured by quantifying the percentage of the 12th through 14th intersomitic vessels in which a cell nucleus was positioned at the distal tip of the vessel, indicating complete migration of the cell along the length of the vessel. Cell migration is impaired in a dose-dependent manner with SERCA inhibition and reflects the defects in vessel height, length, branching, and total number of vessels per embryo. A defect in SERCA-dependent cell motility therefore explains the measured impairments in intersomitic vessel growth and branching from SERCA inhibition.

outgrowth and branching to form the intersomitic vessels may require a particular pattern of changing calcium levels to direct cell motility. Inhibition of both arms of the calcium cycle–calcium release and calcium uptake–may not reconstitute the dynamic fluctuations necessary for vessel formation.

3.1 Summary

We conclude from these studies of the effects of SERCA inhibition on zebrafish intersomitic vascular growth that inhibition of SERCA activity impedes vessel outgrowth and branching. The dorsal aorta and posterior cardinal vein become increasingly malformed with higher doses of SERCA inhibitor, and the individual intersomitic sprouts are shorter and possess fewer branches compared with controls after the same incubation time. The rate of branching earlier in the vessel's formation may be more severely affected than branching when the vessel is more mature. Vessel outgrowth and branching decrease dose-dependently with increasing SERCA inhibition, and the effect is reversed upon removal of the inhibitor. Thus, SERCA's regulation of calcium serves as a dynamic cue that instructs cell behavior, and the proper dynamic can resume as soon as SERCA activity is restored. Cell position within the more developed vessels rather than the number of cells accounts for the measured differences. This suggests that impaired cell migration accounts for the reduction in vessel growth and branching, which is consistent with previous work showing that the vessels form principally by cell migration (*Childs et al.*, 2002). Activation of PKC to reduce calcium release into the cytoplasm does not compensate for the impaired

calcium uptake into the ER to rescue zebrafish intersomitic vessel outgrowth.

Zebrafish intersomitic vascular development relies principally on the migration of individual endothelial cells between the somites. Some cell division does occur, however. While these studies indicate that SERCA-dependent defects in cell migration give rise to the observed vascular phenotype, we wished to determine whether cell migration can fully account for SERCA-dependent budding defects. For this we turned to a system where branching proceeds in the complete absence of cell proliferation.

Chapter 4

PKC-regulated SERCA governs *Drosophila* tracheal and neural morphogenesis

To determine whether SERCA regulates branching across tissues and species, and whether it regulates branching in a system that relies exclusively on cell migration, we studied SERCA activity in *Drosophila* embryos. PKC activation was also tested to see whether it could rescue SERCA inhibition in the context of tracheal and neural development by reducing ER calcium release. The *Drosophila* embryonic nervous system, unlike the zebrafish vasculature, depends on both cell migration and considerable proliferation. In contrast, the embryonic tracheal system is a network of epithelial tubules that forms exclusively by the migration of individual tracheal cells following complete cessation of cell proliferation. It is thus a useful system to assay the extent to which SERCA regulates branching by directing cell migration.

To determine whether SERCA is important for the formation of the embryonic *Drosophila* tracheal network and CNS development, embryos were permeabilized and treated with DMSO (control) or drug through embryonic development. The specific

pan-SERCA inhibitor, CPA, and protein kinase C activator, PMA, were administered alone or in combination. Embryos were fixed around stage 15 to 16 when the CNS and tracheal network have formed. Antibody staining for Fasciclin II and tracheal lumen protein reveal CNS tracts and motor axons, and tracheal structure, respectively.

Figure 4.1 shows whole mount images of embryos treated with (A) DMSO (control), (B) 20μM CPA, (C) μM CPA washed out at stage 12 (early organogenesis), (D) 100nM PMA, and (E) 20μM CPA + 100nM PMA. The normal tracheal network (cyan) is evident in controls (Fig. 4.1A) with interconnected segments and continuous dorsal and lateral trunks (refer to Fig. 1.4 on page 14 for the names of the different branches). The nervecord can be seen with tracts (magenta) running along the ventral side of the embryo and axons projecting dorsally alongside segments of the trachea. The embryo permeabilization does not cause developmental perturbations in controls, however, it is effective for administering drugs as the tracheal network and nerves are disrupted with CPA treatment (Fig. 4.1B). The trachea and nerve networks can be seen for each treatment, albeit with faint dorsal trunk labeling for the washout and PMA treatments (Fig. 4.1C,D, arrowheads). Of note is the normal-looking embryo treated with CPA and PMA (Fig. 4.1E) compared with the embryo treated with SERCA inhibitor (Fig. 4.1B), where the tracheal structure is fragmented. There are breaks in the dorsal trunk (yellow arrowheads), lateral trunk (blue arrowheads), and the longitudinal nerve fascicles (pink arrowheads).

A closer look at just the trachea in whole mount embryos labeled with antibody to tracheal lumen protein shows that compared with controls (Fig. 4.2A), the trachea

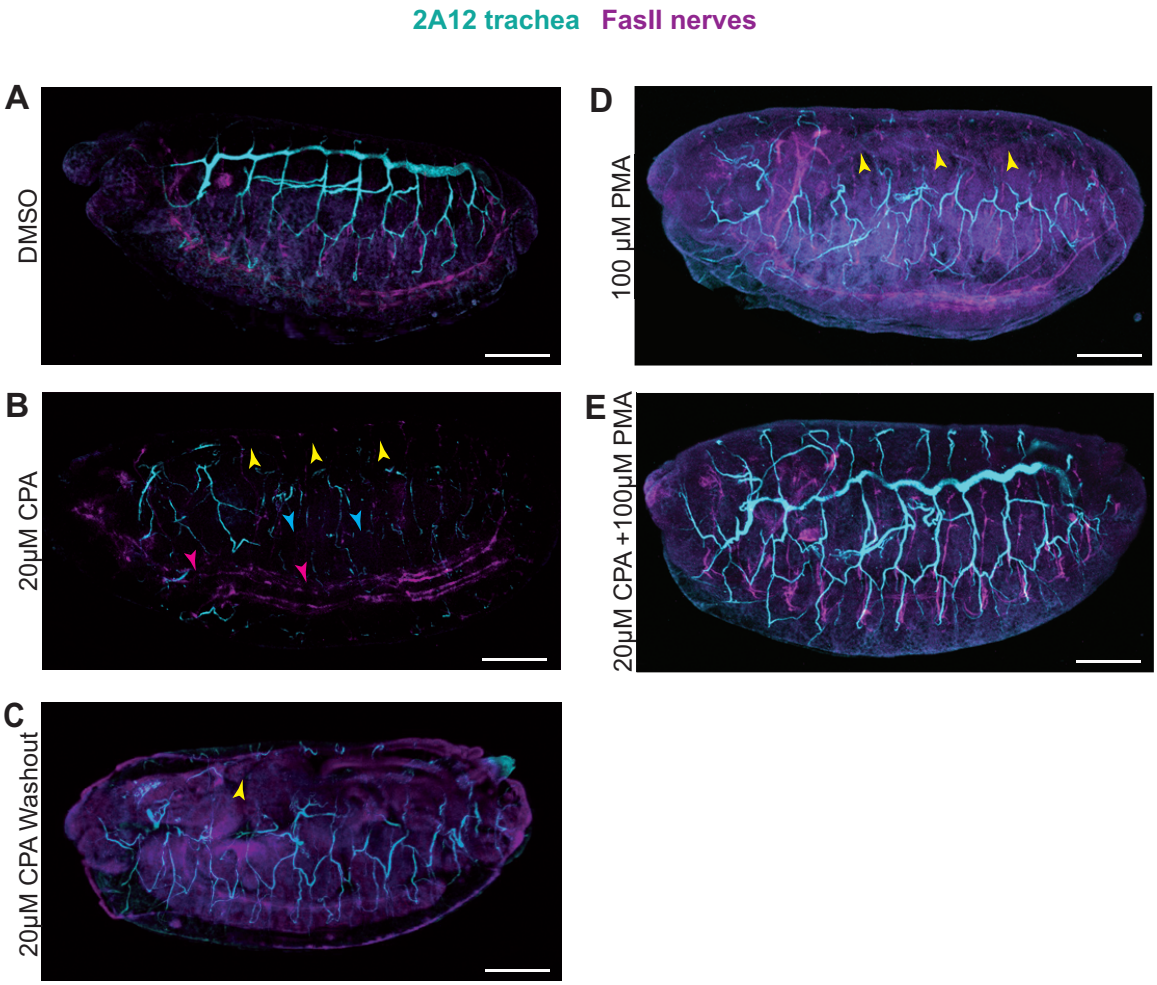

Figure 4.1: Dual label of *Drosophila* trachea and nerves demonstrates that the permeabilization of the embryos itself causes no phenotype but permits drug treatment. (A) Permeabilized controls treated with DMSO. (B) Embryos treated with SERCA inhibitor display breaks in the dorsal trunk (yellow arrowheads), lateral trunk (cyan), and ventral nervecord (pink). (C) Washout of SERCA inhibitor at stage 12 improves tracheal and nerve networks, although incompletely (arrow). (D) The dorsal trunk is not visible in embryos treated with PKC activator, but they otherwise look normal. (D) Dual treatment with SERCA inhibitor and PKC activator normalizes tracheal and neural structure. Scale bars=50μm. 2A12 labels tracheal lumen. FasII marks longitudinal fascicles and motor axons.

of the CPA-treated embryo (Fig. 4.2B) is highly disorganized and discontinuous. The dorsal trunk is absent (yellow arrowheads), and the lateral trunk is severely fragmented with few connected segments (yellow arrows). In this severe case, the visceral branches cannot be distinguished from the transverse connectives, and some of the glial branches appear to be missing (open arrowheads). Following removal of SERCA inhibitor at stage 12 with drug-free culture to stage 16 (Fig. 4.2C), the embryo exhibits a relatively normal tracheal network. The dorsal trunk stains faintly in this particular embryo, which may indicate a defect in lumenization or lumen protein secretion; however, it is largely continuous except for one gap (arrowhead).

The most striking appearance is the exuberant branching at the tips of tubes of the visceral branches and glial branches (open arrowheads). Many of the tubes are have a squiggly structure as though the tube is longer than it needs to be, and the tips project farther than in controls. These features suggest that removal of the SERCA inhibitor either resulted in an over-compensatory branching and migration of the cells, or that these behaviors are normally restrained and that this restraining mechanism recovered more slowly than SERCA's activity to promote migration upon removal of the inhibitor. In addition, the gross recovery of tracheal structure following washout of the inhibitor suggests that the defects are not a result of perturbed extracellular matrix or other cues that the tracheal cells require in order to migrate to their proper positions. Instead, the effect is more likely a reversible cell-autonomous defect in migration, and when inhibition of the SERCA pump is relieved, the cells are able to resume migration and recover their proper positions. In the embryo treated with PKC

activator (Fig. 4.2D), the tracheal network appears normal apart from the missing dorsal trunk (outlined by yellow dots), which is investigated further in Figure 4.3. In (Fig. 4.2E), the embryo treated with the combination of the SERCA inhibitor and PKC activator recovers a remarkably normal tracheal structure with continuous trunks and segmental projections.

Visualizing the *Drosophila* embryonic trachea using an antibody to tracheal lumen protein suggests defects in tracheal structure from SERCA inhibition and perturbed dorsal trunk formation from PKC activation. However, this could be an artifact of the antibody used if tube lumenization, rather than cell migration to form tubes, is affected. To ascertain that the observed defects are actual gaps in the tracheal structure due to mispositioning of tracheal cells, we used a transgenic fly line to genetically label all tracheal cells by the early tracheal-specific promoter *Breathless* (*Btl*). In the *w; Btl:Gal4, UAS-dsRed-NLS, UAS-actin-eGFP* line, tracheal cell nuclei are red and eGFP fused to actin labels the outline of the cells. These embryos were permeabilized and treated with SERCA inhibitor and/or PKC activator as before and stained with anti-GFP antibody to visualize all tracheal cells regardless of lumenization.

The panels in Figure 4.3 show images of the trachea from embryos filleted to remove gut autofluorescence. Dashed yellow lines outline the dorsal trunk in each panel. Tracheal structure is normal in permeabilized embryos treated with DMSO (Fig. 4.3A), with continuous dorsal and lateral trunks. In embryos treated with SERCA inhibitor (Fig. 4.3B), complete gaps between segments (arrowhead) and

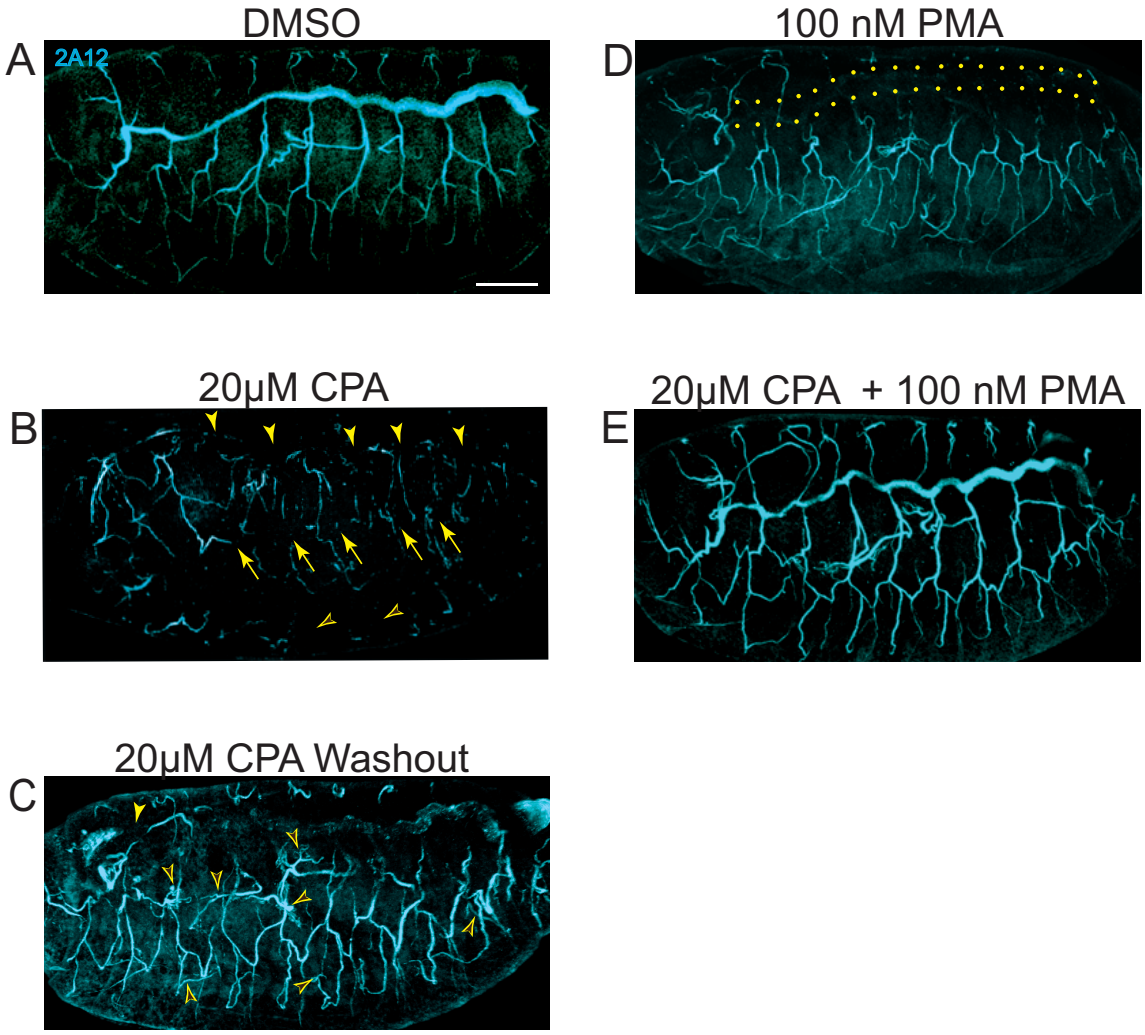

Figure 4.2: SERCA inhibition disrupts tracheal morphogenesis and PKC activator rescues. (A) Control embryos treated with DMSO. (B) Embryos that develop in the presence of SERCA inhibitor have grossly disrupted tracheal development. Breaks persist in the dorsal trunk (arrowheads), lateral trunk (arrows), and glial branches (open arrowheads). (C) Washout of SERCA inhibitor at stage 12 and continued development in the absence of drug results in exuberant sprouting and long, wavy tubules (open arrowheads). The overall tracheal structure is vastly recovered, although a break persists in the dorsal trunk (closed arrowhead). (D) Development with the PKC activator alone results in an apparently missing dorsal trunk by lumenal staining but otherwise normal trachea (also see Fig. 4.3. (E) Co-culture with SERCA inhibitor and PKC activator rescues tracheal development. Scale bars=50μm. 2A12 labels tracheal lumen protein, and embryos were imaged with confocal microscopy.

tenuous cell projections between segments (arrow) are commonly seen. In embryos from which the inhibitor was washed out at stage 12 (Fig. 4.3C), fewer segmental gaps (solid arrowhead) are observed, and in general the tracheal structure is more complete. These embryos frequently exhibit hyper-sprouty and long tracheal tubes (open arrowheads). Interestingly, a supernumerary lateral trunk sometimes forms partially or completely as demonstrated here (arrows), and the embryo is slightly larger. These phenotypes suggest compensatory behaviors to recover tracheal distribution following removal of SERCA inhibitor.

Embryos treated with PKC activator alone (Fig. 4.3D) always possess an intact dorsal trunk by *Btl* actin-eGFP labeling. Therefore, the lack of dorsal trunk that is seen in some embryos based on lumen protein staining likely reflects a defect in lumenization or lumen protein secretion. The tracheal structure is normal in embryos treated with PKC activator alone based on the positions of tracheal cells. To further investigate these defects in lumenization that may be occurring as a result of PKC activation, *w; Btl:Gal4, UAS-dsRed-NLS, UAS-actin-eGFP* embryos treated with DMSO or PMA were jointly stained with anti-GFP antibody to label all tracheal cells and the 2A12 antibody to label lumen protein. In Figure 4.4, the first column of panels shows all tracheal cells by eGFP label. The second column shows 2A12 lumen protein staining, and the third column is the merged image. The top row shows control embryos (Fig. 4.4A) with continuous lumenization of the dorsal trunk near the top of the center image and lumenization throughout each of the smaller branches of the developing tracheal network. The panels in row (B) show an example

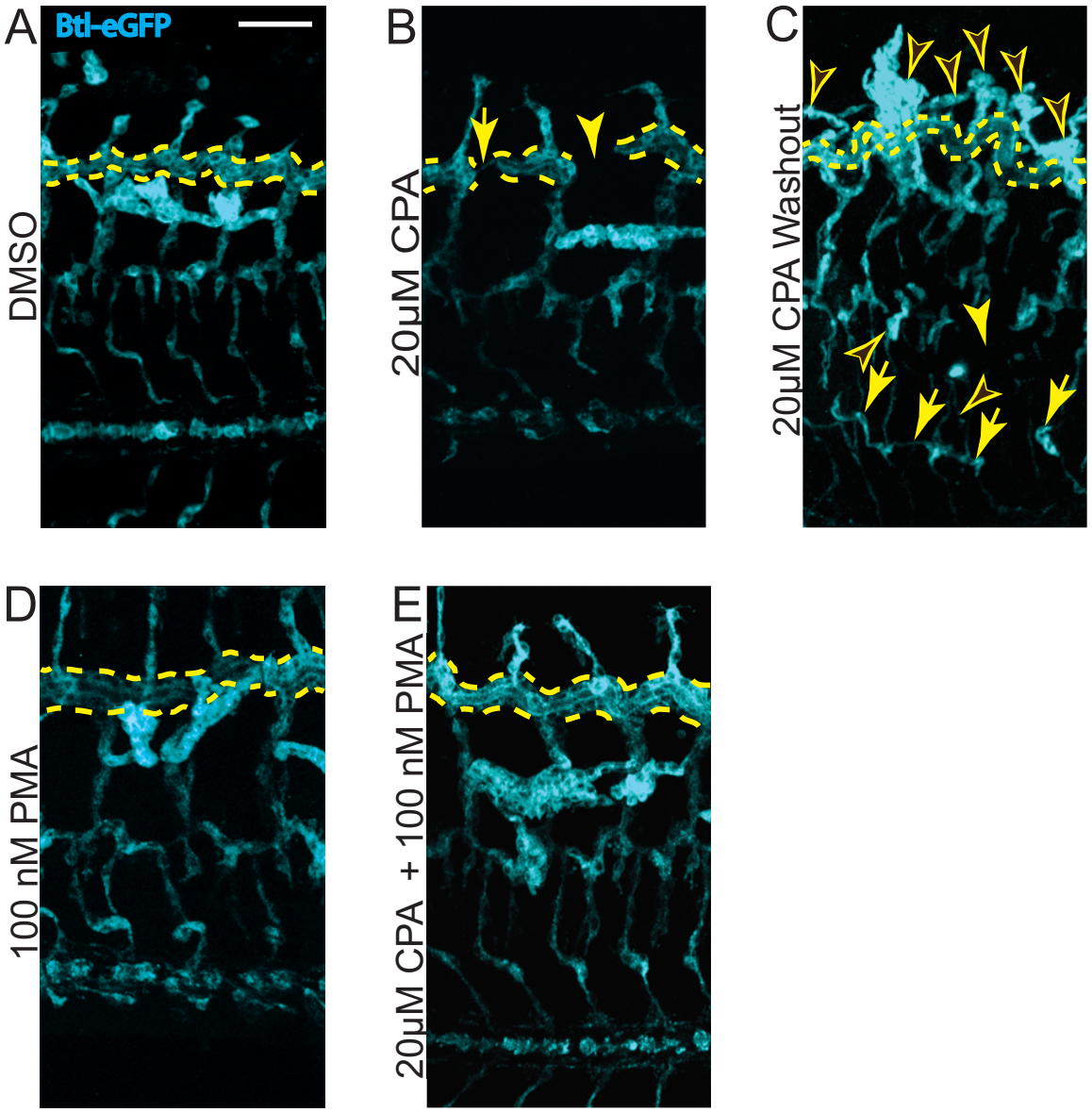

Figure 4.3: PKC activation does not perturb tracheal structure and rescues defects from SERCA inhibition. Tracheal cells are genetically labeled by expression of the tracheal marker *Breathless* (*Btl*) driving eGFP fused to actin. The dorsal trunk is outlined with dotted yellow lines in each panel. (A) Control embryos treated with DMSO. (B) Incubation with SERCA inhibitor results in breaks in the dorsal trunk (arrowhead) and tenuous cytoplasmic connections between segments (arrow). (C) Removal of SERCA inhibitor at stage 12 generally results in fewer gaps (solid arrowhead) but instead an exuberance of sprouting and thickened, wavy tubules (open arrowheads). In some cases, an extranumerary lateral trunk forms partially or completely (arrows). (D) Treatment with the PKC activator alone gives normal tracheal structure based on label of tracheal cells, with continuous dorsal and lateral trunks. (E) Co-treatment with SERCA inhibitor and PKC activator fully rescues tracheal development. Scale bar=50μm throughout.

of an embryo treated with PKC activator where half of the dorsal trunk stains for lumen protein, but the other half does not (dotted yellow lines in center panel). The tracheal cells are clearly present by *Btl* eGFP label, and yet the lumen protein deposition abruptly stops at one of the segments of the dorsal trunk. A lumen is also clearly visible continuing through the dorsal trunk despite the lack of 2A12 labeling (arrowheads in merged panel). Similarly, row (C) shows an example of an embryo in which the dorsal trunk is continuous by *Btl* eGFP labeling (left panel), but there is no lumen staining throughout the entire trunk (center panel, dotted yellow lines). As in example (B), a lumen is clearly visible throughout the trunk (arrowheads in merged panel). Tracheal cell nuclei (yellow) are still positioned normally through these trunks where lumen label is absent, confirming the presence of the cells (Fig. 4.5, arrows).

Thus, PKC activation does not interfere with structural formation of the tracheal network, as evidenced by visualizing *Breathless* expressing cells by actin-eGFP labeling. Likewise, the tubes lumenize; however, there is sometimes a defect in production, secretion, or modification of the chitinous lumenal protein identified by the 2A12 antibody.

Embryos co-incubated with both SERCA inhibitor and PKC activator (Fig. 4.3E) display an astonishingly normal tracheal network with orderly segments and connected trunks. This remarkable finding indicates that in the context of *Drosophila* tracheal development, PKC activation compensates for SERCA inhibition to rescue tracheal development. Interestingly, the lumen protein defect that is often seen in embryos treated with PKC activator alone is less commonly observed in embryos

treated concurrently with SERCA inhibitor and PKC activator. Rebalancing calcium uptake and release must contribute to lumenal maturation. Yet, dual drug treatment does not fully correct the lumen protein defect in all embryos. It is likely that calcium feeds into the secretion or maturation of lumenal proteins.

Rescue of *Drosophila* tracheal development by PKC activation in the background of SERCA inhibition differs from the case of zebrafish intersomitic vascular development, where PKC activation did not rescue. To probe whether rescue could be achieved in another *Drosophila* tissue and whether it might relate to tracheal formation being dependent solely on migration in the absence of proliferation, we investigated the effects of drug treatment on CNS longitudinal tract formation. Like the zebrafish vasculature, formation of these tracts relies primarily on axonal extension but also involves cell proliferation.

Figure 4.6 shows images of the ventral nervecord longitudinal tracts that form bilaterally on either side of the ventral midline in embryos from each of the drug treatment groups. Antibody staining against Fasciclin II labels the longitudinal tracts and motor axons. Controls treated with DMSO (Fig. 4.6A) have three parallel tracts on each side of the midline with segmental peripheral axon projections. Treatment with SERCA inhibitor (Fig. 4.6B) disrupts the parallel bundles and midline barrier. The separation between different bundles is compromised, with merging of multiple tracts or general disorder, as seen in fig. 4.6B. Rather than axons following parallel bundles, random projections can be seen (white arrowheads), and sometimes there are breaks in the tracts. These mutants also often exhibit aberrant midline crossings

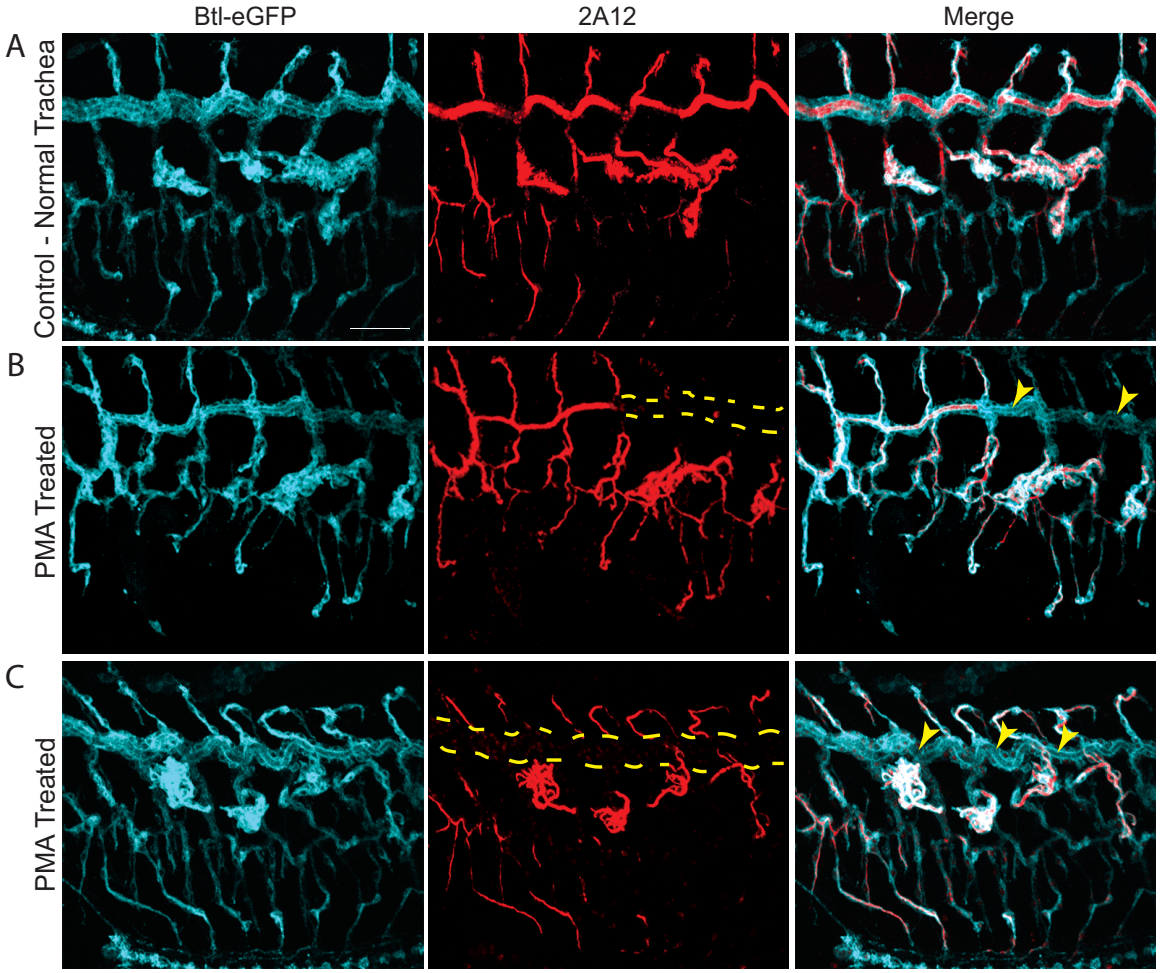

Figure 4.4: Tracheal structure is normal following treatment with PKC activator, but dorsal trunk lumen proteins are affected. Embryos were treated with DMSO (control) or PKC activator (PMA). Tracheal cells are genetically labeled by expression of the tracheal marker *Breathless* (*Btl*) driving eGFP fused to actin (left column, cyan), and stained with the 2A12 antibody against lumen protein (center column, red). The right column shows the merged images. (A) The top row depicts control embryos with continuous lumenization of the dorsal trunk. (B and C) show embryos treated with PKC activator where the dorsal trunk is fully continuous by *Btl* eGFP expression (cyan), but lumen protein label is absent in part or all of the dorsal trunk (dotted yellow outlines). Despite lack of lumen protein label, the trunk is visibly lumenized (yellow arrowheads). Scale bar=50μm throughout.

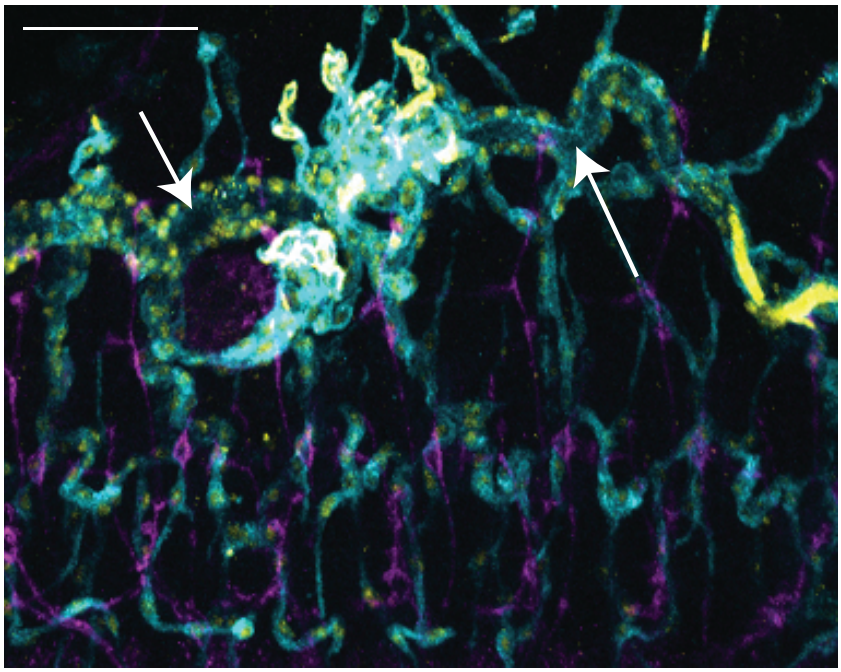

Figure 4.5: The positions of tracheal cells are normal following treatment with PKC activator, but dorsal trunk lumen proteins are affected. Embryos were treated with DMSO (control) or PKC activator (PMA). Tracheal cells are genetically labeled by actin-eGFP (cyan) and nuclear dsRed (yellow spots). Antibody staining with the 2A12 antibody labels lumen protein (yellow lumenal label). FasII-positive nerves are labeled in purple. The dorsal trunk is fully continuous by *Btl* eGFP expression (cyan), and where lumen protein label is absent in part of the dorsal trunk, the cell nuclei (yellow spots) are still present and normally distributed (white arrows). Scale bar=50μm.

and merging of the bilateral tracts at the midline (red arrowheads).

In embryos from which the SERCA inhibitor has been removed at stage 12 (Fig. 4.6C), the CNS longitudinal tracts are vastly normalized, although sometimes the spacing between the bundles is a bit wider than in controls. This may reflect increased expression of Robo receptors or Slit to repel axons further from the midline. During tracheal development, removal of SERCA inhibitor resulted in an over-compensatory sproutiness. In the case of neural development, if inhibition of SERCA can cause abnormal midline crossings and mergings at the midline as observed, then removal of the inhibitor may result in transient over-compensation and slight over-repulsion of axons from the midline. This could explain the slightly wide tract spacing.

In comparison, treatment of embryos with PKA activator gives normal CNS longitudinal tracts and FasII-positive axons (Fig. 4.6D). The axon bundles are parallel with more or less normal spacing. In embryos treated with the combination of SERCA inhibitor and PKC activator (Fig. 4.6E), the longitudinal tracts again are normal. Therefore, co-activation of PKC concomitant with SERCA inhibition rescues *Drosophila* CNS nervecord development just as it rescues tracheal development. These results indicate that the rescue of SERCA blockade by PKC operates in contexts that involve cell proliferation and not exclusively cell migration. The difference in rescue is more likely organism-dependent, perhaps with different PKC isoforms that are differentially expressed between zebrafish and *Drosophila*. Regardless, the rescue of SERCA blockade by PKC in both *Drosophila* neural and tracheal development demonstrates that PKC-dependent SERCA regulates cell migration and can do so in

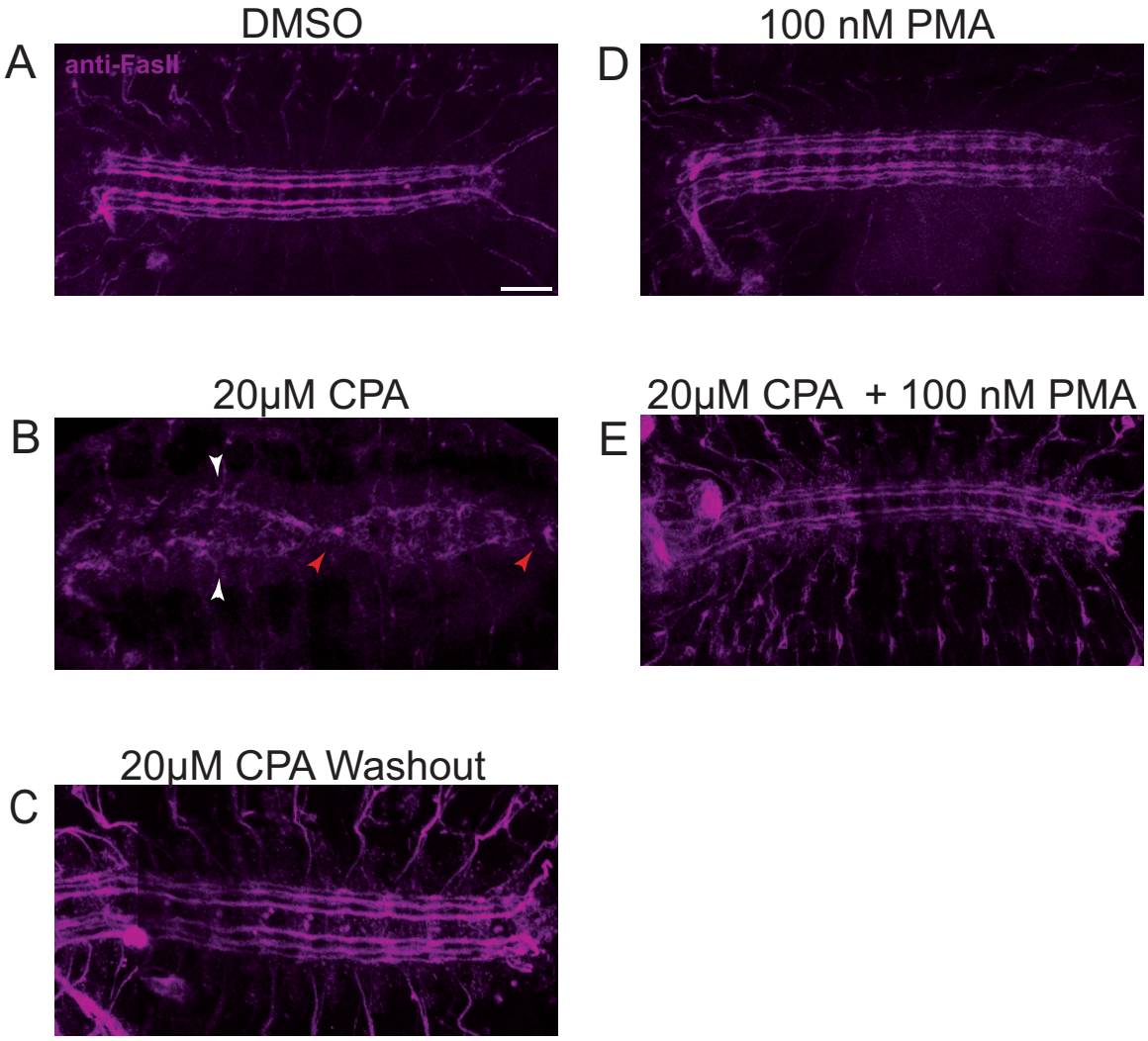

Figure 4.6: PKC activation in the background of SERCA inhibition rescues CNS neural development. CNS longitudinal tracts and some peripheral axons are labeled by FasII expression in permeabilized embryos treated with or without drug. (A) Control embryos have normal longitudinal axons and peripheral projections. (B) In embryos treated with SERCA inhibitor, the parallel axon bundles are disarrayed and frequently merged with random axon projections rather than parallel order (white arrowheads). Aberrant midline crossing and merging of bilateral tracts often occurs (red arrowheads). (C) Washout of SERCA inhibitor at stage 12 vastly normalizes the CNS tracts, although their spacing is sometimes slightly wider than normal. (D) Incubation with PKC activator gives normal CNS longitudinal axons. (D) Co-incubation with SERCA inhibitor and PKC activator rescues CNS longitudinal axon tracts. Scale bar=50μm throughout.

the context of cell proliferation. SERCA can also modulate cell proliferation, but its dominant role appears to be regulation of cell migration (data not shown).

To quantify the severity of *Drosophila* tracheal and neural perturbation and rescue, phenotypes were categorized as normal, moderate, or severe (Fig. 4.7). To be considered normal, an embryo had to have normal tracheal and neural structure, as depicted in the left-hand panels (Fig. 4.7A). The embryo was classified by the most severe phenotype it exhibited. A moderate phenotype was one with complete tracheal or neural structure but slight disorder, exuberant sprouting, or excessively wavy branches (Fig. 4.7B). A severe phenotype was one with overt breaks, missing sections, fused longitudinal tracts or midline crossings, or generally severe disorder (Fig. 4.7C).

Figure 4.8 plots the distributions of phenotype severity for each treatment group. At least 70 embryos were counted per treatment. The embryos that were permeabilized and treated with DMSO (control) are mostly normal (89%). Inhibition of SERCA results in a severe phenotype in 86% of embryos, with only a few percent that look normal. Washout of SERCA inhibitor at stage 12 significantly normalizes tracheal and neural development, with 28% being normal, 36% having a moderate phenotype, and 36% severe. Co-incubation with PKC activator and SERCA inhibitor gives 68% of embryos with normal nerves and trachea, 25% with a moderate phenotype, and just 7% with a severe phenotype. A p value of less than 0.001 by Chi-square analysis distinguishes the washout and CPA+PMA rescue from the CPA-treated embryos, with PKC activation coincident with SERCA inhibition producing

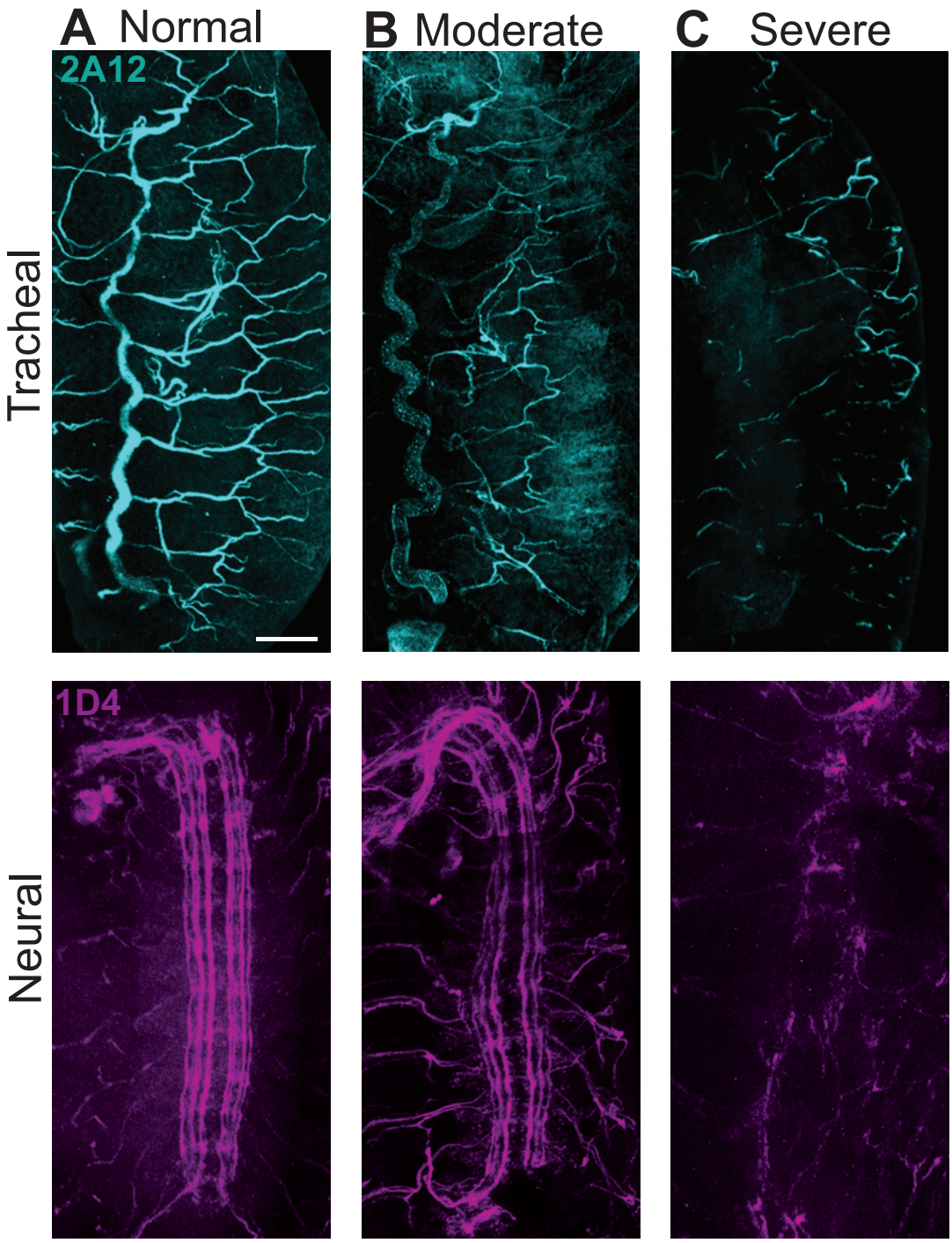

Figure 4.7: Classification of *Drosophila* tracheal and neural phenotypes. Embryos were categorized by the most severe phenotype they exhibited. (A) Embryos with normal tracheal and neural structure as depicted were classified as normal. (B) A moderate phenotype was one in which the trachea had exuberant sprouting, wavy tubes, or slight disorder, or the neural longitudinal bundles were slightly disordered. (C) A severe phenotype was one with overt breaks in the trachea or longitudinal fascicles, severe disorder and missing segments, or merged tracts and aberrant midline crossings. Scale bar=50μm throughout.

the most substantial rescue. For additional examples of the phenotypes observed, see Figs. B.1 and B.2.

Inhibition of the SERCA pump is expected to operate cell-autonomously whereby the functions of cells that take up the inhibitor would be perturbed. However, perturbations of individual cells can have an effect on neighboring cells. To assess whether defects in FasII-positive neurons or the trachea affected the other or if the perturbations were mostly occurring independently of the other in each cell type, *Btl* eGFP tracheal cells and FasII-positive cells were stained in fillet preparations. Figure 4.9A shows an example where SERCA inhibition resulted in breaks in the dorsal tracheal trunk. Arrows in the top panel indicate a gap and a section with a thin connection between trunk segments. The middle panel shows that the nerves are normal, and it is apparent in the merged image that the peripheral neural axons still properly project to the segments with disrupted trachea. Similarly, Figure 4.9B shows an example where the tracheal structure is normal but there is a midline crossing of the longitudinal fascicles (arrow in middle panel). The tracheal cells are still properly located along the longitudinal tracts (merge). These results are consistent with the tracheal and neural disruptions arising in a cell-autonomous manner in cells affected by the inhibitor. Nevertheless, in severe cases it is still likely that disruptions of one cell type cause perturbations of nearby interacting tissues. Targeted disruption in specific cell types and analysis of many different tissues would be required to definitively assess how disruptions in SERCA activity in one cell type affect neighboring tissues.

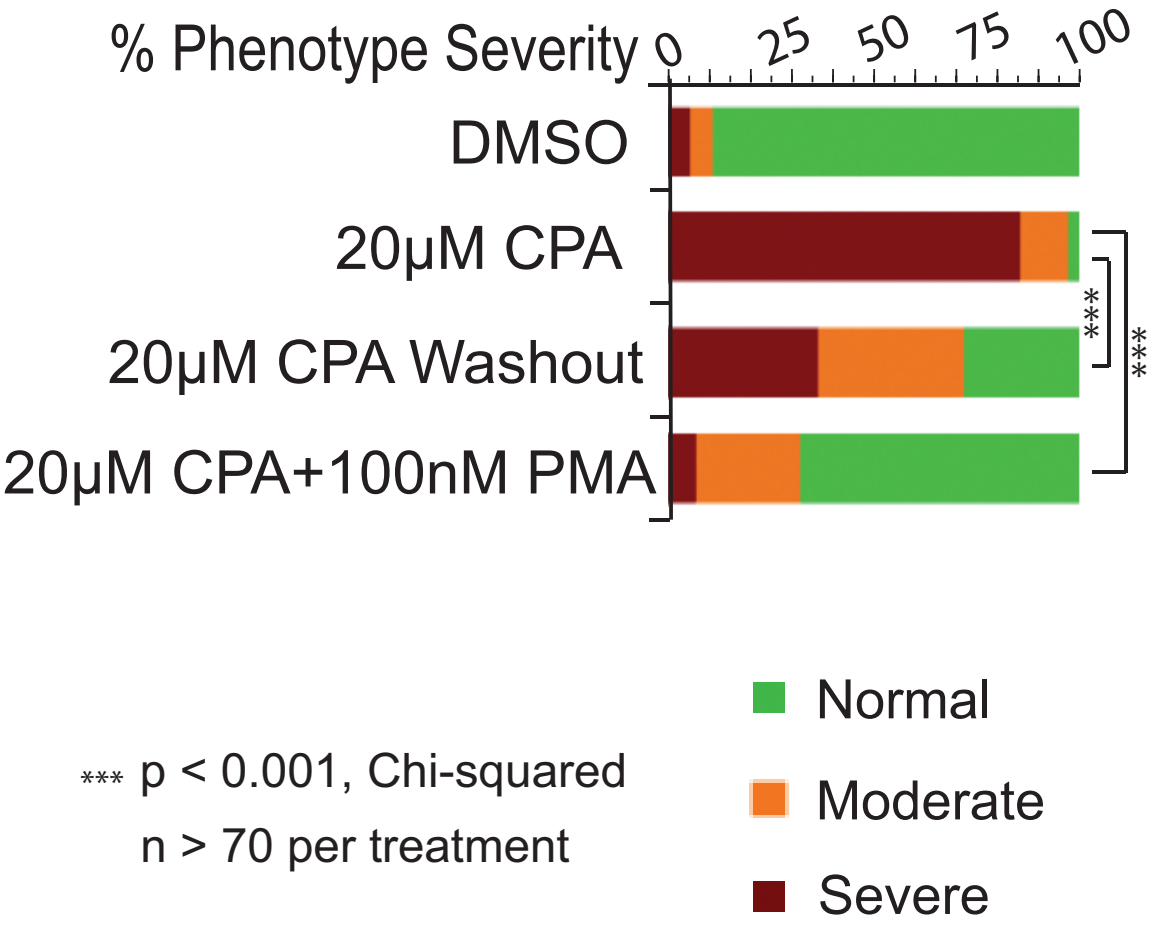

Figure 4.8: Quantification of *Drosophila* tracheal and neural phenotypes demonstrates the most significant rescue by SERCA inhibition by PKC activation. Embryos were categorized by the most severe phenotype they exhibited. In controls that were permeabilized and treated with DMSO, 89% of embryos have both normal trachea and nerves and 5.6% have a severe disruption. In contrast, 86% of embryos treated with SERCA inhibitor display a severe neural or tracheal phenotype, with only 2.6% being normal. Washout of SERCA inhibitor at stage 12 normalizes 28% of embryos, leaving 36% with a moderate phenotype and 36% with a severe phenotype. Co-treatment with PKC activator and SERCA inhibitor results in 68% of embryos having normal trachea and nerves, 25% with a moderate phenotype, and only 7% with a severe phenotype. The washout and dual drug treatment rescue are statistically significant to less than 0.001 by Chi-square analysis, with PKC activator in the background of SERCA inhibition producing the most substantial recovery.

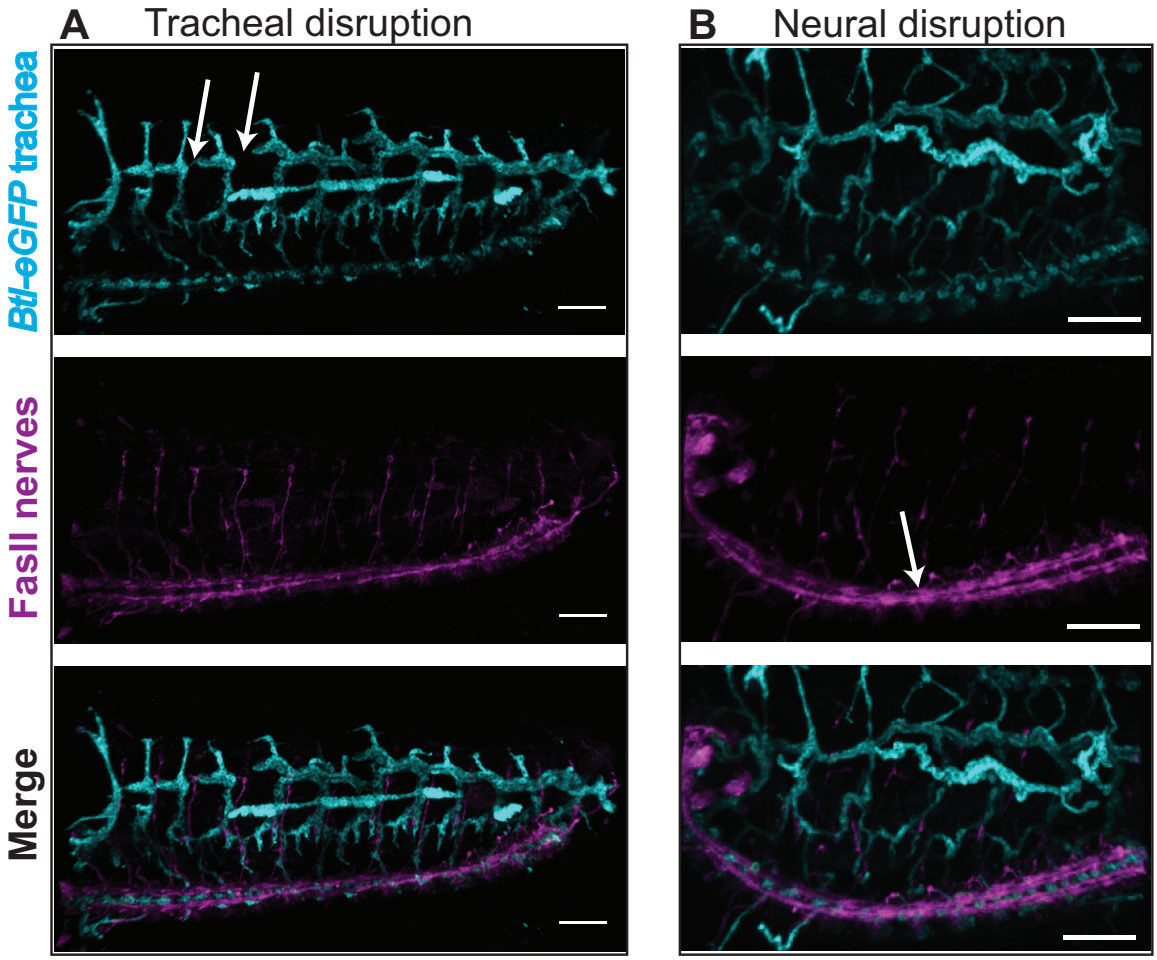

Figure 4.9: Perturbations in trachea and nerves arise independently. Tracheal cells and FasII-positive nerves were labeled to determine whether tracheal and neural defects coincided or tended to occur independently. The top panel depicts *Btl* eGFP tracheal cells in fillet preparations; the middle panel shows FasII-positive nerves, and the bottom is the merged image. (A) shows an example of an embryo with gaps in the dorsal tracheal trunk (arrows) but normal nerve structure and segmental axon projections despite the tracheal breaks (merge). (B) shows an example of an embryo with normal tracheal structure but a midline crossing of longitudinal fascicles (arrow). The tracheal cells are still properly located along the nerve tracts (merge). Scale bars=50μm.

4.1 Summary

Treatment of *Drosophila* embryos with SERCA inhibitor demonstrates that blockade of SERCA activity disrupts tracheal and neural development. Formation of the tracheal system occurs entirely by cell migration following the complete cessation of cell proliferation, and inhibition of SERCA disrupts the proper patterning of the trachea, resulting in segmental gaps, broken trunks, or severe fragmentation of tubes. Likewise, SERCA inhibition during neural development manifests with breaks in the longitudinal connectives, improper tract mergings, and structural disorder indicative of perturbed pathfinding or migration. These tracheal and neural effects are ameliorated upon removal of inhibitor, although defects persist. Inhibitor washout also frequently results in a phenotype of exuberant sprouting of tracheal tips and elongated tubes. In contrast, simultaneous treatment of embryos with SERCA inhibitor and PKC activator substantially rescues tracheal and neural development. Based on these results, dynamic analysis of cell migration during non-proliferative tracheal development is necessary to confirm that migratory defects account for the observed phenotypes.

Chapter 5

SERCA inhibition disrupts cell migration

Results from inhibition of the SERCA pump in zebrafish vascular growth and *Drosophila* tracheal and neural development implicate SERCA in regulating cell migration. Dynamic imaging and analysis of embryonic *Drosophila* tracheal development was used to ascertain whether disrupted cell migration explains the phenotypes observed with SERCA blockade. This system excludes any contributing effects on cell proliferation since the embryonic tracheal network assembles in the absence of cell division.

Transgenic w; Btl:Gal4, UAS-dsRed-NLS, UAS-actinGFP flies label all tracheal cells with GFP-tagged actin and nuclear dsRed fluorophore. Therefore, the cytoskeleton and nuclei of the cells can be spectrally distinguished and followed over time. Three embryos per group were treated with DMSO (control) or SERCA inhibitor (CPA) and dynamically imaged with confocal microscopy. Every 3 to 3.5 minutes, a stack of images was collected to follow tracheal development on one side of the embryo. Individual lateral trunk cells were tracked based on the positions of their nuclei from approximately stage 14 to early stage 16, during which time the lateral

trunk should fuse across adjacent segments.

Figure 5.1 shows three timepoints during lateral trunk development in control embryos that were permeabilized and treated with DMSO. Figure 5.1A shows the embryo at the beginning of this time period, and the white dots mark the nuclei of opposing cells in neighboring segments that must meet to form a continuous trunk. Panel B depicts the embryo 35 minutes later. The cells in neighboring segments have migrated towards each other. The dragon tails on each spot indicate each cell's path over the previous 10 timepoints, and they show how the pairs of cells are moving towards each other. In Figure 5.1C, the neighboring cells are closer together still, and the lateral trunk is becoming a continuous structure.

In comparison, an embryo that was permeabilized and treated with SERCA inhibitor and imaged over the same period of development is shown in Figure 5.2. Cells were tracked on both sides of affected segments where lateral trunk fusion fails to occur. Over the timecourse from Figure 5.2A through C, the cells in opposing segments move more or less parallel to each other, being carried along with the outward expansion of the tissue as the embryo develops. Unlike in the control, the cells do not converge with their neighbors, and the lateral trunk remains discontinuous. A gap in the dorsal trunk also persists even as the rest of the trunk lumenizes, indicating that those cells are likewise affected by the inhibitor. Some of the lateral trunk segments do, fuse, however. This is consistent with SERCA acting in a cell-autonomous manner to direct individual cell behaviors.

The paths of migration and overall displacement of the tracked lateral trunk cells

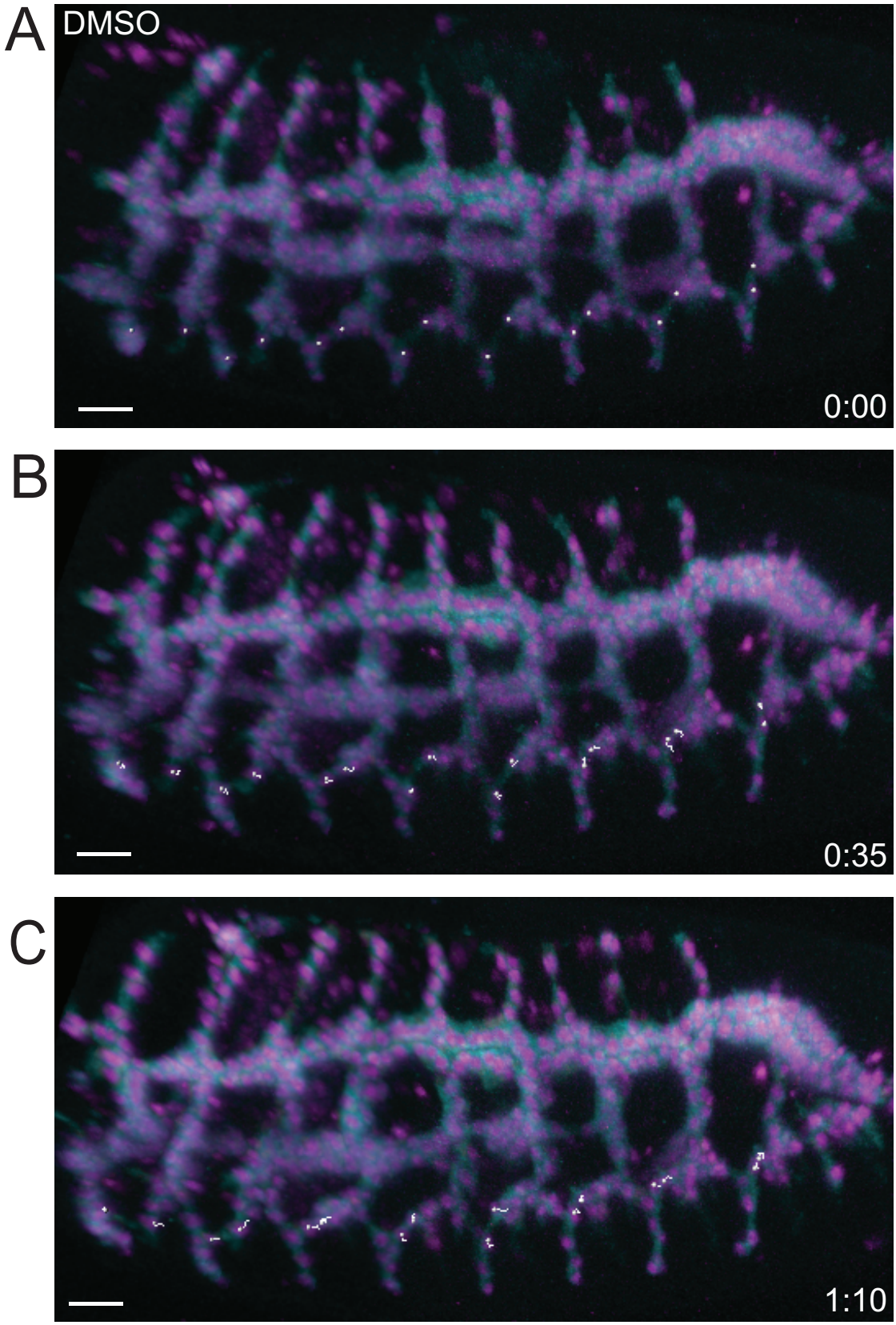

Figure 5.1: Caption next page.

Figure 5.1: In control embryos, tracheal cells in adjacent segments migrate towards each other to form the lateral trunk. Live *Drosophila* embryos with fluorescently labeled tracheal cells were imaged with confocal microscopy to trace cell movements over time in controls treated with DMSO. (A) shows the embryo at stage 14 when the lateral trunk is beginning to form. White spots mark the positions of cell nuclei over time in adjacent segments that fuse to form the continuous trunk. The lower panels show timepoints 35 minutes (B) and 70 minutes (C) later as the trunk is fusing. Dragon tails on the spots depict the cells' movements over the previous 10 timepoints. Over the timecourse, the opposing cells in the lateral trunk of adjacent segments move closer together, and a continuous lateral trunk forms. Scale bars=20μm. Actin cytoskeleton is cyan and nuclei are magenta.

in the control and SERCA-inhibited embryo are compared in Figure 5.3. In each case, the squiggly path traces the migration route of the tracked cell nucleus. The path progresses from yellow to orange to red over the timecourse. White arrows indicate the overall displacement of each cell nucleus. It is clear by the converging pairs of displacement arrows that in the control (Fig. 5.3A), lateral trunk cells from adjacent segments move towards each other and meet. They fuse to form an uninterrupted lateral trunk. This is contrary to two of the segments of the SERCA-inhibited embryo (B), where the displacement arrows for cells in opposing segments are more or less parallel to each other. These cells are passively moving with tissue expansion but are not substantially narrowing the distances between them. The result is discontinuities in the lateral trunk between these affected segments. A break in the dorsal trunk is also evident, despite lumenization of the trunk on either side. These breaks persist through the remainder of the embryo's development. At the same time, cells from some of the segments do converge to form a fused lateral trunk between them. It is likely that SERCA is not sufficiently inhibited in these individual cells to disrupt their migration.

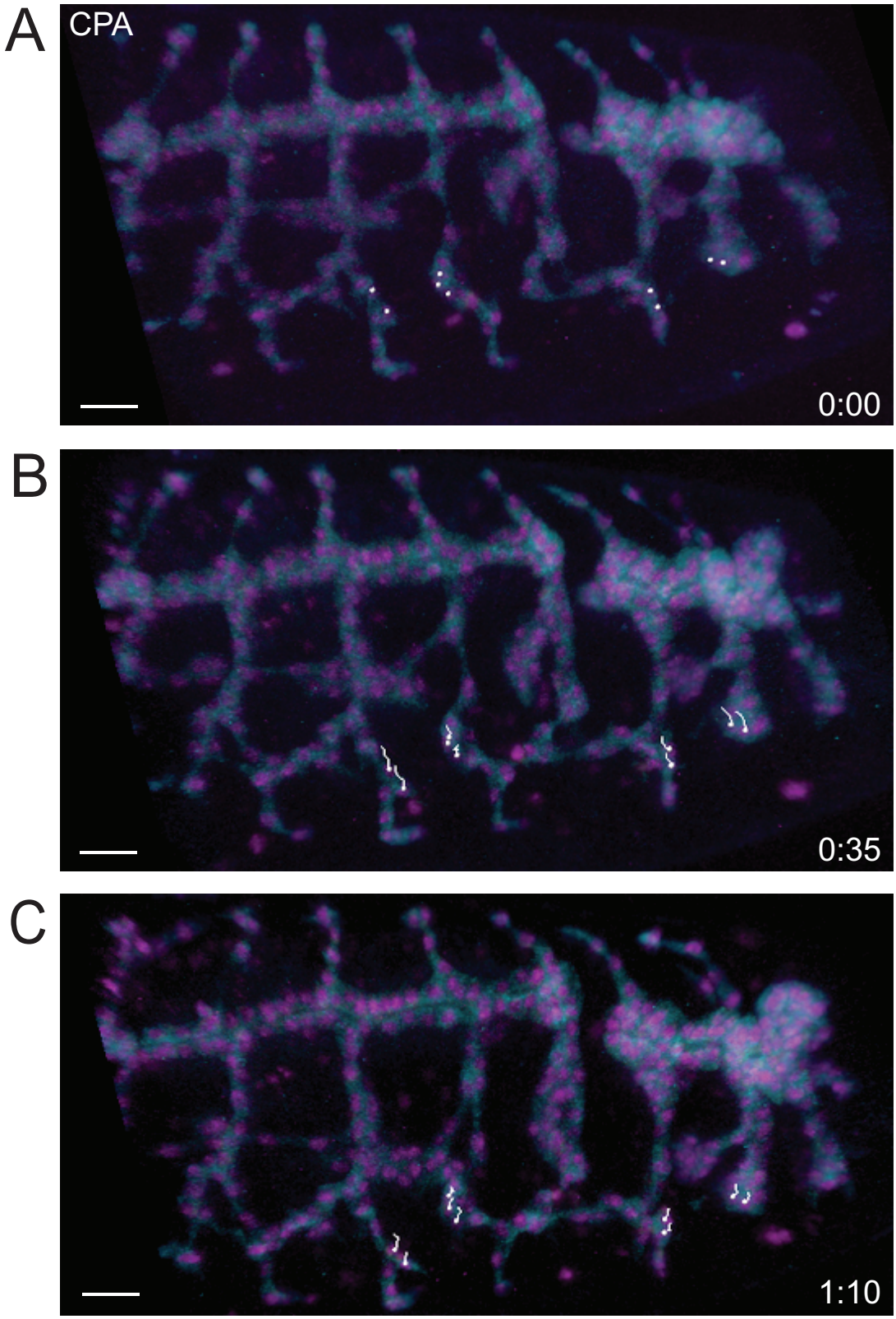

Figure 5.2: Caption next page.

Figure 5.2: When SERCA is inhibited, tracheal cells destined to form the lateral trunk do not converge, leaving discontinuities. Live transgenic *Drosophila* embryos were treated with SERCA inhibitor, and tracheal development was imaged dynamically with confocal microscopy. (A) depicts the tracheal structure at approximately stage 14. White spots mark the nuclei of cells on opposing sections of trachea that should converge to form the lateral trunk. Dragon tails in (B) and (C) trace the path of the cells over the prior 10 timepoints. The panels at 35 minutes (B) and 70 minutes (C) demonstrate that these cells move more or less parallel to each other with overall tissue expansion, rather than converging. Some segments do connect, whereas the cells that are sufficiently affected by SERCA inhibition fail to migrate. Scale bars=20μm. Actin cytoskeleton is cyan and nuclei are magenta.

To quantify the migration defect in embryos treated with SERCA inhibitor, the relative convergence of neighboring cells in adjacent segments was determined. The three-dimensional position of each tracked cell at the start and end of the time period were exported to MATLAB, and the angle of convergence or divergence formed by the displacement vectors for each pair of cells was calculated. Throughout this time, passive movement from overall embryo development is pushing tracheal cells in different directions and by different amounts at different positions in the tracheal tree. It is therefore difficult to remove this passive motion without inadvertently altering the movement that is attributed to cells as active migration. Simply measuring speed of overall movement is also not informative because of this passive motion. For this reason, we calculated the migration of one cell relative to its partner to negate any contribution from passive motion.

Figure 5.4A plots the vectors of directional movement of one cell in each pair relative to its partner. Arrows pointing to the right indicate the angle of convergence of the pair of cells, while arrows pointing left indicate the angle of divergence. The vertical line references parallel movement. Red arrows represent the relative migration

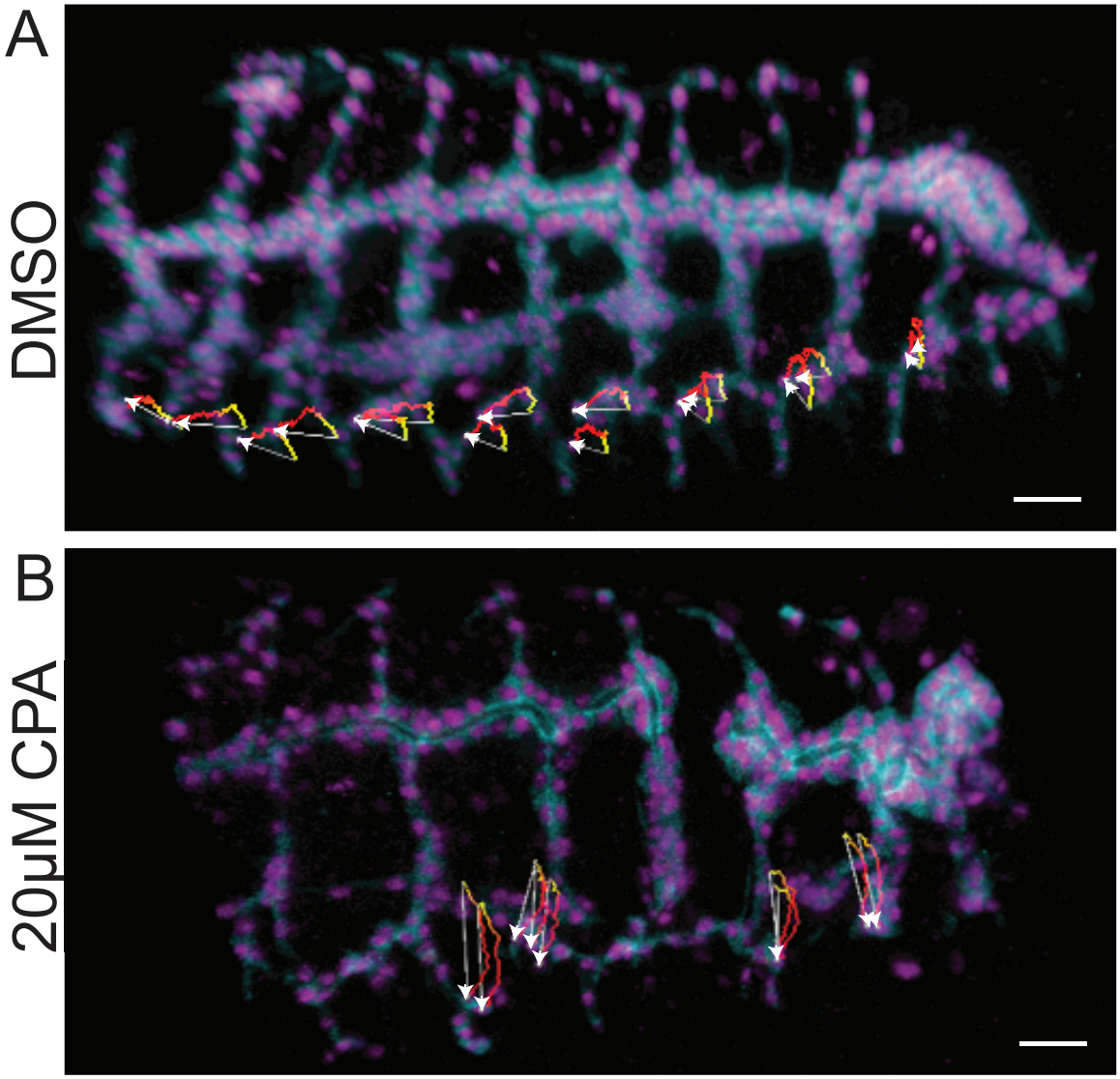

Figure 5.3: Tracking individual cells through a dynamic timeseries shows that cells migrate convergently to form a trunk in controls but drift in parallel when SERCA is inhibited, leaving structural gaps. Overall migration paths and total displacements of tracheal cells tracked during the formation of the lateral trunk are shown for DMSO-treated controls (A) and embryos treated with SERCA inhibitor (B). The yellow-to-red traces map the positions of the individual cell nuclei during the timecourse. In controls (A), the cell displacement arrows illustrate the convergence of cells from adjacent segments to form the continuous lateral trunk. In contrast, with SERCA inhibition (B), the displacements of cells in neighboring segments are approximately in parallel directions, and the lateral trunk remains broken through the remainder of the embryo's development. Scale bars=20μm. Actin cytoskeleton is cyan and nuclei are magenta.

of pairs of cells from embryos treated with SERCA inhibitor, and black arrows represent pairs of cells from DMSO-treated control embryos. The thick arrows represent the median for each treatment group. Pairs of cells from control embryos converge at a median angle of 31 degrees. This convergence is expected as the cells from adjacent segments must move together in order to form a continuous lateral trunk. In contrast, pairs of cells from affected segments of SERCA-inhibited embryos do not migrate towards each other, but instead have a median divergence of 9 degrees.

The difference in migratory behavior between control and SERCA-inhibited embryos is also apparent by calculating the actual amount that cells from adjacent segments move closer together. Pairs of cells from control embryos reduce the starting separation between them by an average of 58% during the measured time period, while cells from embryos treated with SERCA inhibitor on average increase their separation by 5% (Fig. 5.4B). Thus, individual cells fail to migrate properly when the SERCA pump is blocked, and this results in the breaks in the tracheal network that characterize these mutants.

To gain more insight into specific migratory behaviors that are affected in cells with sufficiently inhibited SERCA, we looked more closely at tracheal cells on either side of a gap in the dorsal trunk. Cell migration entails active protrusion of the cytoskeleton, and this might be absent in cells affected by SERCA inhibitor. The panels in figure 5.5 show snapshots from consecutive timepoints every 3.5 minutes in a timeseries of a live embryo treated with SERCA inhibitor. A gap in the dorsal trunk is evident (Fig. 5.5A, space occupied by white arrow). The cell on the right side

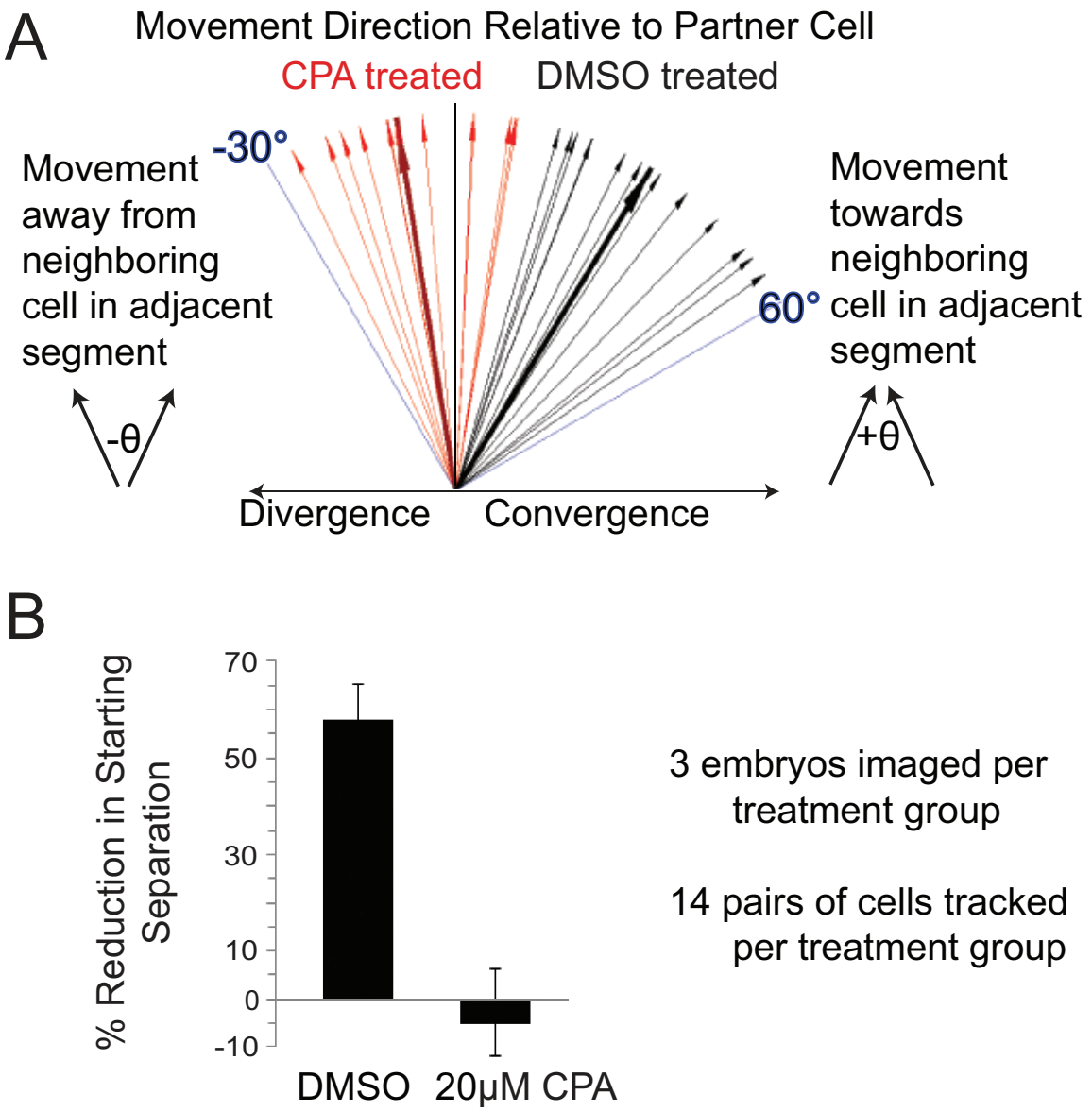

Figure 5.4: Cells in neighboring segments that form the lateral tracheal trunk actively migrate towards each other in control embryos but fail to migrate when affected by SERCA inhibitor. The displacement vector for each tracked cell was determined from the positions of cell nuclei at stage 14 before lateral trunk formation and at the end of the time period of study. (A) The angle of convergence or divergence was calculated for each pair of cells that should join to form the lateral trunk. The vectors of directional movement of one cell in each pair relative to its partner are plotted for controls (black) and SERCA-inhibited embryos (red). In controls, pairs of cells converge between neighboring segments, at a median angle of 31 degrees, while pairs of cells in CPA-treated embryos do not move towards each other, but rather diverge at a median angle of 9 degrees. (B) The start and end separation between the pairs of cells was calculated for each treatment group. In controls, cells in adjacent segments of the lateral trunk reduce the separation between them by 58% on average, while in SERCA-inhibited embryos, the separation increases by 5% on average.

of the gap is extending a cytoskeletal projection that is visible by actin labeling in cyan (white arrow). On the contrary, the opposing cell on the other side of the gap is not reciprocating (red arrow). Through the timecourse, the cell on the right appears to actively search the space for a partner as it extends the cytoskeletal projection (Fig. 5.5A-L). However, the opposing cell does not participate, and through the end of embryonic development of this embryo, the gap in the trunk persists.

Interestingly, cells within the dorsal branch of these segments (Fig. 5.5A, yellow arrow) interact with each other. A cell in the left branch which is not at the tip responds to the tip cell of the branch on the right and extends towards it (Fig. 5.5F, yellow arrow). In panel G they fuse with each other. These branches would normally fuse with dorsal branches extending from the contralateral side of the embryo, and the tip cell on the left branch seems to still be searching for a contralateral partner (Fig. 5.5J,L, green arrows). The gap in the dorsal trunk between these ipsilateral segments may somehow be leading them to fuse with each other as well. Perhaps this helps to balance tension from lumenal fluid pressure or some other property of the tubes. Both of the cells from these dorsal branches appear to be actively engaged in the interaction to create this fusion, while in the dorsal trunk, the cell on one side is not participating to close the gap. The defect in extending cytoskeletal projections is likely analogous to the branching defect observed in zebrafish endothelial cells, where fewer cytoplasmic projections were seen.

To definitively know whether SERCA is inhibited in both of these cells on either side of the gap or just in the quiescent cell on the left, and what the calcium

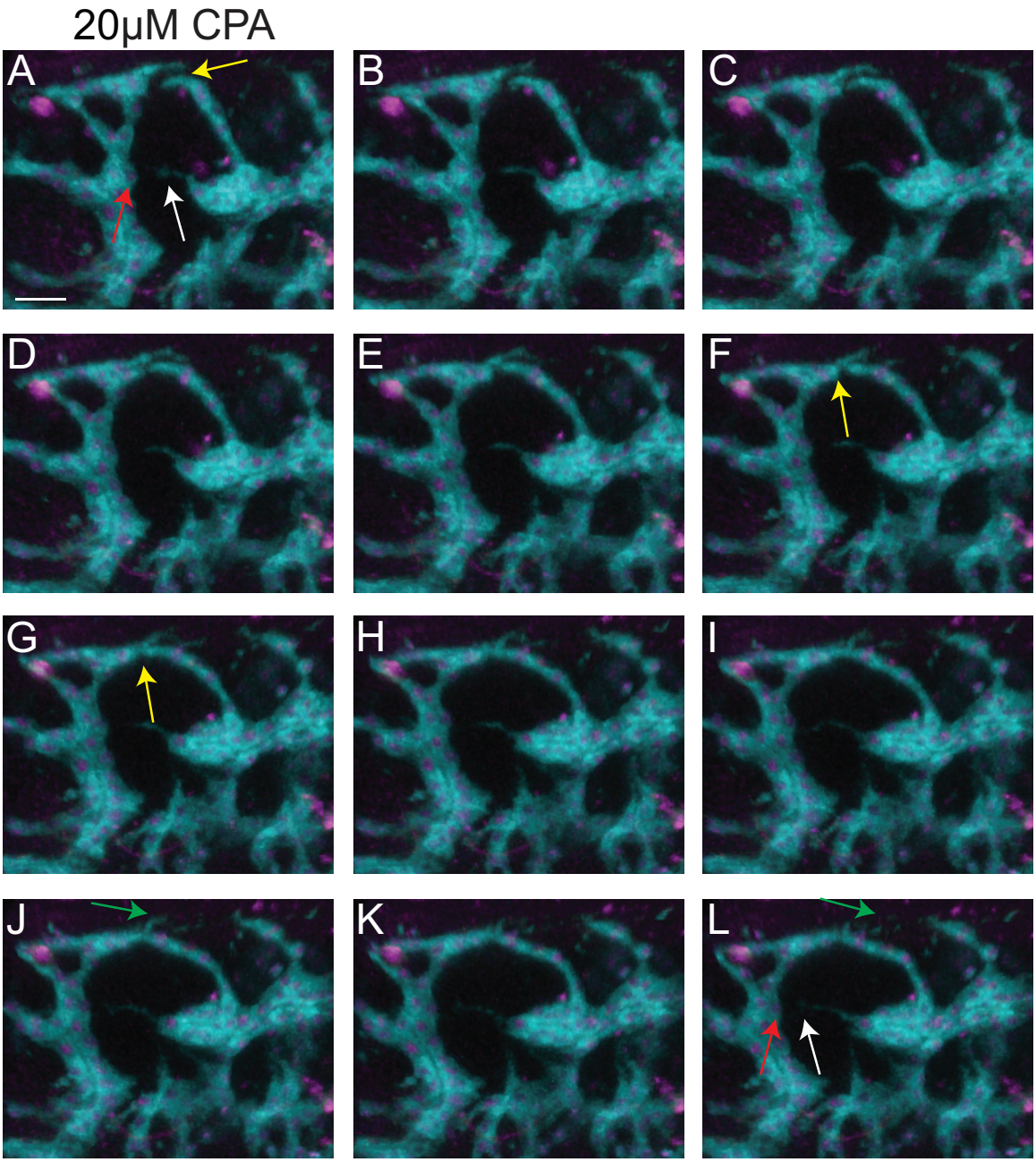

Figure 5.5: Active cytoskeletal dynamics are lacking where gaps remain in the tracheal network. The panels are from consecutive timepoints every 3.5 minutes from a timelapse of tracheal cells in an embryo treated with SERCA inhibitor. (A) At a gap in the dorsal trunk, the cell on the right extends a cytoplasmic projection towards the adjacent segment (white arrow), but the partner in that segment does not respond (red arrow). (A-L) Through the timecourse, the cell on the right continues to search, but the cell on the left does not reciprocate, and the gap persists. The yellow arrow in (A) points to cells in neighboring dorsal branches that extend projections towards each other (F, yellow arrow), and in (G) they fuse. These branches normally fuse with contralateral dorsal branches. (J,L) The left dorsal branch tip cell may still be extending towards a contralateral partner (green arrows). Scale bar=20μm.

signature is that instructs cells to migrate, it is necessary to look at the actual calcium dynamics of individual cells. The interplay between IP3-mediated release of calcium from the ER and calcium sequestration by the SERCA pump could be establishing an oscillating dynamic of calcium within the cell, or periodic spikes, or steady state calcium levels. Specific patterns of calcium activity could drive cytoskeletal rearrangements or other behaviors for cell motility. The GCamp3 calcium indicator permits visualization of dynamic calcium activity because it fluoresces upon binding to calcium, so the intensity of fluorescence can be used to quantify the relative amount of calcium present in the cell cytoplasm.

Drosophila embryos with Btl driving expression of GCamp3 only in tracheal cells (Btl-Gal4, UAS-GCamp3/CyO) were imaged with 2-photon light sheet microscopy to analyze the dynamics of calcium in individual cells during tracheal development. With light sheet microscopy, or selective plane illumination microscopy (SPIM), a thin sheet of light is generated to illuminate an entire plane of the sample rather than raster scanning a point focus across the two-dimensional plane. The entire plane is imaged simultaneously with a camera. Only the plane of focus is illuminated, so there is no out-of-focus fluorescence that must be excluded. The technique affords a time resolution on the order of milliseconds to capture an image, which is about 30 times faster than using conventional confocal microscopy. The time resolution of the light sheet microscope is sufficient to capture changes in calcium dynamics, and preliminary imaging demonstrates a calcium spiking behavior in tracheal epithelial cells (Fig. 5.6A-C). Dramatic calcium spikes are observed throughout the tracheal

system in embryos at stage 15 to 16, and they propagate through adjacent cells as the cells become electrically coupled. At stages 15 to 16, the individual spikes last on average 20-30 seconds within an individual cell and exhibit a definitive spike shape (Fig. 5.6D).

Preliminary analysis of the calcium dynamics of individual cells in controls reveals an oscillatory pattern of calcium activity in cells of the lateral trunk which are migrating to form a continuous trunk (Fig. 5.6E, arrows). Figure 5.6F depicts the intensity profile over time for one of these cells, which shows oscillations in calcium levels by GCamp3 fluorescence. In embryos treated with SERCA inhibitor, these oscillations are absent (Fig. 5.6G, H). Further analysis of controls, SERCA-inhibited embryos, and embryos treated with the combination of SERCA inhibitor and PKC activator should clarify the precise calcium activity that drives cell migration and that is absent in SERCA-inhibited embryos.

5.1 Summary

In summary, dynamic imaging of embryonic *Drosophila* tracheal development demonstrates that the migration of cells is indeed affected in embryos treated with SERCA inhibitor. This migration problem accounts for the observed defects in tracheal development. Each defect is a manifestation of individual cells being affected by the drug and failing to migrate, leaving gaps in the tracheal network. A failure to mobilize the cytoskeleton and extend cytoskeletal projections may characterize these cells. Dynamic imaging of the calcium dynamics of individual cells reveals dramatic

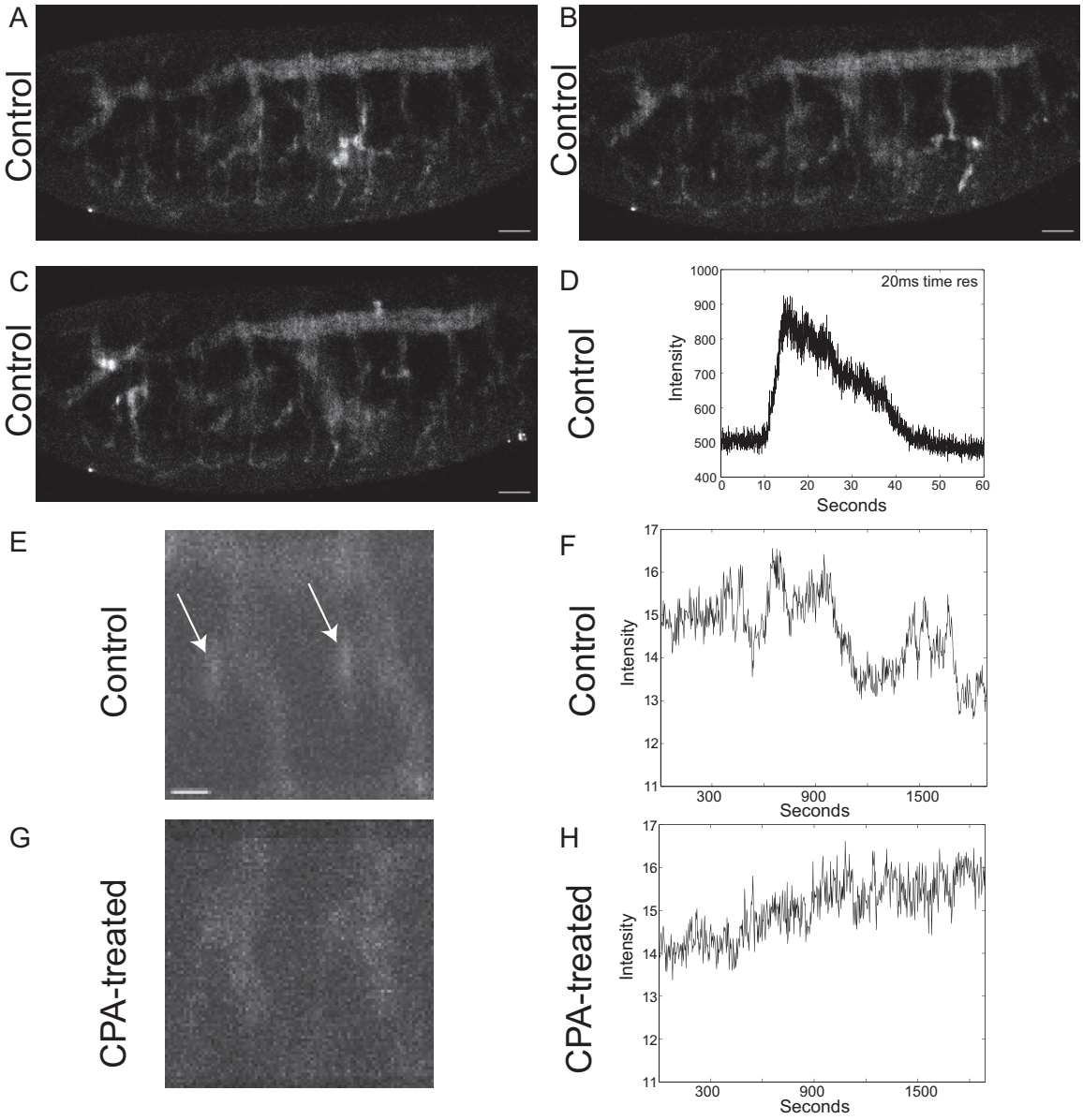

Figure 5.6: Tracheal cells exhibit an active calcium spiking behavior. (A–C) Z-stack projections at individual timepoints of control embryos expressing GCamp3 in tracheal cells reveal calcium spikes that propagate through electrically coupled cells. Different cells are spiking in each image, demonstrating activity across the tracheal network. (D) An example intensity profile of a spiking cell with 20ms time resolution shows the typical shape and duration of these spikes, which on average last 20-30 seconds. (E,G) Zoomed-in views of Z-stack projections of the cells destined to form the lateral trunk in control (E) and SERCA-inhibited (G) embryos show calcium activity in the migrating control cells (E, arrows) that is absent in the non-migratory cells of the CPA-treated embryo (G) that fail to form the lateral trunk. (F,H) Intensity profiles of these cells reveal calcium oscillations in the control cells but not in the SERCA-inhibited cells. Scale bars in A—C=50μm. Scale bar for E, G=10μm.

calcium spiking activity and should elucidate the precise signature of calcium activity that directs cell motility in normal cells based on a lack of that dynamic in cells that fail to migrate.

Chapter 6

Conclusions and discussion

Inhibition of the SERCA pump during zebrafish vascular development and *Drosophila* tracheal and neural development impedes proper outgrowth and structural formation consistent with defects in cell migration. Zebrafish intersomitic vessels remain shorter and less branched; *Drosophila* trachea and nerves exhibit breaks, aberrant fusions, and disorder. These phenotypes could result from disruption of various cell behaviors, such as cell migration, shape change, or cell adhesion. The *Drosophila* tracheal network forms in the absence of proliferation and as such is a useful system for dissecting the role of SERCA activity for cell migration without contributions from proliferation.

6.1 Tracheal structural determinants

Tracheal tube shape is determined by genetic specification as well as cell polarization and lumenization. Signaling molecules encoded by *decapentaplegic* (DPP) and epidermal growth factor (EGF) and their downstream transcription factors, *knirps* and *spalt*, respectively, are important for specifying tracheal branch identity and migration (*Affolter et al.*, 1994; *Beitel and Krasnow*, 2000; *Chen et al.*, 1998; *Vincent et al.*,

1997; *Wappner et al.*, 1997; *Ruberte et al.*, 1995). The breaks in tracheal structure observed with SERCA inhibition are reminiscent of some of the phenotypes seen when *knirps* and *spalt* signaling are altered (*Chen et al.*, 1998). In that study, proper positional migration of cells was perturbed by deleting or misexpressing these genes, so cells would not migrate to their proper destination and would thus fail to form specific segments of the tracheal network. Depending on the combination of over- or under-expression of genes, specific tracheal tubes were affected. Following inhibition of SERCA activity, we observed similar breaks in segments; however, inhibition of SERCA caused disruption of different segments in different embryos, collectively affecting all parts of the tracheal tree. Therefore, while the genetic perturbation studies specifically misdirected particular tracheal cells, SERCA inhibition broadly perturbed tracheal morphogenesis. This suggests that SERCA inhibition affected the migration of cells possessing sufficient levels of inhibitor, and the phenotype that resulted depended on which cells were inhibited.

The necessity for SERCA activity for proper cell migration is consistent with the results of the zebrafish intersomitic vasculature development, and it explains how inhibiting SERCA in the *Drosophila* tracheal system can produce such severe deformities. The similarity of phenotypes that result from SERCA inhibition and some of the *knirps* and *spalt* mutations also suggest that DPP and EGF signaling through *knirps* and *spalt* may eventually act through calcium activity to direct cell migration. It would be interesting to see if modulation of SERCA and PKC activity affected the phenotypes observed following ectopic *knirps* or *spalt* expression.

6.2 Lumenization and tube shape

Individual cell shape was not different between control and SERCA-inhibited *Drosophila* embryos, but tube length and lumen alterations were observed following inhibitor washout and PKC activation, respectively. Tracheal tube size is controlled by various chitinous proteins which are secreted into the tracheal lumen at different stages of tracheal development (*Beitel and Krasnow*, 2000). These proteins play an important role in directing the final shape and dimensions of the tracheal tubes. At early stages, the proteins serve to induce lumenal widening (*Devine et al.*, 2005; *Wang et al.*, 2006), but at later stages, the proteins signal to cells to stabilize the lumen at a certain size and prevent over-dilation or lengthening (*Araújo et al.*, 2005; *Swanson et al.*, 2009). Maturation of the lumen proteins through these different stages requires modifications of the lumen contents by two secreted deacetylases, Vermiform and Serpentine (*Luschnig et al.*, 2006; *Nelson et al.*, 2010; *Schottenfeld et al.*, 2010). These modifications are highly dependent on proper cell polarization. Apical secretion of Verm and Serp into the lumen requires intact adherens junction and septate (tight) junctions (*Wang et al.*, 2006), which also organize basolateral polarity complexes. Mutations in the septate junction disrupt lumenal secretion (*Llimargas et al.*, 2004; *Nelson et al.*, 2010; *Swanson et al.*, 2009). Thus, perturbing septate junctions blocks lumenal maturation, and the tubes elongate excessively and form cysts or constrictions (*Llimargas et al.*, 2004).

Following washout of SERCA inhibitor from *Drosophila* embryos at stage 12, the resulting tracheal tubes were often excessively elongated and convoluted (Fig. 4.2C

and B.1C). The elongated nature of these tubes could be a result of lumen protein defects that have been reported to result in long tubes. However, 2A12 staining in these embryos was not perturbed, and the tube widening and constrictions described in conjunction with the tube length mutants are not observed with SERCA blockade. Thus, the fragmentation and segment breakages are likely a result of defects in a different process.

6.3 Feedback regulation

The elongated tubes and hyper-sprouty phenotype following removal of SERCA inhibitor could simply be an over-correction to the inhibited state. If cell migration was blocked by the drug, the cells may be trying to 'catch up' to where they should be and in the process extend excessive cytoplasmic projections and over-stretch, forming convoluted tubes. Alternatively, there may be a negative feedback mechanism dependent on SERCA activity that constrains the SERCA-dependent migratory activity of cells. This could be analogous to activator-inhibitor feedback in seashell patterning or FGF signaling that promotes tracheal and lung branching but activates an inhibitor, *sprouty*, which restrains the branching activity by modulating downstream FGF signaling (*Meinhardt*, 2009; *Mailleux et al.*, 2001). Upon removal of SERCA inhibitor, cell migration could be rapidly activated, but the feedback to constrain it would have a slight delay in turning on, enabling the migratory activity to get ahead of itself. This could explain the hyper-sprouty and wavy tubes often observed after washout of SERCA inhibitor.

Interestingly, in a few cases, an extra partial or complete lateral trunk formed after washout of SERCA inhibitor (Fig. 4.3C). This astounding phenotype was much less common than the phenotype with normal structure but sprouty, convoluted branches. Yet it indicates that there may be flexibility in tracheal network structuring or branch specification. One possibility is that the formation of the tracheal trunks involves activators and inhibitors that lay out a global pattern like in seashell stripes. Alternatively, a particular calcium dynamic may specify the lateral trunk fate. If this dynamic is achieved in more cells than normal following washout of the SERCA inhibitor, it is possible that it instructs the cells to form more than one lateral trunk. The calcium-mediated signal could, however, occur over an expanded time window rather than a spatial window, instructing a first batch of cells to form the lateral trunk as normal, and then if it persisted or occurred again, it might instruct a second batch of cells to form a second lateral trunk. Analysis of the calcium behavior of individual cells during tracheal development might reveal such a signature calcium dynamic that instructs lateral trunk formation.

In comparison, embryos treated with PKC activator alone commonly display a phenotype of lack of label of the 2A12 lumen protein antigen in the dorsal trunk, but normal tracheal network structure and lumen dimensions. These findings suggest that ectopic PKC activation alters lumen protein maturation such that the 2A12 antigen is reduced or absent. But there must be lumen protein present and sufficient redundancy in the function of the different proteins to achieve proper lumenization and homogeneous widening. Cell junctions and apical secretion must not be perturbed,

otherwise dilations and constrictions as seen in the septate junction mutants would be expected. Likewise, cell migration and positional information remains normal as the tracheal cells are present and the network structure is normal in these embryos. The actin cytoskeletal network is also not affected (based on actin-eGFP localization), so vesicle transport is unlikely to be the cause of the 2A12 perturbation (*Massarwa et al.*, 2009). Since cell polarity, cytoskeletal, and secretion problems are not apparent, the defect may be limited to localization of the particular lumen protein recognized by the 2A12 antibody.

6.4 Neural guidance

The longitudinal nerve tracts of the CNS form primarily by patterned axonal extension but do involve cell proliferation, and again in this system, SERCA inhibition produces a range of breaks, tract mergings, aberrant midline crossings, and general disorder (see Fig. B.2). Migration of glial cells, primary neurons, or follower axons could be affected, and the merging of tracts seen at the level of A4—A5 (Fig. 4.6B, center red arrow) may also reflect perturbed cell migration during germ band retraction, as migration problems often manifest in these segments. Pioneer axons depend on a combination of guidance cues from glia, interneurons, and each other to form the longitudinal fascicles (*Hidalgo and Booth*, 2000; *Kuzina et al.*, 2011; *Learte and Hidalgo*, 2007; *Raper and Mason*, 2010). The glial cells are not stationary; they migrate along with and ahead of some of the pioneer axon growth cones and appear to attract the axons, which extend more slowly in the absence of glia (*Hidalgo and*

Booth, 2000; *Parker and Auld*, 2004).

Rearrangement of the first fascicle by defasciculation and refasciculation to ultimately form three fascicles on each side of the midline depends on the presence of glial cells. The fusion of fascicles sometimes seen following SERCA inhibition could be a result of SERCA blockade affecting glial cell migration and, in turn, pioneer axon pathfinding. Rather than organizing into three bundles, they may remain as a single tract in sections. Misexpression of adhesion proteins, such as FasII, could also affect the alignment of fascicles and result in improper joining of different pathways (*Goodman*, 1996).

Abnormal midline crossing could also reflect changes in expression of repulsion signals or receptors, or midline glial cell behaviors (*Ratnaparkhi and Zinn*, 2007). Affecting the migration of the midline glia could mis-guide commissural axons. However, it is also possible that axon guidance itself is perturbed by SERCA inhibition with neurons failing to migrate properly despite the presence of proper guideposts and signals. Furthermore, as axons-axon interactions are important for primary and follower axon pathfinding, disruption of these interactions could explain some of the neural phenotypes observed (*Imai and Sakano*, 2011). It would be interesting to determine whether Eph or Ephrin receptor expression is perturbed in these mutants, as this would affect axon sorting and guidance interactions (*Imondi et al.*, 2000; *Reber et al.*, 2004).

6.5 PKC activation

Co-treatment of *Drosophila* embryos with SERCA inhibitor and PKC activator rescues tracheal and neural development. This suggests that balancing the reduced SERCA activity with reduced IP3-mediated calcium release from the ER can compensate for reduced calcium sequestration, and cell migration can proceed sufficiently normally to generate the typical neural and tracheal networks. While PKC activation rescues in *Drosophila*, in zebrafish intersomitic vessels, PKC activation in the background of SERCA inhibition produced results similar to those of SERCA inhibition alone, with a sometimes more severe effect. This difference may be specific to tissue type, although PKC activation also rescued *Drosophila* neural development. Species-specific differences likely contribute, with different expression of various PKC isoforms that are variably involved in regulating different cell behaviors through distinct downstream targets.

In zebrafish vascular development, PLCγ1 acts downstream of the VEGFR2 homolog, kdrl and is important for endothelial differentiation and morphogenesis (*Lawson et al.*, 2003). PLCγ1 activity is required cell-autonomously in endothelial cells to migrate from the dorsal aorta and posterior cardinal vein and form the intersomitic vessels (*Covassin et al.*, 2009). PLCγ1 knockout embryos do not form intersomitic vessels. Activation of PLCγ1 can lead to MAPK or Akt signaling, but activation of these pathways does not rescue intersomitic vascular development, meaning these are not the downstream effector pathways. This is consistent with our findings that regulation of calcium activity is the important readout of this pathway and that it

modulates cell migration.

Therefore, in the context of zebrafish intersomitic vessel development, both prolonged or elevated calcium exposure, which is expected by SERCA inhibition, and insufficient production of IP3 following PKC activation are likely to disrupt cell motility. This is consistent with our findings that concomitant inhibition of SERCA and activation of PKC can result in an additive detrimental effect on intersomitic vessel outgrowth.

On the contrary, PKC activation has previously been reported to rescue calcium currents in *Drosophila* (*Gu and Singh*, 1997). In larval skeletal muscle, a mutation in PLCβ, *norpA*, decreases muscle calcium transients through the membrane dihydropyridine (DHP)-sensitive calcium channel, and activation of PKC rescues the current. The DHP-sensitive calcium channel is different from the IP3R channel on the endoplasmic reticulum that responds to IP3 for calcium release, but similar regulatory mechanisms may be at play. It is possible that PKC is directly phosphorylating the channels. However, in the case of the skeletal muscle rescue, the effect is to increase calcium transient, whereas in the trachea and nerves, rescue is presumably achieved by reducing calcium release to balance the SERCA inhibition. It is still unclear exactly how PKC is mediating rescue of calcium dynamics in both of these cases. Analysis of the actual calcium activity in tracheal cells under the influence of SERCA and PKC modulators will hopefully shed light on the regulatory pathway. Regardless, the different combination of activities and isoforms of proteins involved in the calcium release from the endoplasmic reticulum likely contribute to the difference in PKC-

mediated effects in zebrafish vasculature versus *Drosophila* trachea and nerves.

6.6 Conserved regulation of migration and branching

Dynamic analysis of the tracheal development reveals that SERCA-dependent defects in cell migration indeed account for disrupted tracheal development, and likely serves the same role in neural and endothelial migration and branching. Individual cells fail to migrate to their destined locations and interact with partner cells in adjacent segments, and the result is the persistence of breaks between segments that should be connected. The migration defect is consistent with a requirement for SERCA activity to modulate calcium levels and direct individual cell movement, and this is applicable across species and tissue types. The extent of the phenotype correlates with the location and number of cells that are sufficiently affected by the SERCA inhibitor. Similarly, budding activity by extending cytoskeletal projections is affected in both zebrafish and *Drosophila*. Thus, SERCA serves as a general regulator of cell migration and branching across species, tissues, and developmental programs. Modulation of calcium dynamics to encode a branching program is a conserved, generalizable mechanism that obviates the need for specific morphogenetic signals to direct branch formation in each developmental system.

Part II

Lung branching takes nerve

Chapter 7

Nerves are required for branching morphogenesis in mammalian lung and *Drosophila* trachea

7.1 Introduction

The lungs develop as a bud from the foregut that forms in the fourth week of human gestation and at embryonic day 9.5 (E9.5) in the mouse (*Costa et al.*, 2001; *Warburton et al.*, 2000, 2005). Numerous morphogens, including fibroblast growth factors (FGFs) from the heart and bone morphogenic proteins (BMPs) and retinoic acid (RA) produced in the foregut endoderm and mesenchyme are necessary to pattern the anterior-posterior fates of the foregut endoderm (*Chen et al.*, 2010; *Tiso et al.*, 2002; *Cardoso and Lü*, 2006; *Serls et al.*, 2005; *Warburton et al.*, 1998). Wnt and RA signaling in the mesenchyme around the ventral foregut are involved in inducing Nkx2.1 and sonic hedgehog (Shh) in the ventral foregut, which are necessary for lung bud specification (*Desai et al.*, 2004; *Harris-Johnson et al.*, 2009; *Goss et al.*, 2009). Sox2 expression in dorsal foregut limits lung induction to the ventral region

(*Que et al.*, 2007). Loss of Nkx2.1 results in formation of only rudimentary lung buds and failed separation from the esophagus (*Litingtung et al.*, 1998; *Minoo et al.*, 1999; *Jacobs et al.*, 2012). Shh is also necessary for separation of the lungs and trachea from the foregut and for epithelial branching, but the epithelial cells that are present can differentiate (*Pepicelli et al.*, 1998).

RA integrates Wnt and Tbx4 signaling in the mesenchyme to induce mesenchymal expression of Fgf10 (*Chen et al.*, 2010), which is restricted by Shh to the mesenchyme surrounding the growing tips of lung buds (*Morrisey and Hogan*, 2010; *Pepicelli et al.*, 1998). Tgfβ from the trachea and proximal bronchi inhibits Fgf10 expression there to confine branching to distal regions (*Serra et al.*, 1994; *Zhao et al.*, 1996; *Pelton et al.*, 1991). This localized Fgf10 expression is necessary for epithelial bud outgrowth to form the iterative branched structure of the lung. The pattern of branches that generate the mammalian lung is highly stereotyped, with the sequence of branches that form being nearly identical from one individual to the next (*Metzger et al.*, 2008). The basic pattern of branches is first laid out, and then at later stages in lung development, cells differentiate into specific subtypes to form alveoli and provide the secretory, absorptive, and gas exchange functions of the lungs (*Morrisey and Hogan*, 2010).

Fgf10 acts on FGF receptor (Fgfr) 2b in the adjacent bronchial epithelium to induce bud outgrowth (*Bellusci et al.*, 1997; *Min et al.*, 1998). Excess Fgf10 increases lung branching. Conversely, over-expression of Shh suppresses Fgf10, and branching is reduced. Fgfr signaling in turn upregulates Sprouty2 (spry2) in the epithelium.

Spry2 limits downstream MAPK signaling to restrain branch outgrowth except right at the tip of the growing bud (*Mailleux et al.*, 2001; *Tefft et al.*, 2002).

Depletion of endothelial cells from lungs *in vivo* using an inducible VEGF decoy receptor results in a reduction of branching overall, and particular inhibition of orthogonal branches that make the lungs thicker (*Lazarus et al.*, 2011). However, the epithelium continues to proliferate, generating more cystic, dilated airways. To the contrary, exogenous Vegf164 (an isoform of Vegf-A) promotes mesenchymal proliferation and epithelial branching, likely by indirectly stimulating growth-promoting factors in the mesenchyme (*Moral et al.*, 2006). Furthermore, endothelial cells and the epithelium interact through Shh signaling, as vasculature is reduced in Shh knock-outs (*Pepicelli et al.*, 1998), and Shh signaling is perturbed following vascular depletion, resulting in diffuse mesenchymal Fgf10 expression (*Lazarus et al.*, 2011). Thus, endothelial cells also play a role in directing stereotyped lung branching.

Various basement membrane proteins are expressed throughout the lung and play a role in branch formation. At branch tips, epithelial cells produce laminin A, and this can interact with laminins B and C produced by the mesenchyme to form a basement membrane (*Thomas and Dziadek*, 1994). Nidogen cross links the laminins, collagen IV, and heparan sulfate to form a stable structure (*Paulsson et al.*, 1987; *Aumailley et al.*, 1989; *Battaglia et al.*, 1992). The basement membrane at the tips of epithelial buds is discontinuous, and epithelial and mesenchymal cells are seen interacting via cellular projections through the basement membrane (*Riso*, 1983; *Gallagher*, 1986). Collagen bundles are arranged parallel to epithelial stalks and are often found

associated with endothelial cell clusters (*Hilfer*, 1996; *Thomas and Dziadek*, 1994). Fibronectin deposition is key to the formation of epithelial branchpoints by reducing cell adhesion, and knockdown of fibronectin reduces branching (*Sakai et al.*, 2003; *Onodera et al.*, 2010; *De Langhe et al.*, 2005).

Thus, a myriad of morphogens as well as interactions between epithelium, the surrounding mesenchyme, basement membrane components, and developing blood vessels contribute to regulating lung branching morphogenesis. In addition, neurons are known to be present within the lungs shortly after the branching program begins (*Burns et al.*, 2008; *Tollet et al.*, 2001; *Sparrow et al.*, 1995). As branching proceeds, ganglia of neural cell bodies coalesce, and a network of nerves extends down the growing epithelial tubules to innerve vascular and bronchial smooth muscle. However, it remains unknown whether these nerves may be playing a role in regulating epithelial branching itself. It has recently been demonstrated in a similar branching organ, the submandibular gland, that parasympathetic innervation is necessary for growth and branching of the epithelium (*Knox et al.*, 2010). Therefore, we set out to investigate the role of neurons in the early branching program of the lung.

7.2 Methods

7.2.1 Lung explant culture

Lungs were explanted from embryos at the desired stage of development and cultured at the air-liquid interface on culture inserts as previously described (*Aguayo et al.*,

Table 7.1: Concentrations of drugs and dyes used for lung branching studies.

Substance	[Stock]	[Final]	Product Info
4-DAMP	25mM in DMSO	10 to 20μM	Tocris Biosci 0482
Heparin	2mg/mL in H_2O	50ng/mL	Sigma H3393
rmFgf10	100μg/mL	400ng/mL	R&D 6224-FG-025/CF
Topro3-iodide	1mM	1μM	Life Technologies T3605

1994; *Jesudason et al.*, 2000). Briefly, the embryonic lungs were gently separated from the esophagus and heart in phosphate buffered saline (PBS) at room temperature. They were transferred in a small volume of PBS to a 0.4μm Millicell polytetrafluoroethylene culture insert using a pipet with the tip cut to enlarge the opening. The lungs were carefully arranged to lie relatively flat on the insert, and excess PBS was removed, leaving a small volume of fluid around the lungs. The insert was placed in a 6-well culture dish floating on top of 1.5 to 2mL of 50% DMEM-50% F12 media plus 2% fetal calf serum (FCS) and 100U penicillin/100μg streptomycin (1:100 dilution). Explants were cultured at 37 degrees Celsius with 5% CO_2. Fresh media was provided approximately every 24 hours.

7.2.2 Drug treatment of lung explants

Lungs were explanted and placed on culture inserts as described. The appropriate amount of desired drug was diluted into the media in the culture well.

7.2.3 Widefield imaging of lung explants and morphometry

Widefield transilluminated and epifluorescent images of cultured lung explants were captured with an Olympus stereoscope. The number of buds were counted to quantify the extent of branching, and the fold change in number of buds was calculated.

7.2.4 Laser ablation

Lungs were placed in a small volume of media in coverslip-bottomed imaging dishes. The ablation procedure was limited to one hour per sample, and then the lungs were quickly returned to culture at the air-liquid interface on culture inserts. Ablations were performed using a long-working-distance, high-numerical aperture objective for a small focal volume with a digital zoom of 3x. A z-stack was first collected with confocal imaging using 488nm wavelength light from an argon laser. The same region was then imaged with low intensity 820nm infrared light with a pulse frequency of 80MHz from a titanium-sapphire laser. The collimating lens for the infrared light was adjusted until the focal plane was the same as for the 488 nm visible light. A nerve or axon of interest was then identified with confocal imaging, and a small region of interest was drawn within the cell or axon. That region of interest was imaged with approximately 350 to 700mW of average power (30-60% power) at 820nm with a pixel dwell time of 164μs/px. The area was again imaged with 488 nm light to verify liquidation of the target. The number of scans performed for an ablation was counted, and the same number of scans was performed in a control ablation on another sample. For control ablations, scattered mesenchymal cells were targeted. Epithelium, blood vessels, and nerves were avoided.

7.2.5 Topro cell death assay

1μM of Topro3 iodide was added to lung explant media right before targeted ablation was performed and immediately before each subsequent timepoint after culture.

Topro3 iodide 642 was excited with 633nm light and was well separated from eGFP emission.

7.2.6 Antibodies used

Table 7.2: Antibodies used for mammalian lung or *Drosophila* studies.
(DSHB= Developmental Studies Hybridoma Bank)

Antibody target	Dilution	Product Info
β3-tubulin	1:250	Covance MMS-435P
Cleaved caspase 3	1:500	R&D AF835
E-cadherin	1:100	BD Pharmingen 610181
Fasciclin II	1:3	DSHB 1D4
eGFP	1:1000	Invitrogen A11122
HNK1	1:50	DSHB 3H5
Isotype specific donkey secondary antibodies	1:500	Invitrogen
Isotype specific goat secondary antibodies	1:500	Invitrogen
Phosphohistone H3	1:500	Millipore 06-570
QH1	1:50	DSHB QH1
Stranded at second	1:1000	D. Cavener, Vanderbilt U.
Tracheal lumen 2A12	1:2	DSHB 2A12
VEGFR2	1:25	BD Biosci 560680

7.2.7 Antibody staining of lung explants

Lung explants were fixed with 4% crystalline PFA overnight at 4 degrees C then washed 4 times with PBS to remove the PFA. Lungs were mounted in 3% agarose and vibratome sectioned approximately perpendicular to the length of the explants at a thickness of 75μm. A vibrational amplitude of 8 and speed of 2.5 were used. Sections were placed in Lab-Tek 8 well chambered slides and blocked for 3 hours in blocking solution (PBS/0.8% TritonX-100/1%fraction 5 BSA/10% goat serum). Primary antibodies were applied in fresh blocking solution overnight for 2 to 4 nights

at 4 degrees C with gentle nutation. Primary antibody solution was removed and sections were washed in PBS/0.3% TritonX-100 at room temperature 4 to 6 times over approximately 4 hours and then overnight at 4 degrees C. Secondary antibodies were applied at a 1:500 dilution in blocking solution overnight at 4 degrees C. Secondary antibody solution was removed and sections were washed approximately 4 times over 4 hours at room temperature and overnight at 4 degrees C in PBS/0.3% TritonX-100.

Antibody staining of the lung explant in Figure 7.1A was performed as described in *Lazarus et al.* (2011).

7.2.8 Imaging antibody-stained lungs

To image stained sections, the sections were mounted between two coverslips with a small amount of PBS and placed on a copper slide holder for ease of flipping the sample over to image both sides. Confocal and two-photon imaging were performed with a Zeiss LSM 710 microscope with the following collection parameters: 5.5-6% 730 nm excitation, 371-455nm collection; 5.8-6.0% 488 nm excitation, 500-558nm collection; 0.05% 561 nm excitation, 592-631nm collection; 0.8-3% 633nm excitation, 650-746nm collection. Identical settings were used across samples except when signal was saturating, and then the laser power was adjusted to obtain comparable signal at the surface and depth between samples. The pinhole size for confocal imaging was 4μm, and the pinhole was open all the way for 2-photon imaging. The z-step interval was 4μm, and the pixel dwell time was 2.55μs/px.

Whole mount fixed avian lungs were mounted in 3% agarose, and extra agarose

was trimmed parallel to the ventral or dorsal lung surface. To image the whole lung, confocal and two-photon microscopy were used on parallel collection tracks to image approximately 150μm of the surface of the sample with overlapping tiled z-stacks. Approximately 75μm was then removed from the imaged surface with a vibratome, and the process was repeated to image the next section. Overlapping z-stacks were stitched using Fiji plugins (*Preibisch et al.*, 2009).

Imaging of the lung explant in Figure 7.1A was performed as described in *Lazarus et al.* (2011).

7.2.9 Confocal imaging of live lung explants

Lungs were placed in coverslip-bottomed imaging dishes in a small amount of media and imaged with a Zeiss LSM 510 meta or Zeiss LSM 710 microscope. A 488 nm wavelength from an argon laser was used to image eGFP. To image multiple fluorophores in combinatorial antibody staining, two-photon excitation at 730 nm was used to excite A350 dyes, 488 nm was used for FITC or A488 dyes, 561 nm was used for A568 and A594 dyes, and 633 nm was used to excite A633 and A647 dyes, and bandpasses were set to collect non-overlapping emissions. A Plan-Apochromat 20X/0.8 NA air or LD C-Apochromat 40X/1.1 water objective were used with a pinhole set to 4-6.8μm. Tiled z-stacks of images were collected with a pixel dwell time of 2.55 to 3.22μs and a z-interval of 2 to 6μm.

7.2.10 Statistics

Individual cells were counted in antibody-stained sections, and numbers were normalized by the volume of tissue imaged. Ratios were calculated for the treatment group compared to the controls. Means and standard errors of the mean were calculated and plotted using MATLAB. Endothelial cell cluster sizes were also plotted using MATLAB. Statistical significance in differences in branching of lung explants was determined by the Mann-Whitney U test for continuous variables that may or may not have a normal distribution.

7.2.11 Fly crosses

For pan-neural ablation, the *elav*-gal4 driver line was crossed to the UAS-RicinA/CyO line. Embryos with neural ablation were clearly distinguishable from normal embryos with no ablation by neural antibody staining. To visualize the cells affected by this ablation, the *elav*-gal4 driver line was crossed to the UAS-dsRed stinger line, which expresses nuclear dsRed in cells expressing the driving promoter following heat shock. Embryos were collected on grape jelly plates in egg-laying chambers and kept moist until they had developed to the stage of interest. For the UAS-dsRed cross, embryos were heat shocked for 2 hours at 29 degrees Celsius five hours before imaging to activate the nuclear dsRed expression, and then they were imaged live 3 hours later.

7.2.12 *Drosophila* embryo fixation

For whole mount preparation, when embryos reached stages 13 to 16, they were transferred to glass vials and treated with heptane and 5% PFA in PBS for 15 minutes at room temperature to fix. The PFA was removed and 100% methanol was added, and the embryos were shaken to remove the vitelline membrane. The heptane was aspirated and the embryos were incrementally rehydrated through 70%, 50%, 30%, 0% methanol in PBS and then transferred to PBT (PBS + 0.05% TritonX-100 + 0.1% BSA).

7.2.13 *Drosophila* embryo antibody staining

For antibody staining, embryos were blocked for 1 hour at room temperature in 5% normal goat serum (NGS) then incubated with primary antibodies in PBT + 2% NGS overnight at 4 degrees C. Embryos were washed 6 times for 30 minutes at room temperature in PBT then blocked for 20 minutes in 5% NGS. Secondary antibodies (Invitrogen) were used at 1:500 in PBT + 2% NGS overnight at 4 degrees C. Embryos were washed 6 times for 30 minutes at room temperature and transferred to PBT/14% glycerol.

Fillet preparations were performed as previously described (*Lee*, 2009). Briefly, following drug treatment embryos were spread on glass slides with guts removed and a wax line drawn around them on the slide. They were fixed in 5% PFA for 30 minutes at room temperature and washed 4 times for 5 minutes in PBS and again in PBT on the slides. Blocking was performed for 30 minutes in 5% NGS, and fillets

were incubated with primary antibodies as above at 4 degrees overnight. Fillets were washed 6 times for 10-30 minutes and incubated with secondary antibodies as above at 4 degrees overnight, then washed again 6 times for 10 minutes. Coverslips were mounted and sealed with nail polish.

7.2.14 Imaging of *Drosophila* embryos

Whole mount *Drosophila* embryos were arranged on glass slides with permafluor (for fixed embryos) or PBS (for live nuclear dsRed labeled embryos) and coverslipped for imaging. Coverslipped fillet preparations were imaged the same way as whole mount embryos. Confocal and two-photon tiled z-stacks were collected with a Zeiss LSM 510 meta or Zeiss LSM 710 microscope using a 2μm pinhole (for confocal) and 1.5μm z-step interval. Appropriate excitation wavelengths and collection bandpasses were selected as above for the fluorophores used. Images were assembled using Fiji stitching plugins (*Preibisch et al.*, 2009) and viewed in 3D using Imaris software (Bitplane).

7.3 Results

To assess whether the intrinsic nerves of the lungs grow and elaborate with the epithelial branching program during early pseudoglandular development, we studied lung explants, which are detached from external inputs yet continue to branch in a stereotyped fashion in culture. Explant culture also enables non-genetic perturbation studies. To analyze the structure of the nerve network near the beginning of the branching program, fresh lung explants from embryonic day E12.5 were stained with

antibodies against E-cadherin to label the epithelium and β3-tubulin to label the nerves (Fig. 7.1A). Axon tracks extend along the bronchial epithelium into each major lobe of both lungs. The vagus nerve is also visible as the thick nerve bundle down the center between the lungs.

We next determined whether the nerves are visible in live explants without the aid of antibody staining. The microtubule-associated protein tau eGFP (MAPT) knockin mouse line has eGFP inserted in the tau protein locus and labels all neuron cell bodies and axons with eGFP (*Tucker et al.*, 2001). Confocal imaging of live E12.5 lung explants from these mice demonstrates that principle nerve bundles to each of the lung lobes are clearly visible and comparable to the fixed sample (Fig. 7.1B). In this sample, the vagus nerve was removed for clarity. Explants were then cultured at the air-liquid interface on culture inserts. Brightfield (Fig. 7.1C) and epifluorescence images (Fig. 7.1D) are shown for a lung freshly explanted from a MAPT positive embryo at E12.5. Figure 7.1E and F show brightfield and fluorescence images, respectively, of the same lung after 46 hours in culture. The nerve tracks to the primary lobes visible in Fig. 7.1D continue to elaborate along the branched epithelial tubes in Fig. 7.1F (examples marked by white arrowheads). Thus, even when disconnected from the central nervous system, neurons persist in the lung and integrate with the branching structure.

Branching of the submandibular gland depends on parasympathetic neural input (*Knox et al.*, 2010). To test whether inhibition of muscarinic acetylcholine receptors affects branching during lung development as it does in the submandibular gland, lung

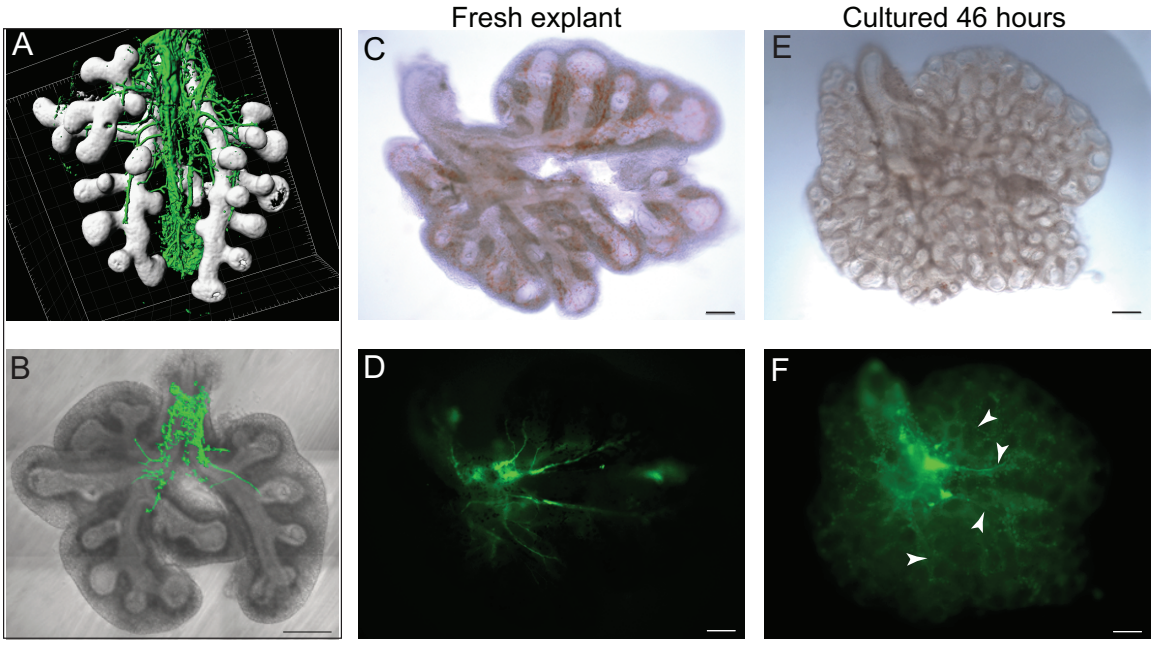

Figure 7.1: Intrinsic nerves elaborate with epithelial branches in lung explants. (A) lung explants from E12.5 mouse embryos were fixed and stained with antibodies against epithelial E-cadherin (white) and neural β3-tubulin (green) to visualize the nerves within the lungs at this stage. Axon bundles are visible along each major lobe. The vagus nerve is visible as the large nerve bundle in the center. (B) These principal neural axons are visible projecting to each lung lobe in live lung explants from the MAPT mouse line without using antibody staining. The vagus has been removed for clarity. Lungs were then cultured to assess whether the nerves survive following explant and continue to elaborate with the epithelium. A fresh explant is seen in brightfield (C) and epifluorescence (D) to visualize the nerves. After 46 hours in culture, the same lung has branched considerably (E, brightfield). (F) By epifluorescence, the nerves are still present and projecting axons along the epithelial branches (examples indicated by white arrowheads). Scale bars=200μm.

explants were treated with or without the irreversible muscarinic inhibitor 4-DAMP (N-2-chloroethyl-4-piperidinyl diphenylacetate) and cultured for two days. Various concentrations of 4-DAMP were tested alone or in combination with heparin and recombinant mouse Fgf10 branching morphogens, and in no case was an inhibitory effect on branching measured. The panels in figure 7.2 show freshly explanted lungs (A and B), where the lung in (A) was treated with 4-DAMP. Figure 7.2C is the same lung after 21 hours in culture, and Fig. 7.2D shows the control lung after the same time in culture. Although these explants were from the same mouse, there can still be variability in the maturity of the individual embryos, and the control in B began slightly less branched than the explant in (A). Therefore, the explant in C has more branches than the one in D, but this is proportional to the starting maturity of each lung. Even so, the muscarinic inhibitor caused no effect on lung branching. Quantifications are provided in Figure 7.7. The complexity of neurons present in the lungs at this stage may be greater than in the submandibular gland, with disruption of one type being compensated by other neural types. Alternatively, acetylcholinergic signaling may not be important at this stage.

It is possible that a combination of inhibitors of different neural receptors could elicit an effect on epithelial branching. However, a role for nerves in early lung development may not involve signaling via neurotransmitters: the nerves could be performing some other function. Acetylcholine receptors are also expressed by many non-neural cells (*Roman and Koval*, 2009; *Wessler and Kirkpatrick*, 2001). Therefore, to test whether the nerves play a regulatory role in bronchial epithelial branching

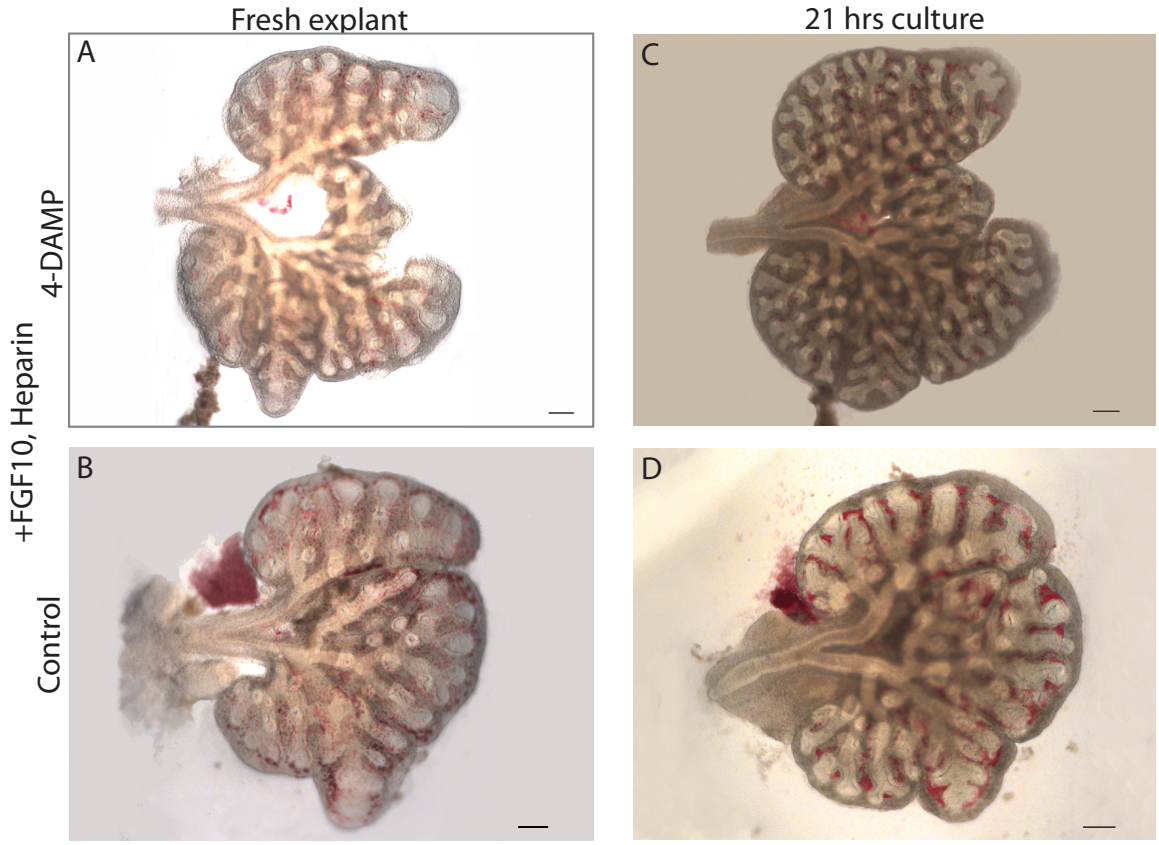

Figure 7.2: Unlike the submandibular gland, inhibition of muscarinic receptors does not affect lung branching. Explants were treated with or without the irreversible muscarinic inhibitor 4-DAMP, alone or in combination with branching mediators heparin and Fgf10. Freshly explanted lungs treated with 4-DAMP (A) or without inhibitor (B) are shown. The same lungs after 21 hours in culture are shown following culture with 4-DAMP (C) or without (D). At no concentration of 4-DAMP was an inhibitory effect on branching measured. The lung in (C) has more branches than the one in (D) owing to its slightly greater maturity upon explant despite coming from sibling embryos of the same pregnant mother. The branching is proportional to their starting maturity. Scale bars=200μm.

without regard to how they exert their influence, a generic method of removing all nerves regardless of subtype was necessary. For this reason, we looked beyond genetic ablation, which might remove only a subset of nerves, and different subsets could be more or less important and give unclear answers. Targeted laser ablation confines a focus of high-energy infrared light to small focus of about $0.1\mu m^3$. At a power of 350 to 700 mW, the beam can liquidate any cell at its point of focus.

We tested whether laser ablation was sufficiently powerful and precise to denervate lung explants. Lungs from MAPT embryos were used to visualize the nerves. Individual cell bodies or axons were identified with confocal microscopy, and a two-photon laser at 820nm was collimated to the same focus point (Fig. 7.3A). A small volume was scanned within a cell or across an axon (Fig. 7.3B, regions shown at higher magnification are outlined). The region was then imaged again with confocal microscopy to assess the results. When a cell body was targeted, a ring of autofluorescence was often seen following ablation of each cell, or sometimes the cell was no longer visible by fluorescence (Fig. 7.3B-1). After targeting slices across an axon, distal eGFP fluorescence that was previously visible in the axon was dissipated (Fig. 7.3B-2). These results suggested that targeted two-photon laser ablation could eliminate cells from live explants.

To test the precision of the laser ablation technique, a stack of confocal images was taken to assess the positions of multiple cells in three dimensions (Fig. 7.4). A neuron was selected for ablation where there was a second neuron positioned one cell width directly behind it in the axial dimension. Figure 7.4A shows the targeted neuron in

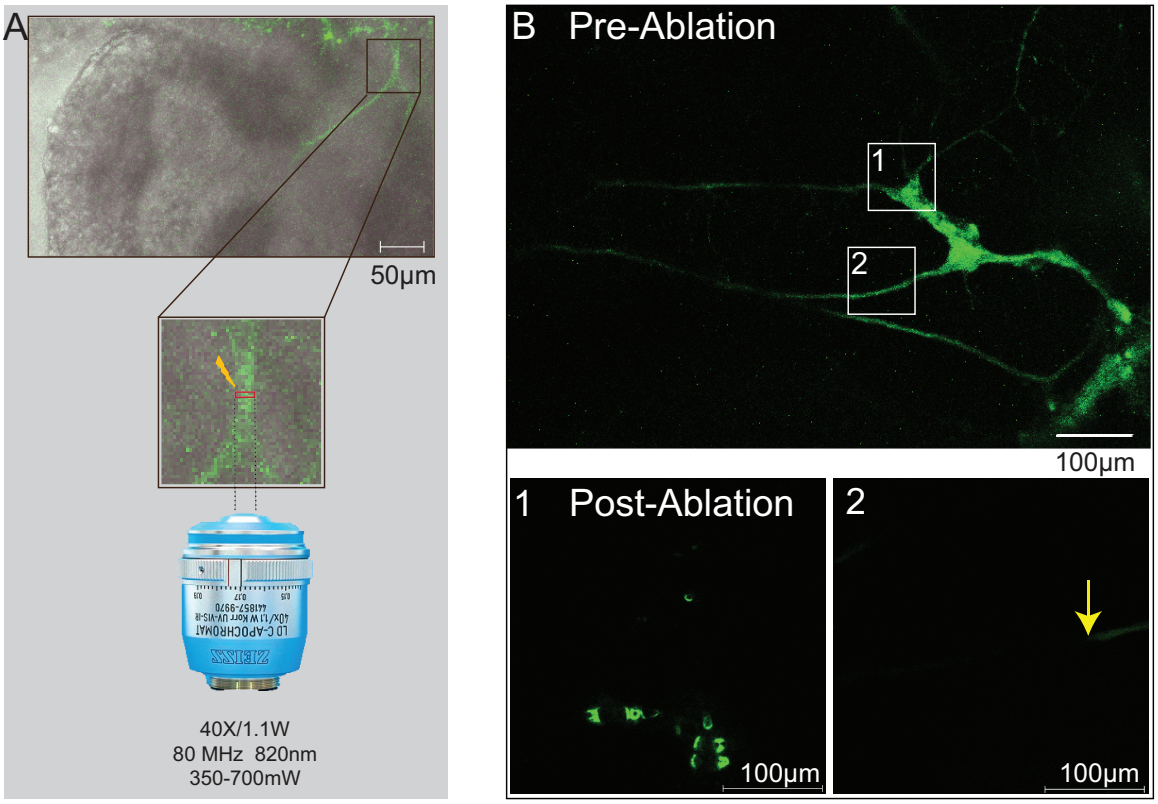

Figure 7.3: High energy two-photon laser power can eliminate cells from explants. (A) Neurons were identified in MAPT lung explants by eGFP fluorescence with confocal microscopy. 820nm infrared light was focused to the same plane to target cell bodies or axons. (B) Neurons were imaged before and after ablation. Cells or axons in the boxed regions of the top panel were targeted and are shown at higher magnification following ablation. (B1) After targeting cell bodies, either a ring of autofluorescence is seen, or the cell is no longer visible by fluorescence imaging. (B2) After slicing axons, the eGFP is dissipated distal to the cuts (yellow arrow).

the X-Y plane before the ablation, with the red circle indicating the ablation focus. Figure 7.4B shows the axial plane with the neuron to be ablated marked in red, and the white arrow indicates the neuron directly behind it. Figure 7.4C-D show the same image volume after ablation. Viewed in the X-Y plane (Fig. 7.4C), a vaporization ring of autofluorescence is seen where the targeted neuron had been (outlined by red box). In the axial dimension (Fig. 7.4D), the vaporized neuron is outlined in red, and the neuron positioned directly behind it has been unaffected by the adjacent ablation (white arrow). Thus, the energy of the ablation is tightly confined to the focus and does not cause immediate damage to nearby cells.

To determine whether heat from the ablation affects bystander cells after a longer period of time, cell death was assessed immediately after ablation and up to 4 hours later. A lung explant was treated with Topro3 iodide dead cell indicator to fluorescently label dead cells with a fluorophore that is spectrally distinct from eGFP. Figure 7.5A shows a projection of an image stack collected of a neuron of interest before ablation. The yellow arrow indicates the cluster of cells to be ablated, and the yellow line marks the laser focus region. Immediately after ablation, a second image stack was collected (Fig. 7.5B). The cells targeted by the ablation are no longer visible, but the adjacent axon remains. The lung was cultured and then re-imaged after two and four hours, with fresh Topro-3 added each time to label dead cells. Figure 7.5C shows the same region of interest after 4 hours when cell toxicity from the ablation would be apparent. A few cells at the point of focus of the ablation are permeable to the indicator (purple). However, there is not general toxicity to bystander cells in

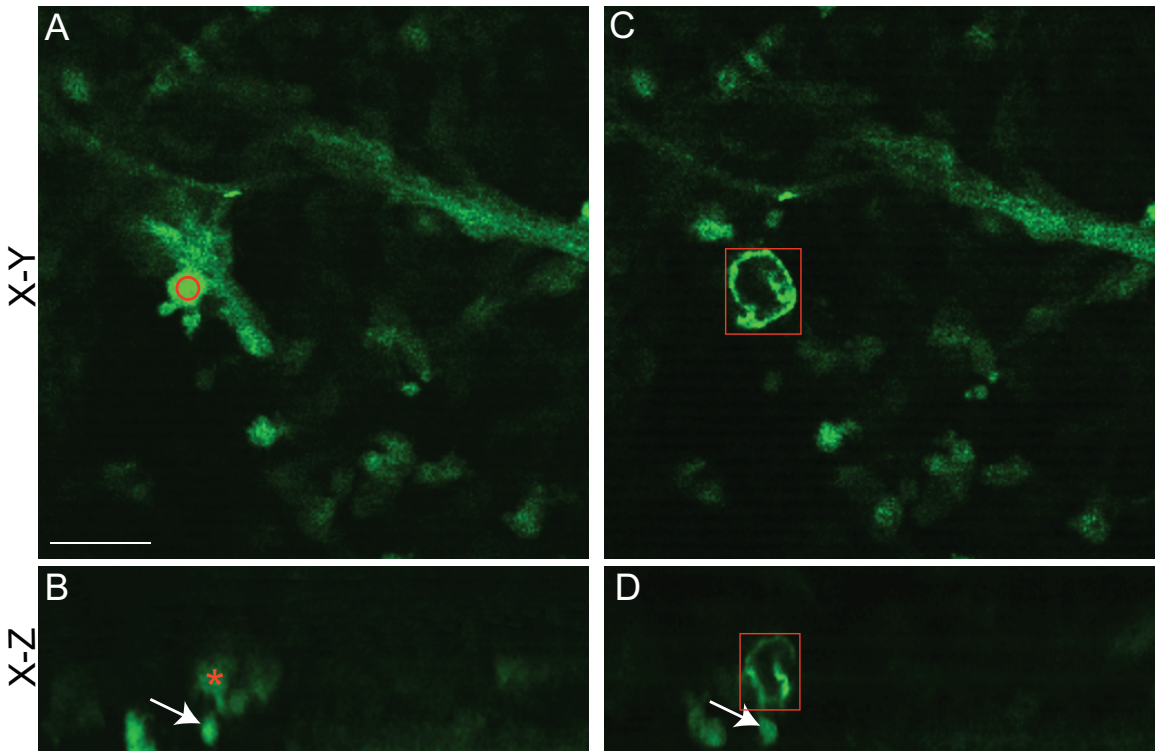

Figure 7.4: Targeting a region of interest within a single cell confines the ablation to that cell. (A) Before ablation, a neuron of interest is shown in the X-Y plane with the red circle indicating the ablation focus. (B) The same neuron is marked in red in the axial plane, and a neuron positioned directly behind it is indicated by the white arrow. (C) Following ablation, a ring of autofluorescence marks where the targeted cell had been (red box outline). (D) Viewed axially, the ablated cell is outlined in red, and the adjacent neuron behind it is unaffected (white arrow). Scale bar=20μm throughout.

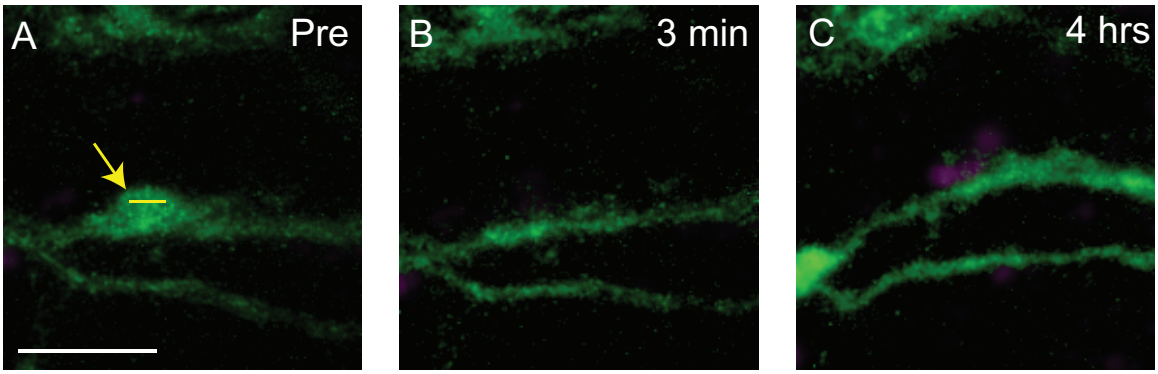

Figure 7.5: Bystander cell death is not observed hours after ablation. Death of neighboring cells in the region of a targeted ablation was assessed up to 4 hours after ablation. A MAPT lung explant was treated with Topro3 dead cell indicator to visualize dead cells. (A) A projected image stack shows a cluster of cells and axons before ablation, with the yellow arrow pointing to the cells that will be targeted and the yellow line indicating the region of laser focus. (B) An image stack was collected immediately after ablation, and the targeted cells are no longer visible by fluorescence imaging. (C) After 4 hours in culture, the explant was freshly treated with Topro3 and the same region of interest was imaged. A few dead cells are permeable to the indicator where the ablation was performed (purple), but there is not generalized death of cells in the surrounding area. Scale bar=30μm throughout.

the surrounding region. The same results were observed after 2 hours in culture.

To assess whether the presence of nerves is necessary for bronchial epithelial lung branching, nerves were laser ablated from MAPT lung explants. Individual neurons and axons were targeted in either the left or right lung of an explant until all or nearly all visible neurons had been lased. To control for the loss of cells and localized heat damage from the ablations, a control ablation was performed on another lung explant from an embryo of the same litter. For these controls, the same lung (right or left) was targeted as in the ablated sample, but instead of hitting neurons or axons, an equivalent number of scattered mesenchymal cells were ablated. Blood cells could often be identified by brightfield morphology, and the epithelium was visible by brightfield, so neurons, endothelial cells, and epithelium were avoided. Control

ablated and nerve ablated explants were then cultured for 43 to 46 hours on culture inserts. Individual epithelial branches were counted immediately after ablation and following 23 and 43-46 hours in culture.

Figure 7.6 shows images of ablated and control ablated lung explants taken at the time of ablation and after two days in culture. The nerves of the left lung in the explant in Fig. 7.6A were ablated. Red asterisks mark the locations of terminal buds present at the time of ablation, and black asterisks mark the positions of terminal buds in the untouched right lung, which serves as a culture control. Fig. 7.6B shows the same lungs after approximately two days in culture. The red asterisks mark the same buds that were present in the fresh explant of the left lung from which nerves were ablated. Black asterisks serve as place holders to mark the positions of the distal buds that were present in the right lung of the fresh explant in (A). It is clear that in the right lung, the epithelium has continued to branch, and numerous distal buds are visible beyond the black asterisks. In contrast, the left lung has grown very little, and only one branch has extended. The epithelium is still clearly visible, which it would not be if the explant had died. Figure 7.6C diagrams the branches that were present in the fresh explant (black) and the new branches that formed during the two days in culture (green). While the right lung branched considerably, the left lung changed very little.

Figure 7.6D-F show the equivalent panels for a stage-matched explant on which a control mesenchymal ablation was performed on the left lung. Black asterisks mark the distal positions of buds present in the fresh explant (Fig. 7.6D). The same

explant is seen after two days in culture, and both lungs have continued to branch (Fig. 7.6E). The new buds that formed are illustrated in green in Figure 7.6F. The right lung branching of the ablated sample (Fig 7.6C) is comparable to the right lung branching of the control (Fig. 7.6F).

Nerve ablation was then performed on the right lung instead of the left. Figure 7.6G-H show the explant at the time of ablation and after two days in culture, respectively. Red asterisks mark the distal buds that were present in the right lung of the fresh explant, while black asterisks mark the untouched left lung (Fig. 7.6G). In Figure 7.6H, the asterisks again serve as place holders marking the buds that were originally present in the right ablation lung (red) and left culture control (black). The right lung has not branched beyond its original structure, while the left lung has continued to branch substantially, as illustrated by green branches in Figure 7.6I. A right lung control mesenchymal ablation was similarly performed, and the black asterisks mark the positions of identical branches at the time of ablation and after two days of culture (Fig. 7.6J-K). As with the left sided control (Fig. 7.6E-F), the right lung control continues to branch proportionally to the unaffected left lung (Fig. 7.6K-L).

These results demonstrate that heat damage from the ablations and elimination of scattered mesenchymal cells from the lungs does not inhibit lung branching. These lungs continue to branch like unperturbed lungs. In contrast, lungs from which the nerves were ablated cease to branch, suggesting that the nerves play a necessary role in enabling epithelial branching.

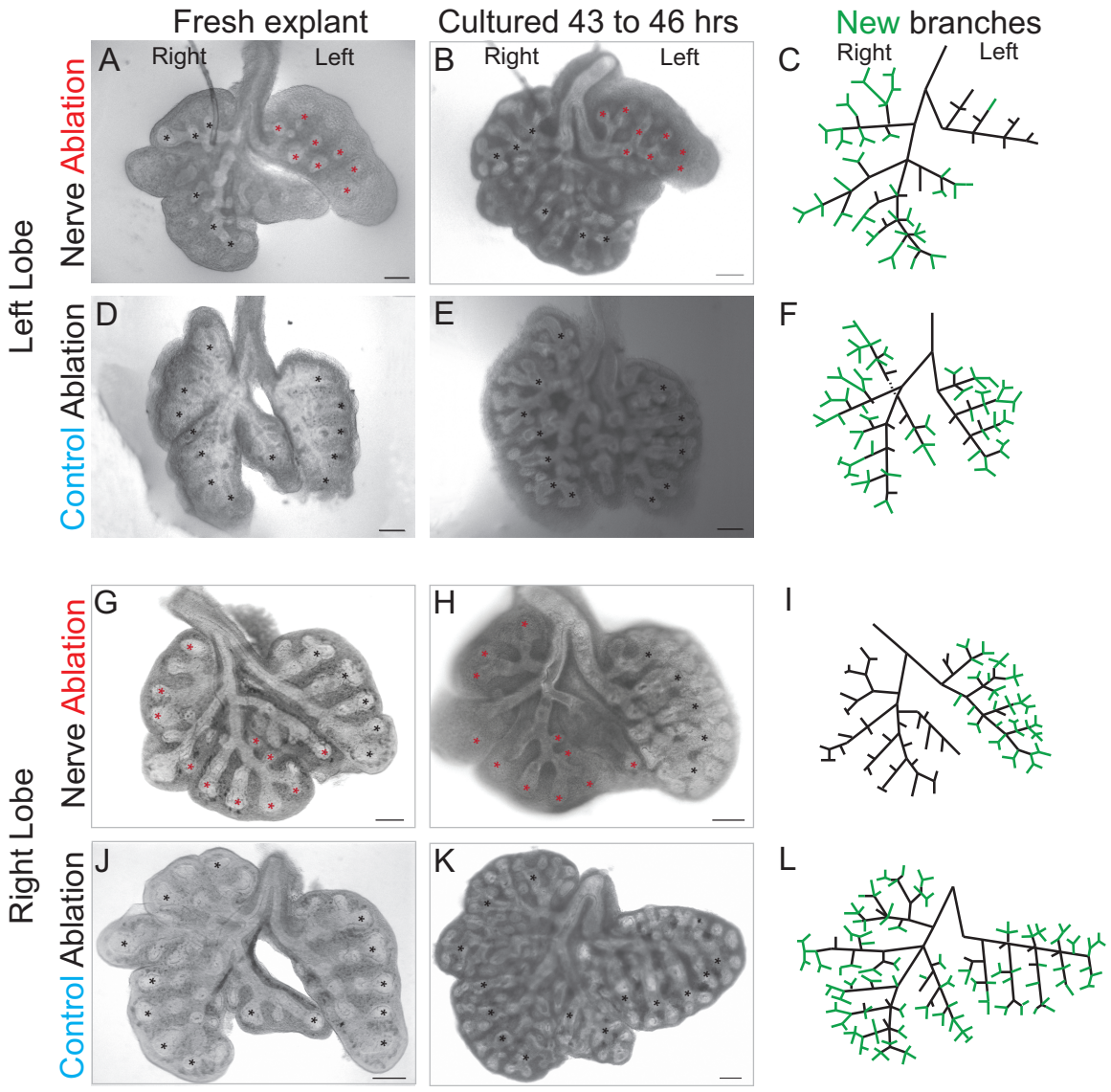

Figure 7.6: Nerve ablation halts lung branching while ablation of scattered mesenchymal cells does not inhibit branching. (A) Nerves were ablated from the left lung of the explant, and the right lung was not manipulated. Red asterisks mark the terminal buds of the left lung at the time of ablation, and black asterisks mark terminal buds in the right lung. (B) The same lung is shown after 43-46 hours in culture, with red asterisks marking the positions of the buds that were present in the left lung two days prior, and black asterisks serving as place holders for the branches that were originally present on the right. Numerous new branches have formed on the right lung distal to the black asterisks, while on the left lung only one branch has extended slightly. (C) The diagram illustrates the branches that were present upon explant (black) and the new branches that formed in culture over two days (green). (D) In parallel, an equivalent number of scattered mesenchymal cells were ablated from the left lung of a stage-matched explant from a sibling embryo to control for heat damage and cell loss. Epithelium, neurons, and endothelium were avoided. Black asterisks mark the terminal buds on the right and left lungs. Caption continued next page.

Figure 7.6: (Continued from previous page.) (E) The explant is seen after two days in culture with black asterisks indicating where the terminal branches had been in the fresh explant. Both lungs, including the left lung with the control ablation, continued to branch substantially, as illustrated in the schematic (I). (G-L) show the same ablation and control ablation for right lung, where the nerves were ablated from the right lung in (G), and a control ablation was performed on the right lung in (J). Like the left lung, nerve ablation in the right lung halts branching (H,I). The left lung paired with the right lung nerve ablation has branched substantially (H,I), as have both lungs of the control ablation sample (K,L). Scale bar=200μm throughout.

The extent of branching for ablations and controls was quantified by counting epithelial branches and calculating the fold change. Figure 7.7 plots the fold change in number of branches. The median change in branches for lungs from which the nerves were ablated was 1.4, while the median fold change for the control ablations was 3.3 (Fig. 7.7A, red lines indicated medians). The p value for statistical difference between these is much less than 0.01 (Mann-Whitney U test for non-parametric populations). In comparison, the median fold change in branching for explants cultured with the muscarinic inhibitor 4-DAMP was 4.5, and the median for controls that were cultured with no inhibitors or ablations was 3.9. There is no statistical difference in branching for samples treated with muscarinic inhibitor compared with controls, nor is there any statistical difference in branching between control mesenchymal ablation samples and explants cultured without any perturbation. These results indicate that neurons are necessary for lung epithelial branching, but their role is independent of parasympathetic muscarinic signaling.

To test whether a genetic neural ablation could produce a lung branching phenotype resembling that from nerve ablation, branching was quantified in lung explants from endothelin B receptor (EDNRB) knock-out mice. EDNRB knock-out mice have

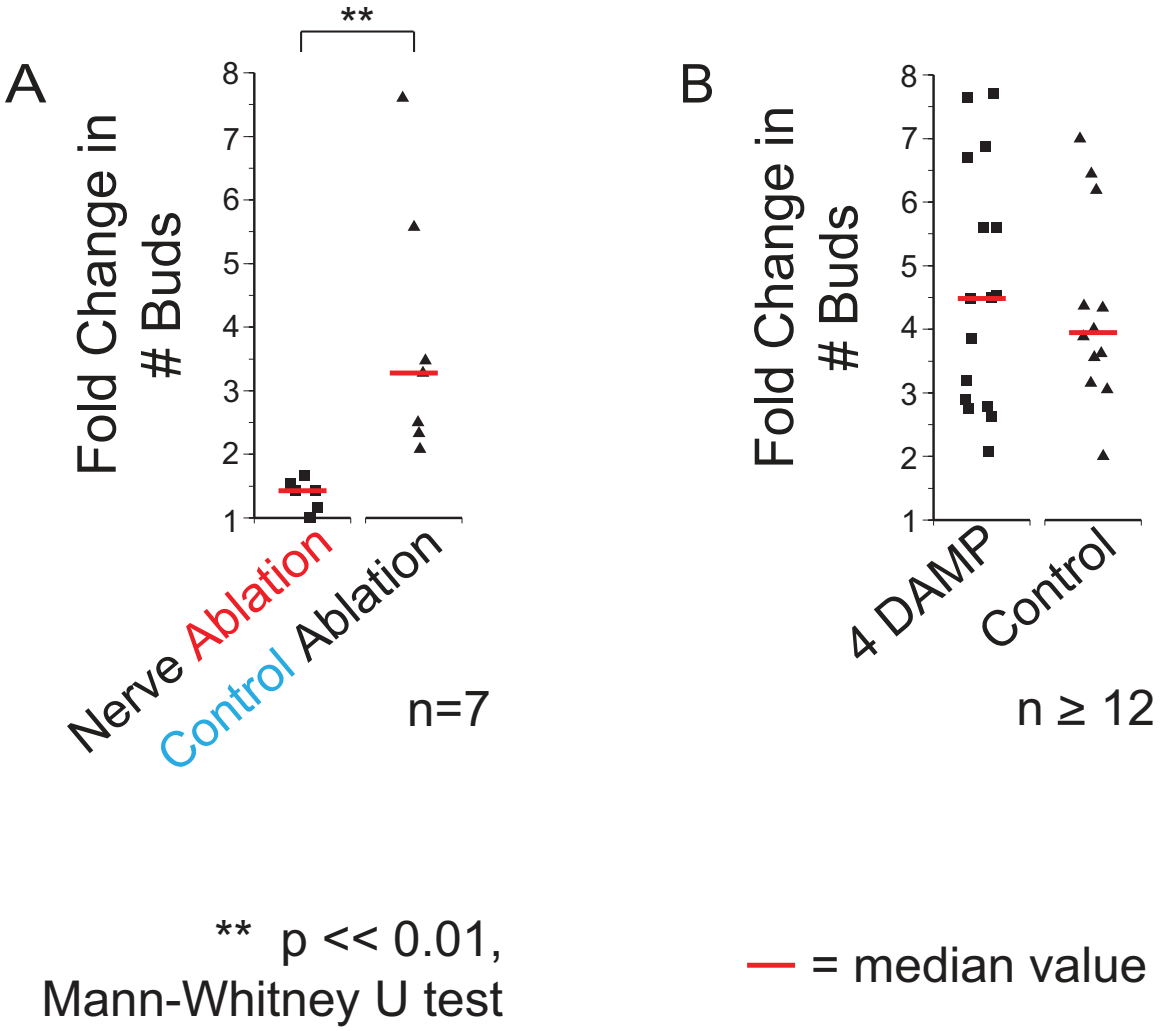

Figure 7.7: Nerve ablation causes a statistically significant blockade of lung branching, while control mesenchymal ablation has no affect on branching. Lung buds were counted in fresh explants and after two days in culture, and the fold change in branching was calculated. (A) The median fold change in branches for lungs following nerve ablation was 1.4 compared with 3.3 for control ablations (p value significantly less than 0.01 by Mann-Whitney U test). (B) No significant difference in branching was found for lungs treated with the muscarinic acetylcholinergic inhibitor 4-DAMP compared to controls. There was also no statistical difference in branching between control ablated lungs and lungs that were simply cultured with no perturbation. Red lines indicate median values.

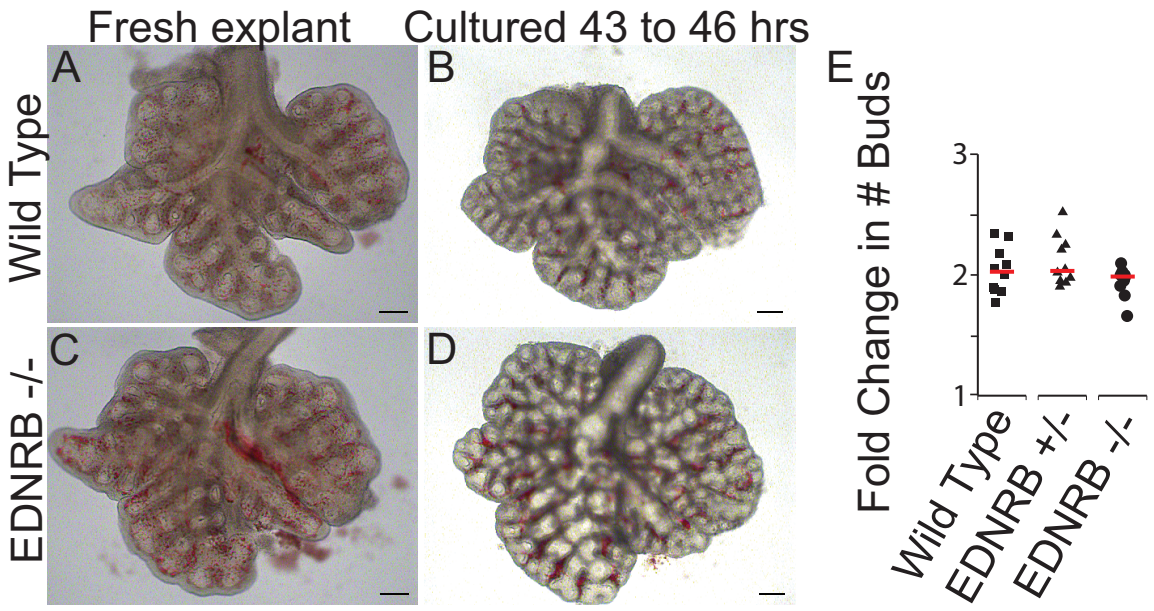

Figure 7.8: Partial lung denervation by genetic knock-out of endothelin receptor B (EDNRB) does not affect lung branching. Lungs were explanted from wild type, heterozygous, and EDNRB knock-out litermates and cultured for two days. Fresh explants from wild type (A) or EDNRB-/- (C) embryos were cultured for 43-46 hours. Cultured wild type (B) and EDNRB-/- (D) branch comparably. (E) Quantification of branching shows no difference between wild type, heterozygous, and knock-out littermates. Scale bars=200μm. Red lines indicate median values.

an aganglionic gut and are reported to have reduced but not eliminated lung innervation (*Hosoda et al.*, 1994). Lung explants from wild type, heterozygous (+/-), and EDNRB knock-out (-/-) mice were cultured as before. Lungs from EDNRB knock-outs branched just as much as those from heterozygote and wild type littermates (Fig. 7.8A-D). Quantification of the fold change in branches showed no difference between the three groups (Fig. 7.8E). Either the subtype of nerve matters at this stage of development, or an insufficient number of neurons were eliminated by genetic ablation.

Antibody staining was performed on the nerve ablation lung explants and control ablation lung explants to investigate what cell behaviors might account for the mea-

sured differences in branching. Figure 7.9A shows a projected z-stack of a section from a control ablation lung, and Figure 7.9B is from a nerve ablation lung. Phosphohistone H3 staining for proliferation (pink), β3-tubulin staining for nerves (cyan), and Vegfr2 staining for endothelial cells (green) are all less frequent in the denervated samples. Quantification of the nerves found in the lung sections from each treatment group demonstrates that the number of nerves in the nerve ablation samples are indeed severely reduced to 6% of that found in controls (Fig. 7.9C).

Cell proliferation in the epithelium and mesenchyme of lungs following nerve ablation is also reduced, which is consistent with the reduced size of these lungs relative to controls. Total cell proliferation in samples with nerve ablation is 20% of that in control ablated samples (Fig. 7.9D). Interestingly, the number of endothelial cells observed in lungs following nerve ablation is also substantially reduced to 27% of that in control ablated lungs. The endothelial cells that are present in the nerve ablated lungs are typically in smaller clusters, while large clusters of cells are seen in the control ablation samples. Figure 7.9F shows the frequency of different endothelial cell cluster sizes present in the two groups. Quantification of the proportion of endothelial cells from each group that are dividing will shed light on whether a proliferation defect in the endothelia accounts for their reduced numbers in lungs denuded of nerves. Preliminary assessment of cell death suggests it is not different between control and denervated samples.

Neurons may play a conserved role in regulating branching morphogenesis during development. In *Drosophila*, the tubular tracheal system for air transport is homolo-

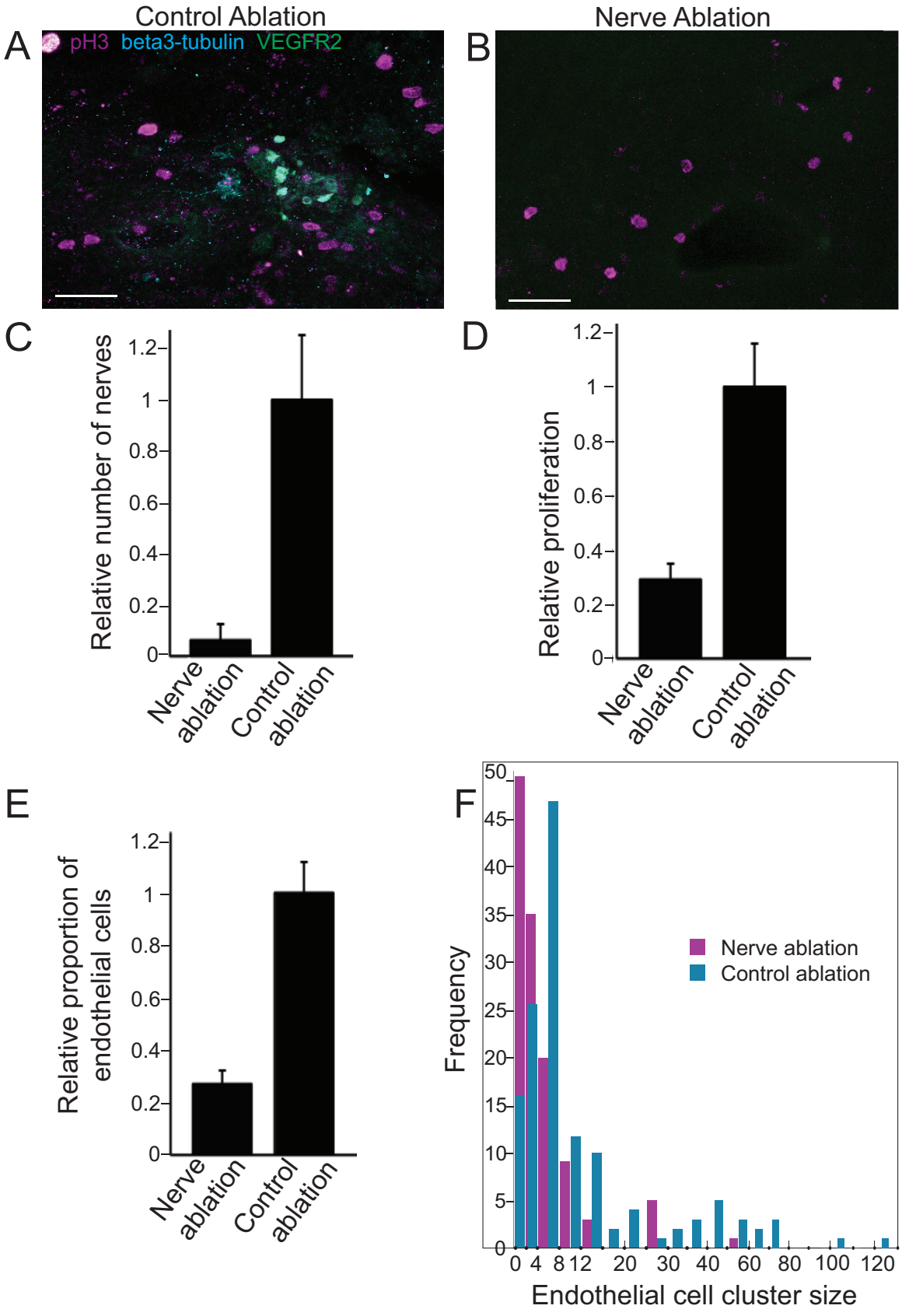

Figure 7.9: Caption next page.

Figure 7.9: Laser ablation denervates the lung and results in fewer endothelial cells and reduced proliferation. Control ablated and nerve ablated lungs were sectioned and stained with antibodies against phosphohistone H3 for proliferating cells (pink), neural β3-tubulin (cyan), and endothelial Vegfr2 (green). Panels show a sample from (A) a control ablated lung and (B) a nerve ablated lung. (C) Nerves are indeed largely eliminated following targeted neural ablation. On average, they are reduced to 6% of the amount seen in controls. (D) In nerve ablated samples, cell proliferation is reduced to a mean of 20% of that of control ablated samples, which is consistent with the lungs being smaller. (E) Fewer endothelial cells are present in denervated samples, with on average only 27% as many observed as in controls. (F) shows the distributions of endothelial cell cluster size for each treatement group. The endothelial cells that are present in denervated lung explants are found in smaller clusters, whereas in controls, large groups of endothelial cells are often seen. Scale bars = 50μm. Error bars represent the S.E.M.

gous to the mammalian lung, and development of the trachea is regulated by many of the same factors that have been characterized to direct mammalian lung development (*Affolter et al.*, 2009; *Cardoso and Lü*, 2006; *Glazer and Shilo*, 1991; *Hacohen et al.*, 1998; *Horowitz and Simons*, 2009; *Morrisey and Hogan*, 2010; *Sutherland et al.*, 1996; *Warburton et al.*, 1998, 1999, 2000). To assess whether neurons are necessary for proper embryonic tracheogenesis in *Drosophila*, neurons were genetically ablated. The *elav* promoter is expressed in all neurons for neural differentiation (*Yao and White*, 1994). The A subunit of the Ricin toxin is a potent inducer of cell death by blocking protein translation (*Hidalgo and Brand*, 1997). The elav:Gal4 driver line was crossed with the UAS-RicinA line to kill neurons. Neural death is expected to begin around stage 11, in time to affect tracheogenesis at stages 12-16.

Figure 7.10A shows a wild type *Drosophila* embryo at approximately stage 16, stained with antibodies against tracheal lumen protein and neural cell adhesion molecule Fasciclin II (FasII), which labels longitudinal tracks of the central nervous system and some motor axons. Figure 7.10B depicts all the cells expressing the

elav promoter by fluorescent label of their nuclei. Neural cell bodies positioned in the central nervous system are visible as a large collection in the region around the longitudinal fascicles, and peripheral nerve cell bodies are visible in each body segment. All of these cells express the *elav* promoter.

When RicinA is expressed in neurons under the control of the *elav* driver, neurons are ablated to varying degrees, but generally many neurons are killed. Concomitantly, tracheal morphogenesis is disrupted. Figure 7.10C-F show examples of embryos expressing the RicinA toxin under the control of the *elav* promoter in neurons. Compared with the wild type embryo in Figure 7.10A, the longitudinal fascicles are typically missing and replaced with short sections of labeled axons (Fig. 7.10D,E, open arrowheads). Some embryos possess one or more fascicles, but they are abnormal. In Figure 7.10D, a single fascicle on each side extends along most of the embryo, but it is broken in sections (arrowheads) and has disordered commissures. In Figure 7.10F, the longitudinal tracks are present but mostly fused together (arrowheads), and the peripheral FasII-positive projections are highly disordered.

Deletion of neurons causes are range of perturbations of tracheal development. In the embryo in Figure 7.10C, cells appear to have formed fragments of a dorsal tube, but it is discontinuous, and it is actually positioned on the ventral side of the embryo instead of the dorsal side (arrows). Similarly, in Figure 7.10D, short tracheal tubes are present by lumen label, but they are discontinuous (arrows). Smaller branches are not evident by lumen staining. In Figure 7.10E, some smaller tracheal tubes have formed and lumenized but are discontinuous (closed arrowheads). Most of a dorsal

trunk is present, but it also has a break (arrow). In Figure 7.10F, the tracheal cells appear to have all clustered into two groups and formed a circuitous ball of lumen (arrows), which is highly abnormal. These phenotypes cannot be a result of toxin being released from dying cells and acting directly on bystander cells because only the A subunit of the toxin is expressed. The B subunit is required to gain entry to viable cells, so any released toxin will have no effect.

To confirm that tracheal cells are indeed misplaced or absent in these mutants and that the defect is not solely in lumenization, embryos were stained with antibodies against the lumen protein as well as an antibody against *stranded-at-second*, which labels the tracheal epithelial cells. Figure 7.10G shows the lumen label in a less severely perturbed mutant, which has more tracheal tubes to analyze. Figure 7.10H shows the tracheal epithelial cells, and Figure 7.10I is the merge. Epithelial cells indeed surround the discontinuous lumens (arrowhead) and are absent where gaps are evident by lack of lumen label (arrow). Thus, deletion of neurons during *Drosophila* embryonic development disrupts tracheal morphogenesis and branching. A role for neurons in proper execution of stereotyped branching is conserved from mammalian lung to *Drosophila* tracheal development.

7.4 Conclusions and Discussion

Neural cell bodies reside within the lung and form ganglia and networks of axons that extend along the bronchial tubules as the epithelium grows and branches during embryogenesis. These neurons play a necessary role in the progression of iterative

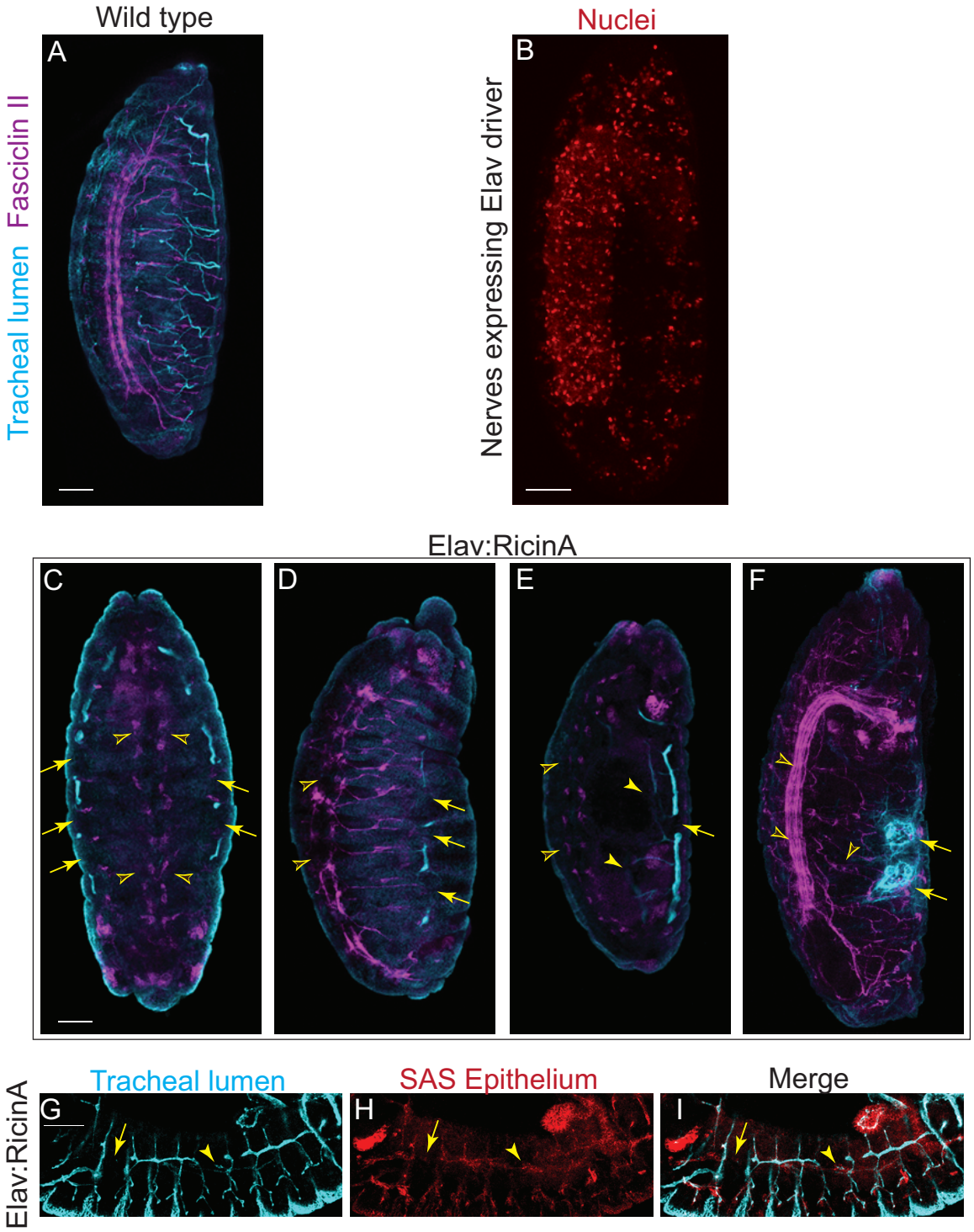

Figure 7.10: Caption next page.

Figure 7.10: Neurons are required for *Drosophila* embryonic tracheal development. Neurons were ablated in *Drosophila* embryos by expressing the A subunit of the potent ricin toxin under the control of the pan-neural driver *elav*. Antibody staining for the FasII adhesion molecule labels the longitudinal tracks of the CNS and some motor nerve axons (magenta). Tracheal structure is visible by staining for lumen protein (cyan). (A) shows the neural and tracheal structure in wild type embryos. (B) Neural nuclei are labeled by the activity of the *elav* promoter to visualize the distribution of cells affected by the ricinA toxin. (C-F) show examples of neural depletion and the effects on tracheal development when ricinA is expressed in neurons. The longitudinal tracks often nearly eliminated (C,E open arrowheads) and sometimes reduced to single disordered tracks with breaks (D, open arrowheads) or merged tracks with disordered peripheral projections (F, open arrowheads). Sections of what appear to be dorsal tracheal trunk form but are fragmented with breaks (C-E, arrows). In (C), the these tracheal cells are actually positioned on the ventral side of the embryo rather than the dorsal side. Smaller tubes are largely absent by lumen staining, and those that are present are incomplete (E, closed arrowheads). In (F), the tracheal cells form circuitous balls of lumenized tube, which are severely abnormal (arrows). (G-I) show labeling of tracheal epithelial cells in fillet preparations to confirm that the gaps are not simply a lumenization problem. Discontinuous tracheal lumens (G) are surrounded by epithelial cells (H) and seen together in the merge(I) (example indicated by arrowheads). Where gaps in the lumen exist, epithelial cells are absent (G-I, arrow). Scale bars=50μm throughout.

branching. Targeted laser ablation is precise and effective at eliminating individual neurons without causing detectable damage to surrounding cells. Deletion of the pulmonary neurons, but not scattered mesenchymal cells, halts epithelial branching. Inhibition of muscarinic receptors does not reproduce the branching phenotype, which contrasts with the submandibular gland. Neither does partial genetic denervation cause a branching defect. Elimination of the neurons significantly reduces the number and cluster size of endothelial cells in the lungs. Quantification of endothelial cell proliferation and apoptosis will reveal whether a proliferative or survival defect, or both, account for the reduced number of vascular cells. Similarly, proliferation of the epithelium and mesenchyme is also compromised in denervated lungs. The requirement for nerves in epithelial branching extends to the embryonic *Drosophila*

tracheal system, where substantial ablation of neurons leads to severe disruption of tracheaogenesis, often with only a few sections forming, and sometimes at the wrong position in the embryo.

Partial pulmonary denervation by genetic ablation did not recapitulate the effects of more complete denervation by laser targeting. This suggests that the subtypes of neurons may matter, or they may be able to compensate among themselves, requiring ablation of a certain proportion of the total population of neurons to inhibit branching.

The reduction in the number of endothelial cells could partly be a result of perturbed endothelial cell migration. Neurons and endothelia interact via ephrins, neuropilin, and other guidance signals (*Affolter et al.*, 2009; *Bagnard et al.*, 2001; *Melani and Weinstein*, 2010). If the pulmonary nerves provide a scaffold for migration of endothelial cells and assembly of vessels to form parallel neurovascular bundles, then elimination of the nerves would be expected to result in fewer endothelia populating the lung parenchyma. Indeed, in embryonic avian lungs, neurons and undifferentiated neural cells that may become glial cells are seen interacting with disorganized endothelial tubules early during lung bud outgrowth from the foregut (Fig. 7.11A, arrows). As the lung matures, progressively more organized networks of nerves and blood vessels align and form a meshwork around distal epithelial tubes (Fig. 7.11B). Cell-cell contacts between endothelial cells and neurons are likely involved in the organization of these networks. This is consistent with descriptions of neurovascular tracks observed in fetal mammalian lungs (*Sparrow et al.*, 1999).

Neurons may also provide growth and survival signals, such as Vegf-A, to stimulate

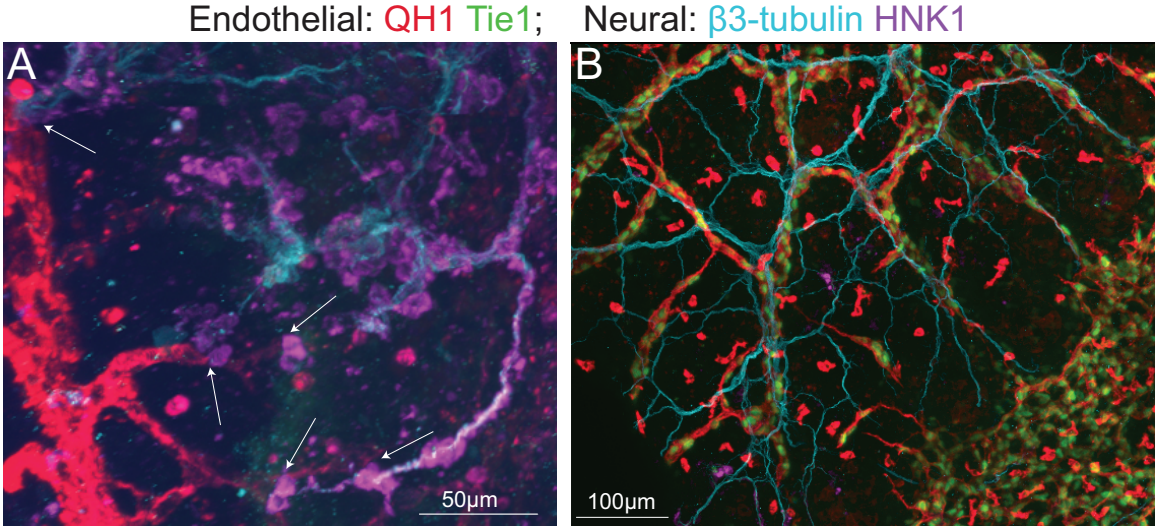

Figure 7.11: Neural and vascular cells interact during early avian lung development and align to form a neurovascular network. Antibody staining for neural crest cells (HNK1, purple), nerve axons (β3-tubulin, cyan), endothelial cell membrane (QH1, red), and endothelial nuclei (tg(*tie1*:H2B-eYFP), green) was performed on lung explants from E3.5 and E7 quail embryos. (A) In E3.5 quail lungs, which consist of two primary bronchi, vascular tubes are forming, and endothelial cells are seen making contact with clusters of neurons (arrows). Neurovascular structure is disorganized. (B) In E7 quail lungs, organized networks of mostly aligned nerves and blood vessels extend down branched epithelial tubes (which are situated in the unlabeled regions of the image).

endothelial survival, proliferation, and vessel sprouting. It is known that reduction of pulmonary vasculature using a VEGF decoy receptor perturbs the epithelial branching program: the extent of branching is reduced overall, and in particular, orthogonal branches that thicken the lung structure form less frequently and at more shallow angles, even in explant cultures disconnected from circulation (*Lazarus et al.*, 2011). Airways are also more dilated from continued epithelial proliferation. Thus, some of the perturbation of epithelial branching may be an indirect result from disrupted vasculogenesis. However, epithelial ramification is halted following pulmonary denervation, which is not observed by vascular ablation. Thus, pulmonary neurons must be necessary for additional aspects of lung development beyond vascularization.

VEGF blockade results in diffuse Fgf10 expression (*Lazarus et al.*, 2011). Elimination of neurons may deplete an important source of Vegf-A, and this could in turn disrupt Shh signaling in the epithelium to generate diffuse Fgf10 expression through the mesenchyme, rather than localized Fgf10 production at the tips of growing buds. Analysis of Fgf10 distribution in denervated explants should elucidate whether this may be a factor in the blockade of branching. Mesenchymal proliferation is also compromised, and if mesenchymal function is perturbed then less Fgf10 may be produced. Gene expression studies should shed light on how epithelial-mesenchymal signaling may be altered.

Exogenous nicotine stimulates lung branching after long-term exposure (*Wongtrakool et al.*, 2007). $\alpha 3$ and $\beta 4$ nicotinic acetylcholine receptors (nAChRs) are expressed on pulmonary nerve fibers at the stage of interest (Fig. 7.12). Nicotinic and

muscarinic acetylcholine receptors are also expressed by many non-neural cell types, including pulmonary endothelia, fibroblasts, macrophages, neuroendocrine cells, and bronchial epithelium, where they modulate calcium and affect cell motility and adhesion (*Conti-Fine et al.*, 2000; *Wessler et al.*, 1999; *Wessler and Kirkpatrick*, 2001; *Zia et al.*, 1997). However, nicotinic inhibitors do not inhibit epithelial branching (*Wongtrakool et al.*, 2007). So it is unlikely that the endogenous role of nerves during early lung development is to provide acetylcholine. Instead, exogenous nicotine (such as from smoking during pregnancy) acts through nAChRs that are expressed on the epithelium and other cell types, but this activity is extrinsic to normal development (*Catassi et al.*, 2008; *Jensen et al.*, 2012; *Li et al.*, 2011).

While muscarinic acetylcholine receptor (mAChR) blockade in the mouse submandibular gland was sufficient to interrupt epithelial branching in that organ (*Knox et al.*, 2010), it caused no effect on pulmonary branching. Considering that nAChR blockade also does not impede branching, either all neural activity must be simultaneously blocked, or the neurons are important for another purpose besides neurotransmitter release. Since many different cell types express ACh receptors, a role for neurotransmitter signaling cannot be determined using receptor inhibitors. Botulinum toxin could be used to block neurotransmitter release at acetylcholinergic nerve terminals to clarify if neurotransmitter signaling is important for epithelial branching (*Schiavo et al.*, 1992; *Rossetto et al.*, 2001).

During limb regeneration in salamanders, nerves are necessary for dedifferentiation of blastema cells and growth of a new limb (*Bryant et al.*, 2002). In this system,

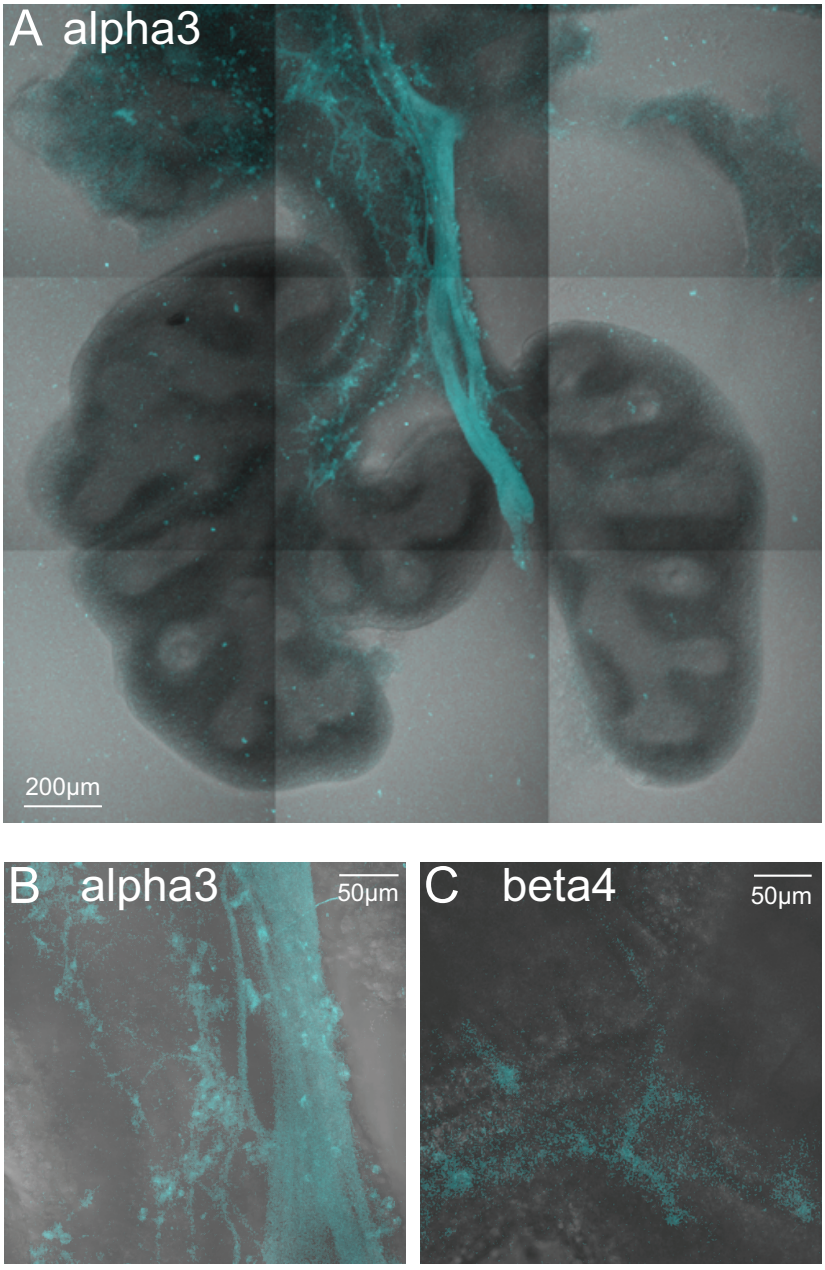

Figure 7.12: Nerves with $\alpha 3$ and $\beta 4$ nicotinic acetylcholine receptor (nAChR) subunits are expressed on pulmonary nerve fibers during early lung development. Lungs were explanted from E12.5 embryos of mice with eGFP-tagged nicotinic receptor $\alpha 3$ or $\beta 4$ subunits and imaged with confocal microscopy. (A) shows a whole lung with $\alpha 3$ nAChR positive nerve fibers around the trachea and extending into the individual lung lobes. The large vagal nerve is also labeled. Higher magnification shows $\alpha 3$ (B) and $\beta 4$ (C) positive axons and cell bodies along the bronchial tubes.

nerves produce and secrete transferrin, which binds and transports iron in the blood for uptake into cells (*Mescher et al.*, 1997). Exogenous transferrin is sufficient to support limb regeneration in the absence of nerves. It is possible that neurons in the developing lung provide transferrin or another growth-promoting molecule to directly support epithelial proliferation and branching.

Neural ablation also impedes proper embryonic *Drosophila* tracheal morphogenesis. In this system, the nerves may serve as a scaffold for tracheal epithelial cells to migrate along to reach their proper destinations. This hypothesis is supported by the formation of what appears to be a partial dorsal trunk at the ventral side of a nerve ablated embryo (Fig.7.10C) and fragments of a trunk at the tips of motor nerve projections that do not extend all the way to the dorsal part of the embryo (Fig.7.10D). The nerves may also provide a growth and migratory promoting signal as in the mammalian lung. Specific ablation of peripheral nerves may clarify if these are the axons necessary for proper tracheal development.

In summary, neural ablation impedes branching morphogenesis in mammalian lung and *Drosophila* trachea. In embryonic mouse lung, endothelial cell numbers are reduced, and epithelial and mesenchymal proliferation are compromised. Acetylcholine receptor inhibition does not explain the defects in growth and branching, suggesting that the nerves regulate branching morphogenesis independent of neurotransmitter signaling. In the developmental condition congenital diaphragmatic hernia, the diaphragm is malformed and lungs are reduced in size with sparse nerves and thickened, constricted blood vessels (*Pederiva et al.*, 2008, 2009). Understanding

the role of nerves in regulating lung branching and subsequent innervation of known targets such as vascular and bronchial smooth muscle may inform interventions to supplement lung growth and vascular development in affected fetuses.

Appendix A

PKC activation in the background of SERCA inhibition fails to rescue zebrafish intersomitic vessel outgrowth and branching

We tested whether reducing the release of calcium from the ER could balance the inhibition of SERCA to pump calcium back into the ER and partially rescue intersomitic vessel growth and branching. The phorbol ester phorbol myristate acetate (PMA) activates PKC and would thus be expected to reduce IP3-driven calcium release (*Castagna et al.*, 1982). Counting the number of intersomitic vessels that form per embryo with DMSO (control), 5μM CPA, 10nM PMA, or a combination of 5μM CPA and 10nM PMA shows no effect of co-incubating CPA with PMA (Fig. A.1A). Approximately the same number of vessels form with PMA+CPA as with just CPA, and PMA alone may cause a slight but insignificant reduction in the number of vessels. With respect to the extent of branching of vessels 13-16 that form during the middle of the incubation period, co-incubation with CPA and PMA results in the same amount of branching as treatment with just CPA (Fig. A.1B). This remained

true with varying degrees of SERCA inhibition and PKC activation.

Quantification of the height, length, and number of branches on individual vessels that form at the end of the incubation period also demonstrated a lack of rescue of intersomitic growth with PKC activation in the background of SERCA inhibition. The measured values for branching (Fig. A.2A,D), length (Fig. A.2B,E), and height (Fig. A.2C,F) were reduced approximately the same for SERCA inhibition alone compared with PKC activation in addition to SERCA inhibition, and for the 19th intersomitic vessel the dual treatment appeared to have an additive effect on vessel length and height.

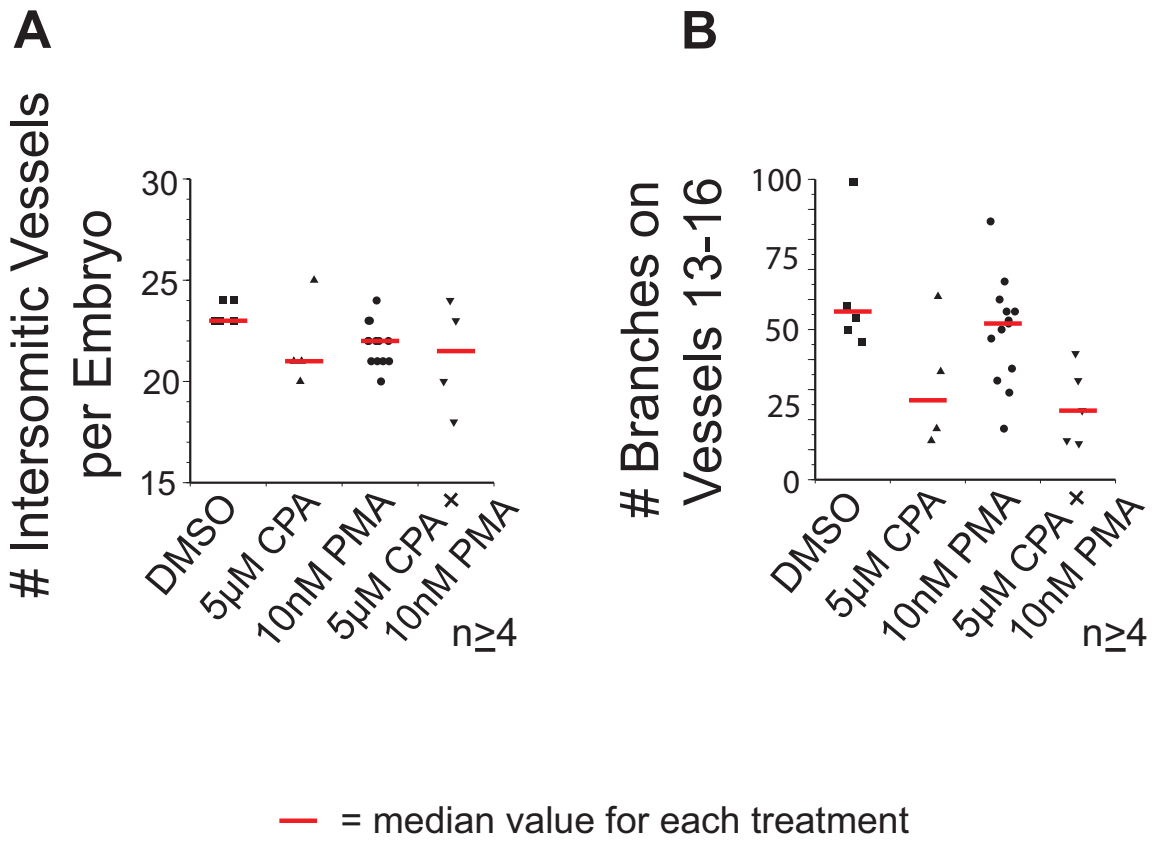

Figure A.1: Activation of PKC in the background of SERCA inhibition fails to rescue the number of intersomitic vessels that form or the extent of branching. (A) The number of intersomitic vessels that form during the period of incubation following just SERCA inhibition or SERCA inhibition plus PKC activation are approximately the same. (B) The extent of branching of vessels that form during the middle of the incubation period is the same for embryos treated with SERCA inhibitor alone or PKC activator in addition to SERCA inhibitor. Median values for each treatment group are indicated by red lines. Compared to controls, both vessel formation and vessel branching are equivalently reduced by SERCA inhibition versus PKC activation in the background of SERCA inhibition. Titrating the levels of SERCA inhibitor and PKC activator gave the same result.

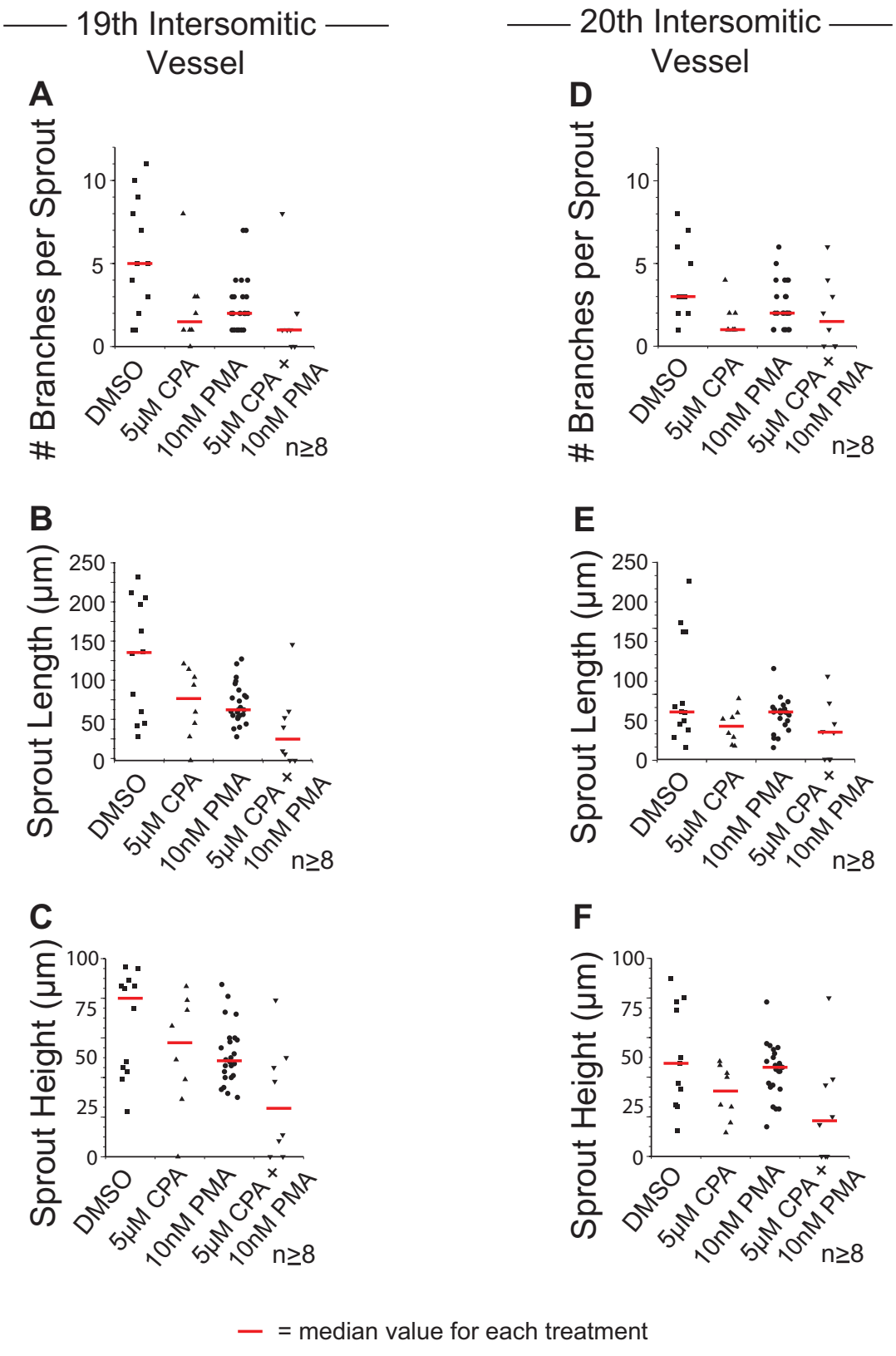

Figure A.2: Caption next page.

Figure A.2: Activation of PKC in the background of SERCA inhibition fails to rescue the branching, length, and height of individual vessels that form near the end of the incubation period. For the 19th and 20th intersomitic vessels, respectively, the number of branches per sprout (A,D), vessel length (B,E), and vessel height from the dorsal aorta (C,F) are similarly reduced following treatment with SERCA inhibitor alone or PKC activator in addition to SERCA inhibitor. For the 19th vessel, the dual treatment may even have an additive inhibitory effect on vessel outgrowth (B,C). Median values for each treatment group are indicated by red lines. Titrating the levels of SERCA inhibitor and PKC activator gave the same result.

Appendix B

Additional examples of tracheal and neural mutants with SERCA inhibition and PKC activation

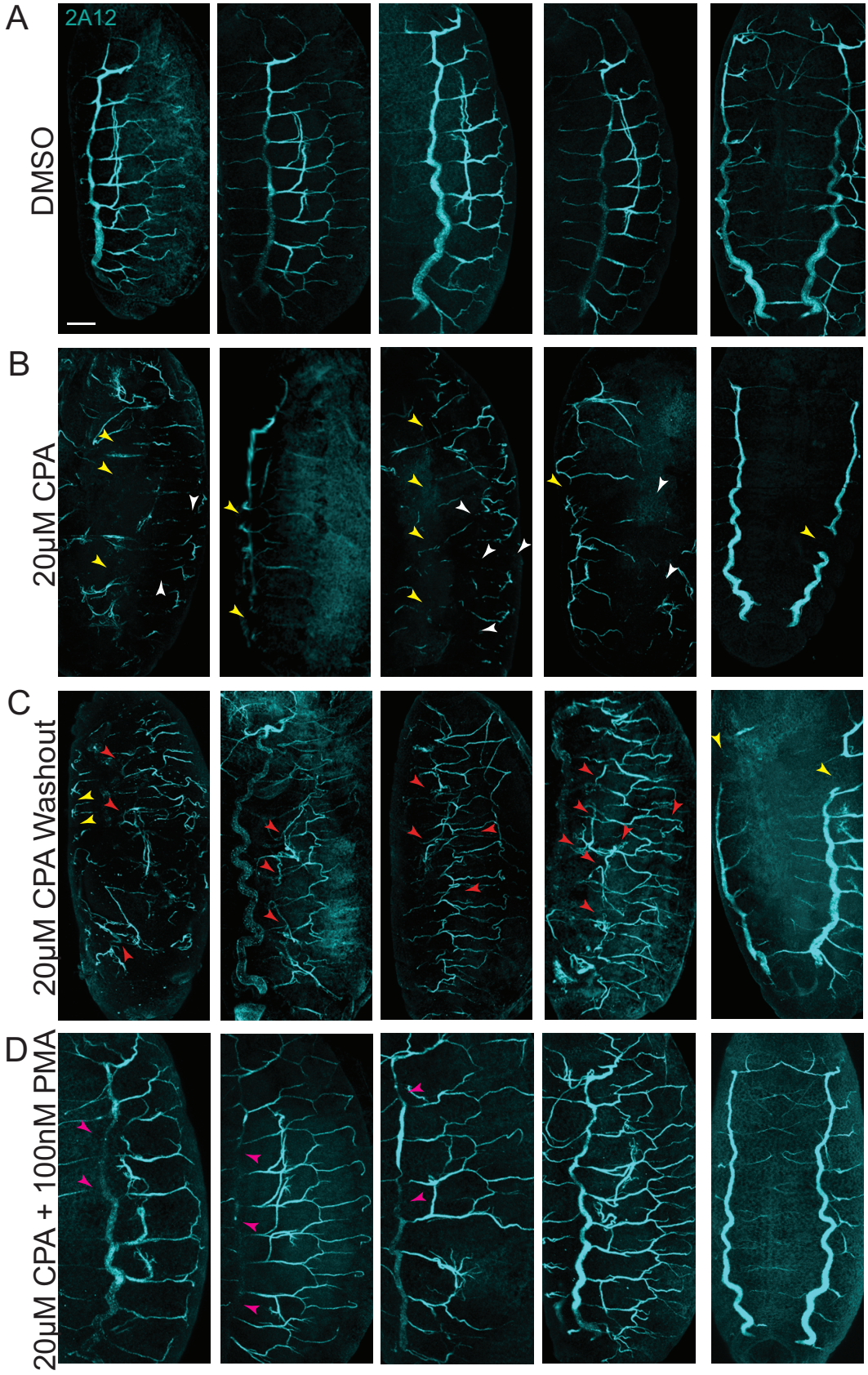

Figure B.1: Caption next page.

Figure B.1: Additional examples of tracheal phenotypes observed following modulation of SERCA activity. (A) Controls permeablized and treated with DMSO. (B) Embryos treated with SERCA inhibitor. (C) Washout of SERCA inhibitor at stage 12. (D) Co-incubation with SERCA inhibitor and PKC activator. Throughout the panels, yellow arrowheads point to breaks in the dorsal trunk, white arrowheads indicate disruptions in smaller tubes, red arrowheads show hyper-sprouty and elongated tubes, and pink arrowheads mark areas of faint lumen label in embryos exposed to PKC activator. Anterior is up. Scale bar=50μm throughout.

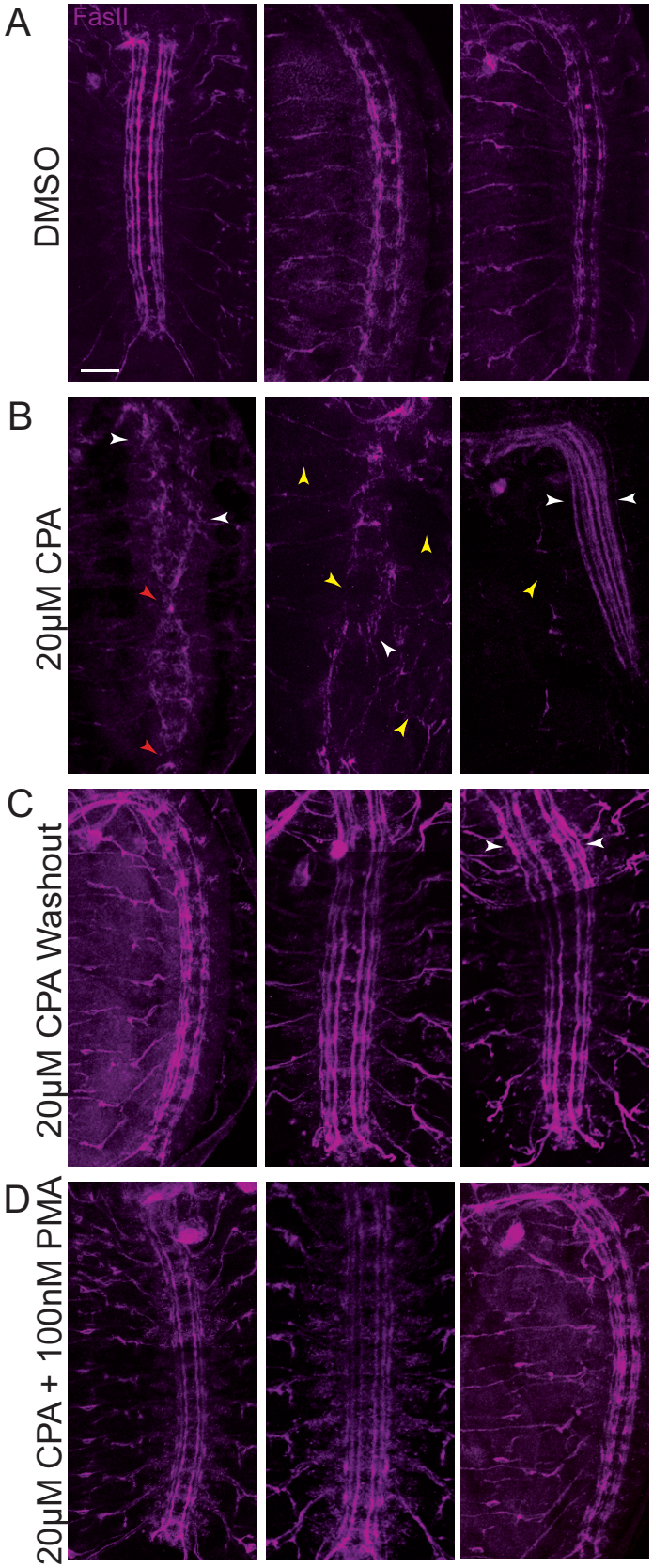

Figure B.2: Caption next page.

Figure B.2: Additional examples of neural phenotypes observed following modulation of SERCA activity. (A) Controls permeablized and treated with DMSO. (B) Embryos treated with SERCA inhibitor. (C) Washout of SERCA inhibitor at stage 12. (D) Co-incubation with SERCA inhibitor and PKC activator. Throughout the panels, yellow arrowheads point to breaks or missing axons, white arrowheads indicate improper spacing of longitudinal tracks, and red arrowheads mark aberrant fusing at the midline. Anterior is up. Scale bar=50μm throughout.

Bibliography

Affolter, M., and E. Caussinus (2008), Tracheal branching morphogenesis in *Drosophila*: new insights into cell behaviour and organ architecture, *Development*, *135*(12), 2055–2064, doi:10.1242/dev.014498.

Affolter, M., D. Nellen, U. Nussbaumer, and K. Basler (1994), Multiple requirements for the receptor serine/threonin kinase *thick veins* reveal novel functions of TGF-beta homologs during *Drosophila* embryogenesis, *Development*, *120*(11), 3105–3117.

Affolter, M., R. Zeller, and E. Caussinus (2009), Tissue remodeling through branching morphogenesis, *Nat. Rev. Mol. Cell Biol.*, *10*, 831–842.

Agostoni, E. (1959), Volume-pressure relationships of the thorax and lung in the newborn, *J. Appl. Physiol.*, *14*, 909–913.

Aguayo, S., W. Schuyler, J. Murtagh, and J. Roman (1994), Regulation of lung branching morphogenesis by bombesin-like peptides and neutral endopeptidase, *Am. J. Respir. Cell Mol. Biol.*, *10*(6), 635–642.

Ahmad, S., et al. (2009), Bcl-2 suppresses sarcoplasmic/endoplasmic reticulum Ca2+-

ATPase expression in cystic fibrosis airways, *Am. J. Respir. Crit. Care Med.*, *179*(9), 816–826, doi:10.1164/rccm.200807-1104OC.

Araújo, S., H. Aslam, G. Tear, and J. Casanova (2005), *mummy/cystic* encodes an enzyme required for chitin and glycan synthesis, involved in trachea, embryonic cuticle and CNS development — Analysis of its role in *Drosophila* tracheal morphogenesis, *Dev. Biol.*, *288*(1), 179–193, doi:10.1016/j.ydbio.2005.09.031.

Arendt, D., and K. Nübler-Jung (1999), Comparison of early nerve cord development in insects and vertebrates, *Development*, *126*(11), 2309–2325.

Aumailley, M., H. Wiedemann, K. Mann, and R. Timpl (1989), Binding of nidogen and the laminin-nidogen complex to basement membrane collagen type-IV, *Eur. J. Biochem.*, *184*(1), 241–248, doi:10.1111/j.1432-1033.1989.tb15013.x.

Bagnard, D., C. Vaillant, S. Khuth, N. Dufay, M. Lohrum, A. Puschel, M. Belin, J. Bolz, and N. Thomasset (2001), Semaphorin 3A-vascular endothelial growth factor-165 balance mediates migration and apoptosis of neural progenitor cells by the recruitment of shared receptor, *J. Neurosci.*, *21*(10), 3332–3341.

Battaglia, C., U. Mayer, M. Aumailley, and R. Timple (1992), Basement membrane heparan-sulfate proteoglycan binds to laminin by its heparan-sulfate chains and to nidogen by sites in the protein core, *Eur. J. Biochem.*, *208*(2), 359–366, doi:10.1111/j.1432-1033.1992.tb17195.x.

Beitel, G., and M. Krasnow (2000), Genetic control of epithelial tube size in the *Drosophila* tracheal system, *Development*, *127*(15), 3271–3282.

Bellusci, S., J. Grindley, H. Emoto, N. Itoh, and B. Hogan (1997), Fibroblast Growth Factor 10 (FGF10) and branching morphogenesis in the embryonic mouse lung, *Development*, *124*(23), 4867–4878.

Berridge, M. (1993), Inositol trisphosphate and calcium signaling, *Nature*, *361*(6410), 315–325, doi:10.1038/361315a0.

Berridge, M., and A. Galione (1988), Cytosolic calcium oscillators, *FASEB J.*, *2*(15), 3074–3082.

Berridge, M., P. Lipp, and M. Bootman (1999), Calcium signaling, *Curr. Biol.*, *9*(5), 157–159.

Berridge, M., M. Bootman, and H. Roderick (2003), Calcium signalling: Dynamics, homeostasis and remodelling, *Nat. Rev. Mol. Cell Biol.*, *4*(7), 517–529, doi: 10.1038/nrm1155.

Bers, D. M. (2000), Calcium fluxes involved in control of cardiac myocyte contraction, *Circ. Res.*, *87*, 275–281, doi:10.1161/01.RES.87.4.275.

Bhat, K. (2005), Slit-roundabout signaling neutralizes Netrin-Frazzled-mediated attractant cue to specify the lateral positioning of longitudinal axon pathways, *Genetics*, *170*(1), 149–159, doi:10.1534/genetics.104.036863.

Blum, Y., H.-G. Belting, E. Ellertsdottir, L. Herwig, F. Lueders, and M. Affolter (2008), Complex cell rearrangements during intersegmental vessel sprouting

and vessel fusion in the zebrafish embryo, *Dev. Bio*, *316*(2), 312–322, doi: 10.1016/j.ydbio.2008.01.038.

Bobe, R., et al. (2011), SERCA2a controls the mode of agonist-induced intracellular Ca2+ signal, transcription factor NFAT and proliferation in human vascular smooth muscle cells, *J. Mol. Cell. Cardiol.*, *50*(4), 621–633, doi: 10.1016/j.yjmcc.2010.12.016.

Brand, A., S. Shanks, V. M. S. Duncan, M. Yang, K. Mackenzie, and N. A. R. Gow (2007), Hyphal orientation of Candida albicans is regulated by a calcium-dependent mechanism, *Curr. Bio*, *17*(4), 347–352, doi:10.1016/j.cub.2006.12.043.

Bryant, S. V., T. Endo, and D. M. Gardiner (2002), Vertebrate limb regeneration and the origin of limb stem cells, *Int. J. Dev. Biol.*, *46*(7), 887–896.

Burns, A. J., N. Thapar, and A. J. Barlow (2008), Development of the neural crest-derived intrinsic innervation of the human lung, *Am. J. Respir. Cell Mol. Biol.*, *38*, 269–275.

Cantero-Recasens, G., C. Fandos, F. Rubio-Moscardo, M. A. Valverde, and R. Vicente (2010), The asthma-associated ORMDL3 gene product regulates endoplasmic reticulum-mediated calcium signaling and cellular stress, *Human Mol. Genet.*, *19*(1), 111–121, doi:10.1093/hmg/ddp471.

Cardoso, W. V., and J. Lü (2006), Regulation of early lung morphogenesis: Questions, facts, and controversies, *Development*, *133*, 1611–1624.

Carmel, J., F. Freiedman, and F. Adams (1965), Fetal tracheal ligation and lung development, *Arch. Pediatr. Adolesc. Med.*, *109*, 452–456.

Castagna, M., Y. Takai, K. Kaibuchi, K. Sano, U. Kikkawa, and Y. Nishizuka (1982), Direct activation of calcium-activated, phosphlipid-dependent protein kinase by tumor-promoting phorbol esters, *J. Biol. Chem.*, *257*(13), 7847–7851.

Catassi, A., D. Servent, L. Paleari, A. Cesario, and P. Russo (2008), Multiple roles of nicotine on cell proliferation and inhibition of apoptosis: Implications on lung carcinogenesis, *Mutat. Res.*, *659*(3), 221–231, doi:10.1016/j.mrrev.2008.04.002.

Chen, C., R. Kuhnlein, K. Eulenberg, S. Vincent, M. Affolter, and R. Schuh (1998), The transcription factors *knirps* and *knirps related* control cell migration and branch morphogenesis during *Drosophila* tracheal development, *Development*, *125*(24), 4959–4968.

Chen, F., Y. Cao, J. Qian, F. Shao, K. Niederreither, and W. V. Cardoso (2010), A retinoic acid-dependent network in the foregut controls formation of the mouse lung primordium, *J. Clin. Invest.*, *120*(6), 2040–2048, doi:10.1172/JCI40253.

Childs, S., J. Chen, D. Garrity, and M. Fishman (2002), Patterning of angiogenesis in the zebrafish embryo, *Development*, *129*(4), 973–982.

Chittenden, T. W., et al. (2006), Selective regulation of arterial branching morphogenesis by synectin, *Dev. Cell*, *10*(6), 783–795, doi:10.1016/j.devcel.2006.03.012.

Conti-Fine, B., D. Navaneetham, S. Lei, and A. Maus (2000), Neuronal nicotinic

receptors in non-neuronal cells: new mediators of tobacco toxicity?, *Eur. J. Pharmacol.*, *393*(1-3, SI), 279–294, doi:10.1016/S0014-2999(00)00036-4.

Costa, R. H., V. V. Kalinichenko, and L. Lim (2001), Transcription factors in mouse lung development and function, *Am. J. Physiol. Lung Cell Mol. Physiol.*, *280*, L823–838.

Covassin, L. D., A. F. Siekmann, M. C. Kacergis, E. Laver, J. C. Moore, J. A. Villefranc, B. M. Weinstein, and N. D. Lawson (2009), A genetic screen for vascular mutants in zebrafish reveals dynamic roles for Vegf/Plcg1 signaling during artery development, *Dev. Biol.*, *329*(2), 212–226, doi:10.1016/j.ydbio.2009.02.031.

De Langhe, S., F. Sala, P. Del Moral, T. Fairbanks, K. Yamada, D. Warburton, R. Burns, and S. Bellusci (2005), Dickkopf-1 (DKK1) reveals that fibronectin is a major target of Wnt signaling in branching morphogenesis of the mouse embryonic lung, *Dev. Biol.*, *277*(2), 316–331, doi:10.1016/j.ydbio.2004.09.023.

Desai, T. J., S. Malpel, G. R. Flentke, S. M. Smith, and W. V. Cardoso (2004), Retinoic acid selectively regulates *Fgf10* expression and maintains cell identity in the prospective lung field of the developing foregut, *Dev. Biol.*, *273*(2), 402–415, doi:10.1016/j.ydbio.2004.04.039.

Devine, W., B. Lubarsky, K. Shaw, S. Luschnig, L. Messina, and M. Krasnow (2005), Requirement for chitin biosynthesis in epithelial tube morphogenesis, *Proc. Natl. Acad. Sci. USA.*, *102*(47), 17,014–17,019, doi:10.1073/pnas.0506676102.

DiFrancesco, D. (1985), The cardiac hyperpolarizing-activated current, i_f. Origins and developments, *Prog. Biophys. Molec. Biol.*, *46*(3), 163–183.

DiFrancesco, D. (2006), Funny channels in the control of cardiac rhythm and mode of action of selective blockers, *Pharmacol. Res.*, *53*, 399–406, doi: 10.1016/j.phrs.2006.03.006.

Dolmetsch, R., K. Xu, and R. Lewis (1998), Calcium oscillations increase the efficiency and specificity of gene expression, *Nature*, *392*(6679), 933–936.

East, M. J. (2000), Sarco(endo)plasmic reticulum calcium pumps: recent advances in our understanding of structure/function and biology, *Mol. Membr. Biol.*, *17*, 189–200, doi:10.1080/09687680010009646.

Featherstone, N., E. Jesudason, M. Connell, D. Fernig, S. Wray, P. Losty, and T. Burdyga (2005), Spontaneous propagating calcium waves underpin airway peristalsis in embryonic rat lung, *Am. J. Respir. Cell Mol. Biol.*, *33*(2), 153–160, doi:10.1165/rcmb.2005-0137OC.

Freeman, A., M. Bowers, A. V. Mortimer, C. Timmerman, S. Roux, M. Ramaswami, and S. Sanyal (2010), A new genetic model of activity-induced Ras signaling dependent pre-synaptic plasticity in *Drosophila*, *Brain Res.*, *1326*, 15–29, doi: 10.1016/j.brainres.2010.02.061.

Gallagher, B. C. (1986), Branching morphogenesis in the avian lung: Electron microscopic studies using cationic dyes, *J. Embryol. Exp. Morph.*, *94*, 189–205.

Glazer, L., and B. Shilo (1991), The *Drosophila* FGF-R homolog is expressed in the embryonic tracheal system and appears to be required for directed tracheal cell extension, *Genes Dev.*, *5*(4), 697–705, doi:10.1101/gad.5.4.697.

Gleason, M. R., R. Armisen, M. A. Verdecia, H. Sirotkin, P. Brehm, and G. Mandel (2004), A mutation in *serca* underlies motility dysfunction in *accordion* zebrafish, *Dev. Biol.*, *276*(2), 441–451.

Goodman, C. (1996), Mechanisms and molecules that control growth cone guidance, *Annu. Rev. Neurosci.*, *19*, 341–377, doi:10.1146/annurev.neuro.19.1.341.

Goss, A. M., Y. Tian, T. Tsukiyama, E. D. Cohen, D. Zhou, M. M. Lu, T. P. Yamaguchi, and E. E. Morrisey (2009), Wnt2/2b and beta-catenin signaling are necessary and sufficient to specify lung progenitors in the foregut, *Dev. Cell*, *17*(2), 290–298, doi:10.1016/j.devcel.2009.06.005.

Grinberg, A., and I. Heath (1997), Direct evidence for Ca2+ regulation of hyphal branch induction, *Fungal Genet. Biol.*, *22*(2), 127–139, doi:10.1006/fgbi.1997.1011.

Gu, G., and S. Singh (1997), Modulation of the dihydropyridine-sensitive calcium channels in *Drosophila* by a phospholipase C-mediated pathway, *J. Neurobiol.*, *33*(3), 265–275, doi:10.1002/(SICI)1097-4695(199709)33:3¡265::AID-NEU5¿3.0.CO;2-#.

Hacohen, N., S. Kramer, D. Sutherland, Y. Hiromi, and M. Krasnow (1998), sprouty encodes a novel antagonist of FGF signaling that patterns apical branching of the *Drosophila* airways, *Cell*, *92*(2), 253–263, doi:10.1016/S0092-8674(00)80919-8.

Harding, R., and S. Hooper (1996), Regulation of lung expansion and lung growth before birth, *J. Appl. Physiol.*, *81*(1), 209–224.

Harris, R., L. Sabatelli, and M. Seeger (1996), Guidance cues at the *Drosophila* CNS midline: Identification and characterization of two *Drosophila* Netrin/UNC-6 homologs, *Neuron*, *17*(2), 217–228, doi:10.1016/S0896-6273(00)80154-3.

Harris-Johnson, K. S., E. T. Domyan, C. M. Vezina, and X. Sun (2009), beta-Catenin promotes respiratory progenitor identity in mouse foregut, *Proc. Natl. Acad. Sci. USA.*, *106*(38), 16,287–16,292, doi:10.1073/pnas.0902274106.

Hartenstein, V., and J. Campos-Ortega (1984), Early neurogenesis in wild type *Drosophila melanogaster*, *Roux's Arch. Dev. Biol.*, *193*(5), 308–325.

Hidalgo, A., and G. Booth (2000), Glia dictate pioneer axon trajectories in the *Drosophila* embryonic CNS, *Development*, *127*(2), 393–402.

Hidalgo, A., and A. Brand (1997), Targeted neuronal ablation: the role of pioneer neurons in guidance and fasciculation in the CNS of *Drosophila*, *Development*, *124*(17), 3253–3262.

Hidalgo, A., J. Urban, and A. Brand (1995), Targeted ablation of glia disrupts axon tract formation in the drosophila CNS, *Development*, *121*(11), 3703–3712.

Hilfer, S. (1996), Morphogenesis of the lung: Control of embryonic and fetal branching, *Annu. Rev. Physiol.*, *58*, 93–113, doi:10.1146/annurev.physiol.58.1.93.

Horowitz, A., and M. Simons (2009), Branching Morphogenesis, *Circ. Res.*, *104*(2), E21, doi:10.1161/CIRCRESAHA.108.191494.

Hosoda, K., R. Hammer, J. Richardson, A. Baynash, J. Cheung, A. Giaid, and M. Yanagisawa (1994), Targeted and natural (piebald-lethal) mutations of endothelin-B receptor gene produce megacolon associated with spotted coat color in mice, *Cell*, *79*(7), 1267–1276, doi:10.1016/0092-8674(94)90017-5.

Imai, T., and H. Sakano (2011), Axon-axon interactions in neuronal circuit assembly: lessons from olfactory map formation, *Eur. J. Neurosci.*, *34*(10, SI), 1647–1654, doi:10.1111/j.1460-9568.2011.07817.x.

Imondi, R., C. Wideman, and Z. Kaprielian (2000), Complementary expression of transmembrane ephrins and their receptors in the mouse spinal cord: a possible role in constraining the orientation of longitudinally projecting axone, *Development*, *127*(7), 1397–1410.

Isogai, S., M. Horiguchi, and B. Weinstein (2001), The vascular anatomy of the developing zebrafish: An atlas of embryonic and early larval development, *Dev. B*, *230*(2), 278–301, doi:10.1006/dbio.2000.9995.

Jackson, S., and I. Heath (1993), Roles of calcium-ions in hyphal tip growth, *Microbiol. Rev.*, *57*(2), 367–382.

Jacob, R. (1990), Calcium oscillations in electrically non-excitable cells, *Biochim. Biophys. Acta*, *1052*(3), 427–438, doi:10.1016/0167-4889(90)90152-4.

Jacobs, I. J., W.-Y. Ku, and J. Que (2012), Genetic and cellular mechanisms regulating anterior foregut and esophageal development, *Dev. Biol.*, *369*(1), 54–64, doi:10.1016/j.ydbio.2012.06.016.

Jacobs, J., and C. Goodman (1989), Embryonic development of axon pathways in the *Drosophila* CNS. 1. A glial scaffold appears before the first growth cones, *J. Neurosci.*, *9*(7), 2402–2411.

Jensen, K., D. Nizamutdinov, M. Guerrier, S. Afroze, D. Dostal, and S. Glaser (2012), General mechanisms of nicotine-induced fibrogenesis, *FASEB J.*, *26*(12), 4778–4787, doi:10.1096/fj.12-206458.

Jesudason, E., M. Connell, D. Fernig, D. Lloyd, and P. Losty (2000), Early lung malformations in congenital diaphragmatic hernia, *J. Pediatr. Surg.*, *35*(1), 124–127.

Jesudason, E., N. Smith, M. Connell, D. Spiller, M. White, D. Fernig, and P. Losty (2006), Peristalsis of airway smooth muscle is developmentally regulated and uncoupled from hypoplastic lung growth, *Am. J. Physiol. Lung Cell Mol. Physiol.*, *291*(4), L559–L565, doi:10.1152/ajplung.00498.2005.

Jesudason, E. C. (2007), Exploiting mechanical stimuli to rescue growth of the hypoplastic lung, *Pediatr. Surg. Int.*, *23*, 827–836, doi:10.1007/s00383-007-1956-0.

Jesudason, E. C., N. P. Smith, M. G. Connell, D. G. Spiller, M. R. White, D. G. Fernig, and P. D. Losty (2005), Developing rat lung has a sided pacemaker region

for morphogenesis-related airway peristalsis, *Am. J. Respir. Cell Mol. Biol.*, *32*(2), 118–127.

Kamei, M., W. B. Saunders, K. J. Bayless, L. Dye, G. E. Davis, and B. M. Weinstein (2006), Endothelial tubes assemble from intracellular vacuoles *in vivo*, *Nature*, *442*(7101), 453–456, doi:10.1038/nature04923.

Kang, M., and H. G. Othmer (2007), The variety of cytosolic calcium responses and possible roles of PLC and PKC, *Phys. Biol.*, *4*, 325–343, doi:10.1088/1478-3975/4/4/009.

Keleman, K., S. Rajagopalan, D. Cleppien, D. Teis, K. Paiha, L. Huber, G. Technau, and B. Dickson (2002), Comm sorts Robo to control axon guidance at the *Drosophila* midline, *Cell*, *110*(4), 415–427, doi:10.1016/S0092-8674(02)00901-7.

Kennedy, T., T. Serafini, J. Delatorre, and M. Tessier-Lavigne (1994), Netrins are diffusible chemotropic factors for commissural axons in the embryonic spinal cord, *Cell*, *78*(3), 425–435, doi:10.1016/0092-8674(94)90421-9.

Kidd, T., K. Brose, K. Mitchell, R. Fetter, M. Tessier-Lavigne, C. Goodman, and G. Tear (1998), Roundabout controls axon crossing of the CNS midline and defines a novel subfamily of evolutionarily conserved guidance receptors, *Cell*, *92*(2), 205–215, doi:10.1016/S0092-8674(00)80915-0.

Klämbt, C., and C. Goodman (1991), The diversity and pattern of glia during axon pathway formation in the *Drosophila* embryo, *Glia*, *4*(2), 205–213, doi:10.1002/glia.440040212.

Klämbt, C., J. Jacobs, and C. Goodman (1991), The midline of the *Drosophila* central nervous system: A model for the genetic analysis of cell fate, migration, and growth cone guidance, *Cell*, *64*(4), 801–815, doi:10.1016/0092-8674(91)90509-W.

Klämbt, C., L. Glazer, and B. Shilo (1992), *breathless*, a *Drosophila* FGF receptor homolog, is essential for migration of tracheal and specific midline glial cells, *Genes Dev.*, *6*(9), 1668–1678, doi:10.1101/gad.6.9.1668.

Knox, S. M., I. M. A. Lombaert, X. Reed, L. Vitale-Cross, J. S. Gutkind, and M. P. Hoffman (2010), Parasympathetic innervation maintains epithelial progenitor cells during salivary organogenesis, *Science*, *329*, 1645–1647, doi: 10.1126/science.1192046.

Kono, T., G. Ahn, D. R. Moss, L. Gann, A. Zarain-Herzberg, Y. Nishiki, P. T. Fueger, T. Ogihara, and C. Evans-Molina (2012), PPAR-gamma activation restores pancreatic islet SERCA2 levels and prevents beta-cell dysfunction under conditions of hyperglycemic and cytokine stress, *Mol. Endocrinol.*, *26*(2), 257–271, doi: 10.1210/me.2011-1181.

Korfei, M., et al. (2008), Epithelial endoplasmic reticulum stress and apoptosis in sporadic idiopathic pulmonary fibrosis, *Am. J. Respir. Crit. Care Med.*, *178*(8), 838–846, doi:10.1164/rccm.200802-313OC.

Korosec, B., D. Glavac, T. Rott, and M. Ravnik-Glavac (2006), Alterations in the ATP2A2 gene in correlation with colon and lung cancer, *Cancer Genet. Cytogenet.*, *171*(2), 105–111, doi:10.1016/j.cancergencyto.2006.06.016.

Kuzina, I., J. K. Song, and E. Giniger (2011), How Notch establishes longitudinal axon connections between successive segments of the *Drosophila* CNS, *Development*, *138*(9), 1839–1849, doi:10.1242/dev.062471.

Lansdale, N., M. G. Connell, N. C. Featherstone, A. Midgley, and E. C. Jesudason (2010), Cyclopiazonic acid (CPA) inhibition of sarco-endoplasmic reticulum Ca2+-ATPase (SERCA) reduces, with similar dose-dependency, prenatal airway branching, peristalsis and cell proliferation and modulates gene expression required for lung development, *Amer. Thoracic Soc. Int. Conf. Abstracts*.

Lawson, N., J. Mugford, B. Diamond, and B. Weinstein (2003), phospholipase C gamma-1 is require downstream of vascular endothelial growth factor during arterial development, *Genes & Development*, *17*(11), 1346–1351, doi:10.1101/gad.1072203.

Lawson, W. E., et al. (2011), Endoplasmic reticulum stress enhances fibrotic remodeling in the lungs, *Proc. Natl. Acad. Sci. USA.*, *108*(26), 10,562–10,567, doi:10.1073/pnas.1107559108.

Lazarus, A., P. M. Del-Moral, O. Ilovich, E. Mishani, D. Warburton, and E. Keshet (2011), A perfusion-independent role of blood vessels in determining branching stereotypy of lung airways, *Development*, *138*, 2359–2368, doi:10.1242/dev.060723.

Learte, A. R., and A. Hidalgo (2007), The role of glial cells in axon guidance, fasciculation and targeting, in *Adv. Exp. Med. Biol.*, Vol. 621, pp. 156–166, Springer-Verlag Berlin, doi:10.1007/978-0-387-76715-4_12.

Lee, T., N. Hacohen, M. Krasnow, and D. Montell (1996), Regulated Breathless

receptor tyrosine kinase activity required to pattern cell migration area branching in the *Drosophila* tracheal system, *Genes Dev.*, *10*(22), 2912–2921, doi: 10.1101/gad.10.22.2912.

Lee, W. A. P. Z. K., H. K. (2009), Live dissection of *drosophila* embryos: Streamlined methods for screening mutant collections by antibody staining, *J. Vis. Exp.*, *34*, e1647, doi:10.3791/1647.

Levina, N., R. Lew, G. Hyde, and I. Heath (1995), The roles of Ca2+ and plasma-membrane ion channels in hyphal tip growth of neurospora-crassa, *J. Cell Sci.*, *108*(Part 11), 3405–3417.

Lewis, M. (1924), Spontaneous rhythmical contraction of the muscles of the bronchial tubes and air sacs of the chick embryo, *Am. J. Physiol.*, *68*(2), 385–388.

Li, Q., X.-D. Zhou, V. P. Kolosov, and J. M. Perelman (2011), Nicotine Reduces TNF-alpha Expression Through a alpha 7 nAChR/MyD88/NF-kappa B Pathway in HBE16 Airway Epithelial Cells, *Cell. Physiol. Biochem.*, *27*(5), 605–612, doi: 10.1159/000329982.

Lin, D., R. Fetter, C. Kopczynski, G. Grenningloh, and C. Goodman (1994), Genetic analysis of fasciclin-II in *Drosophila*: Defasciculation, refasciculation, and altered fasciculation, *Neuron*, *13*(5), 1055–1069, doi:10.1016/0896-6273(94)90045-0.

Litingtung, Y., L. Lei, H. Westphal, and C. Chiang (1998), Sonic hedgehog is essential to foregut development, *Nat. Genet.*, *20*(1), 58–61.

Liu, M., Y. Qin, J. Liu, A. Tanswell, and M. Post (1996), Mechanical strain induces pp60src activation and translocation to cytoskeleton in fetal rat lung cells, *J. Biol. Chem.*, *271*, 7066–7071.

Llimargas, M., M. Strigini, M. Katidou, D. Karagogeos, and J. Casanova (2004), Lachesin is a component of a septate junction-based mechanism that controls tube size and epithelial integrity in the *Drosophila* tracheal system, *Development*, *131*(1), 181–190, doi:10.1242/dev.00917.

Luschnig, S., T. Batz, K. Armbruster, and M. Krasnow (2006), *serpentine* and *vermiform* encode matrix proteins with chitin binding and deacetylation domains that limit tracheal tube length in *Drosophila*, *Curr. Biol.*, *16*(2), 186–194, doi: 10.1016/j.cub.2005.11.072.

Magyar, A., Éva Bakos, and Ándras Váradi (1995), Structure and tissue-specific expression of the *Drosophila* melanogaster organellar-type Ca(2+)-ATPase gene, *Biochem. J.*, *310*, 757–763.

Mahn, K., et al. (2009), Diminished sarco/endoplasmic reticulum Ca2+ ATPase (SERCA) expression contributes to airway remodelling in bronchial asthma, *Proc. Natl. Acad. Sci. USA.*, *106*(26), 10,775–10,780, doi:10.1073/pnas.0902295106.

Mailleux, A., D. Tefft, D. Ndiaye, N. Itoh, J. Thiery, D. Warburton, and S. Bellusci (2001), Evidence that *sprouty2* functions as an inhibitor of mouse embryonic lung growth and morphogenesis, *Mech. Dev.*, *102*(1-2), 81–94, doi:10.1016/S0925-4773(01)00286-6.

Manning, G., and M. Krasnow (1993), *Development of the Drosophila tracheal system*, Vol. 1, 609–685 pp., Cold Spring Harbor Laboratory Press, Cold Spring Harbor, NY.

Massarwa, R., E. D. Schejter, and B.-Z. Shilo (2009), Apical Secretion in Epithelial Tubes of the Drosophila Embryo Is Directed by the Formin-Family Protein Diaphanous, *Dev. Cell*, *16*(6), 877–888, doi:10.1016/j.devcel.2009.04.010.

McCray, P., and T. Joseph (1993), Spontaneous contractility of human fetal airway smooth muscle, *Am. J. Respir. Cell Mol. Biol.*, *8*(5), 573–580.

Meinhardt, H. (2009), *The Algorithmic Beauty of Sea Shells*, fourth ed., Springer-Verlag, Heidelberg, Germany.

Melani, M., and B. M. Weinstein (2010), Common factors regulating patterning of the nervous and vascular systems, in *Annual Review of Cell and Developmental Biology*, *Annual Review of Cell and Developmental Biology*, Vol. 26, edited by Schekman, R and Goldstein, L and Lehmann, R, pp. 639–665, Annual Reviews, doi:10.1146/annurev.cellbio.093008.093324.

Mescher, A., E. Connell, C. Hsu, C. Patel, and B. Overton (1997), Transferrin is necessary and sufficient for the neural effect on growth in amphibian limb regeneration blastemas, *Dev. Growth Differ.*, *39*(6), 677–684.

Metzger, R. J., O. D. Klein, G. R. Martin, and M. A. Krasnow (2008), The branching programme of mouse lung development, *Nature*, *453*, 745–751.

Min, H., D. Danilenko, S. Scully, B. Bolon, B. Ring, J. Tarpley, M. DeRose, and W. Simonet (1998), Fgf-10 is required for both limb and lung development and exhibits striking functional similarity to *Drosophila branchless*, *Genes & Development*, *12*(20), 3156–3161, doi:10.1101/gad.12.20.3156.

Minoo, P., G. Su, H. Drum, P. Bringas, and S. Kimura (1999), Defects in tracheoesophageal and lung morphogenesis in Nkx2.1(-/-) mouse embryos, *Dev. Biol.*, *209*(1), 60–71, doi:10.1006/dbio.1999.9234.

Misquitta, C. M., D. P. Mack, and A. K. Grover (1999), Sarco/endoplasmic reticulum Ca^{2+} (SERCA)-pumps: link to heart beats and calcium waves, *Cell Calcium*, *25*(4), 277–290.

Mitchell, K., J. Doyle, T. Serafini, T. Kennedy, M. Tessier-Lavigne, C. Goodman, and B. Dickson (1996), Genetic analysis of Netrin genes in *Drosophila*: Netrins guide CNS commissural axons and peripheral motor axons, *Neuron*, *17*(2), 203–215, doi:10.1016/S0896-6273(00)80153-1.

Moral, P.-M. D., F. G. Sala, D. Tefft, W. Shi, E. Keshet, S. Bellusci, and D. Warburton (2006), VEGF-A signaling through Flk-1 is a critical facilitator of early embryonic lung epithelial to endothelial crosstalk and branching morphogenesis, *Dev. Biol.*, *290*(1), 177–188, doi:10.1016/j.ydbio.2005.11.022.

Morrisey, E. E., and B. L. M. Hogan (2010), Preparing for the first breath: Genetic and cellular mechanisms in lung development, *Dev. Cell*, *18*(1), 8–23, doi:10.1016/j.devcel.2009.12.010.

Nambu, J., J. Lewis, M., and S. Crews (1993), The development and function of the *Drosophila* CNS midline cells, *Comp. Biochem. Physiol.*, *104*(3), 399–409, doi: 10.1016/0300-9629(93)90439-B.

Nassif, C., A. Noveen, and V. Hartenstein (1998), Embryonic development of the *Drosophila* brain. I. Pattern of pioneer tracts, *J. Comp. Neurol.*, *402*(1), 10–31, doi:10.1002/(SICI)1096-9861(19981207)402:1¡10::AID-CNE2¿3.0.CO;2-5.

Nelson, K. S., M. Furuse, and G. J. Beitel (2010), The *Drosophila* claudin *Kune-kune* Is required for septate junction organization and tracheal tube size control, *Genetics*, *185*(3), 831–839, doi:10.1534/genetics.110.114959.

Nerbonne, J. M., and R. S. Kass (2005), Molecular physiology of cardiac repolarization, *Physiol. Rev.*, *85*(4), 1205–1253, doi:10.1152/physrev.00002.2005.

Nishizuka, Y. (1988), The molecular heterogeneity of protein kinase C and its implications for cellular regulation, *Nature*, *334*(6184), 661–665, doi:10.1038/334661a0.

Onodera, T., T. Sakai, J. C.-f. Hsu, K. Matsumoto, J. A. Chiorini, and K. M. Yamada (2010), Btbd7 regulates epithelial cell dynamics and branching morphogenesis, *Science*, *329*(5991), 562–565, doi:10.1126/science.1191880.

Parker, R., and V. Auld (2004), Signaling in glial development: differentiation migration and axon guidance, *Biochem. and Cell Biol.*, *82*(6), 694–707, doi: 10.1139/O04-119.

Parsons, L., K. Harris, K. Turner, and P. Whitington (2003), *Roundabout* gene family

functions during sensory axon guidance in the *Drosophila* embryo are mediated by both Slit-dependent and Slit-independent mechanisms, *Dev. Biol.*, *264*(2), 363–375, doi:10.1016/j.ydbio.2003.08.020.

Paulsson, M., M. Aumailley, R. Deutzmann, R. Timpl, K. Beck, and J. Engel (1987), Laminin-nidogen complex extraction with chelating agents and structural characterization, *Eur. J. Biochem.*, *166*(1), 11–19, doi:10.1111/j.1432-1033.1987.tb13476.x.

Pederiva, F., R. A. Lopez, L. Martinez, and J. A. Tovar (2008), Abnormal development of tracheal innervation in rats with experimental diaphragmatic hernia, *Pediatr. Surg. Int.*, *24*, 1341–1346, doi:10.1007/s00383-008-2261-2.

Pederiva, F., R. A. Lopez, L. Martinez, and J. A. Tovar (2009), Tracheal innervation is abnormal in rats with experimental congenital diaphragmatic hernia, *J. Pediatr. Surg.*, *44*(6), 1159–1164, doi:10.1016/j.jpedsurg.2009.02.040.

Pelton, R., M. Johnson, E. Perkett, L. Gold, and H. Moses (1991), Expression of transforming growth factor-beta-1, factor-beta-2, and factor-beta-3 messenger RNA and protein in the murine lung, *Am. J. Respir. Cell Mol. Biol.*, *5*(6), 522–530.

Pepicelli, C. V., P. M. Lewis, and A. P. McMahon (1998), Sonic hedgehog regulates branching morphogenesis in the mammalian lung, *Curr. Biol.*, *8*(19), 1083–1086, doi:10.1016/S0960-9822(98)70446-4.

Periasamy, M., et al. (1999), Impaired cardiac performance in heterozygous mice

with a null mutation in the sarco(endo)plasmic reticulum Ca^{2+}-ATPase isoform 2 (SERCA2) gene, *J. Biol. Chem.*, *274*(4), 2556–2562.

Preibisch, S., S. Saalfeld, and P. Tomancak (2009), Globally optimal stitching of tiled 3D microscopic image acquisitions, *Bioinformatics*, *25*(11), 1463–1465, doi: 10.1093/bioinformatics/btp184.

Qi, M., T. R. Shannon, D. E. Euler, D. M. Bers, and A. M. Samarel (1997), Downregulation of sarcoplasmic reticulum Ca^{2+}-ATPase during progression of left ventricular hypertrophy, *Am. J. Physiol. Heart Circ. Physiol.*, *272*, 2416–2424.

Que, J., T. Okubo, J. R. Goldenring, K.-T. Nam, R. Kurotani, E. E. Morrisey, O. Taranova, L. H. Pevny, and B. L. M. Hogan (2007), Multiple dose-dependent roles for Sox2 in the patterning and differentiation of anterior foregut endoderm, *Development*, *134*(13), 2521–2531, doi:10.1242/dev.003855.

Rajagopalan, S., V. Vivancos, E. Nicolas, and B. Dickson (2000), Selecting a longitudinal pathway: Robo receptors specify the lateral position of axons in the *Drosophila* CNS, *Cell*, *103*(7), 1033–1045, doi:10.1016/S0092-8674(00)00207-5.

Rand, M. D., A. L. Kearney, J. Dao, and T. Clason (2010), Permeabilization of *Drosophila* embryos for introduction of small molecules, *Insect Biochem. Mol. Biol.*, *40*(11), 792–804, doi:10.1016/j.ibmb.2010.07.007.

Raper, J., and C. Mason (2010), Cellular strategies of axonal pathfinding, *Cold Spring Harb. Perspect. Biol.*, *2*(9), doi:10.1101/cshperspect.a001933.

Ratnaparkhi, A., and K. Zinn (2007), The secreted cell signal *Folded Gastrulation* regulates glial morphogenesis and axon guidance in *Drosophila*, *Dev. Biol.*, *308*(1), 158–168, doi:10.1016/j.ydbio.2007.05.016.

Ravier, M. A., D. Daro, L. P. Roma, J.-C. Jonas, R. Cheng-Xue, F. C. Schuit, and P. Gilon (2011), Mechanisms of control of the free Ca2+ concentration in the endoplasmic reticulum of mouse pancreatic beta-cells: Interplay with cell metabolism and $[Ca2+]_c$ and role of SERCA2b and SERCA3, *Diabetes*, *60*(10), 2533–2545, doi:10.2337/db10-1543.

Reber, M., P. Burrola, and G. Lemke (2004), A relative signalling model for the formation of a topographic neural map, *Nature*, *431*(7010), 847–853, doi: 10.1038/nature02957.

Regalado, C. (1998), Roles of calcium gradients in hyphal tip growth: a mathematical model, *Microbiology*, *144*(Part 10), 2771–2782.

Ribeiro, C., M. Neumann, and M. Affolter (2004), Genetic control of cell intercalation during tracheal morphogenesis in *Drosophila*, *Curr. Biol.*, *14*(24), 2197–2207, doi: 10.1016/j.cub.2004.11.056.

Riso, J. (1983), Morphology of epithelio-mesenchymal interaction during lung development of the mouse, *Cell Differ.*, *13*(4), 309–318, doi:10.1016/0045-6039(83)90041-6.

Robson, G., M. Wiebe, and A. Trinci (1991a), Low calcium concentrations induce increased branching in fusarium-graminearum, *Mycol. Res.*, *95*(Part 5), 561–565.

Robson, G., M. Wieve, and A. Trinci (1991b), Involvement of Ca2+ in the regulation of hyphal extension and branching in fusarium-graminearum A-3/5, *Exp. Mycol.*, *15*(3), 263–272, doi:10.1016/0147-5975(91)90028-C.

Roman, J. (1995), Effects of calcium-channel blockade on mammalian lung branching morphogenesis, *Exp. Lung Res.*, *21*(4), 489–502, doi:10.3109/01902149509031754.

Roman, J., and M. Koval (2009), Control of lung epithelial growth by a nicotinic acetylcholine receptor: The other side of the coin, *Am. J. Pathol.*, *175*(5), 1799–1801, doi:10.2353/ajpath.2009.090689.

Rossetto, O., M. Seveso, P. Caccin, G. Schiavo, and C. Montecucco (2001), Tetanus and botulinum neurotoxins: turning bad guys into good by research, *Toxicon*, *39*(1), 27–41, doi:10.1016/S0041-0101(00)00163-X.

Ruberte, E., T. Marty, D. Nellen, M. Affolter, and K. Basler (1995), An absolute requirement for both the type-II and type-I receptors, *punt* and *thick veins*, for *Dpp* signaling *in-vivo*, *Cell*, *80*(6), 889–897, doi:10.1016/0092-8674(95)90292-9.

Sakai, T., M. Larsen, and K. Yamada (2003), Fibronectin requirement in branching morphogenesis, *Nature*, *423*(6942), 876–881, doi:10.1038/nature01712.

Samakovlis, C., N. Hacohen, G. Manning, D. C. Sutherland, K. Guillemin, and M. A. Krasnow (1996a), Development of the *Drosophila* tracheal system occurs by a series of morphologically distinct but genetically coupled branching events, *Development*, *122*, 1395–1407.

Samakovlis, C., G. Manning, P. Steneberg, N. Hacohen, R. Cantera, and M. Krasnow (1996b), Genetic control of epithelial tube fusion during *Drosophila* tracheal development, *Development*, *122*(11), 3531–3536.

Sánchez-Soriano, N., and A. Prokop (2005), The influence of pioneer neurons on a growing motor nerve in *Drosophila* requires the neural cell adhesion molecule homolog FasciclinII, *J. Neurosci.*, *25*(1), 78–87, doi:10.1523/JNEUROSCI.2377-04.2005.

Sánchez-Soriano, N., G. Tear, P. Whitington, and A. Prokop (2007), *Drosophila* as a genetic and cellular model for studies on axonal growth, *Neural Dev.*, *2*(9), doi:10.1186/1749-8104-2-9.

Sanyal, S., C. Consoulas, H. Kuromi, A. Basole, L. Mukai, Y. Kidokoro, K. Krishnan, and M. Ramaswami (2005), Analysis of conditional paralytic mutants in *Drosophila* sarco-endoplasmic reticulum calcium ATPase reveals novel mechanisms for regulating membrane excitability, *Genetics*, *169*, 737–750, doi:10.1534/genetics.104.031930.

Sanyal, S., T. Jennings, H. Dowse, and M. Ramaswami (2006), Conditional mutations in SERCA, the Sarco-endoplasmic reticulum Ca^{2+}-ATPase, alter heart rate and rhythmicity in *Drosophila*, *J. Comp. Physiol. B.*, *176*, 253–263, doi:10.1007/s00360-005-0046-7.

Schiavo, G., F. Benfenati, B. Poulain, O. Rossetto, P. Delaureto, B. Dasgupta, and C. Montecucco (1992), Tetanus and botulinum-B neurotoxins block neurotransmit-

ter release by proteolytic cleavage of synaptobrevin, *Nature*, *359*(6398), 832–835, doi:10.1038/359832a0.

Schittny, J. C., G. Miserocchi, and M. P. Sparrow (2000), Spontaneous peristaltic airway contractions propel lung liquid through the bronchial tree of intact and fetal lung explants, *Am. J. Respir. Cell Mol. Biol.*, *23*, 11–18.

Schopper, W. (1935), Embryonales und erwachsenes lungengewebe vom meerschweinchen und huhn in der dultur mit zeitrafferbeobachtungen an flimmerepithel, sog. Alveolarphagocyten und von kontraktionen der bronchialmuskulatur, *Virchows Arch. Pathol. Anat. Physiol.*, *295*(4), 623–644.

Schottenfeld, J., Y. Song, and A. S. Ghabrial (2010), Tube continued: morphogenesis of the *Drosophila* tracheal system, *Curr. Opin. Cell Biol.*, *22*(5), 633–639, doi: 10.1016/j.ceb.2010.07.016.

Schröedl, K., H. Oelmez, M. Edelmann, R. M. Huber, and A. Bergner (2009), Altered Ca2+-homeostasis of cisplatin-treated and low level resistant non-small-cell and small-cell lung cancer cells, *Cell. Oncol.*, *31*(4), 301–315, doi:10.3233/CLO-2009-0472.

Schuster, S., M. Marhl, and T. Hofer (2002), Modelling of simple and complex calcium oscillations - From single-cell responses to intercellular signalling, *Eur. J. Biochem.*, *269*(5), 1333–1355, doi:10.1046/j.0014-2956.2001.02720.x.

Seeger, M., G. Tear, D. Ferresmarco, and C. Goodman (1993), Mutations affecting

growth cone guidance in *Drosophila*- Genes necessary for guidance toward or away from the midline, *Neuron*, *10*(3), 409–426, doi:10.1016/0896-6273(93)90330-T.

Seidler, N. W., I. Jona, M. Vegh, and A. Martonosi (1989), Cyclopiazonic acid is a specific inhibitor of the Ca2+-ATPase of sarcoplasmic reticulum, *J. Biol. Chem.*, *264*(30), 17,816–17,823.

Serls, A., S. Doherty, P. Parvatiyar, J. Wells, and G. Deutsch (2005), Different thresholds of fibroblast growth factors pattern the ventral foregut into liver and lung, *Development*, *132*(1), 35–47, doi:10.1242/dev.01570.

Serra, R., R. Pelton, and H. Moses (1994), TGF-beta-1 inhibits branching morphogenesis and N-Myc expression in lung bud organ cultures, *Development*, *120*(8), 2153–2161.

Siekmann, A. F., and N. D. Lawson (2007), Notch signalling limits angiogenic cell behaviour in developing zebrafish arteries, *Nature*, *445*(7129), 781–784, doi:10.1038/nature05577.

Silverman-Gavrila, L., and R. Lew (2001), Regulation of the tip-high [Ca2+] gradient in growing hyphae of the fungus *Neurospora crassa*, *Eur. J. Cell Biol.*, *80*(6), 379–390, doi:10.1078/0171-9335-00175.

Silverman-Gavrila, L., and R. Lew (2003), Calcium gradient dependence of *Neurospora crassa* hyphal growth, *Microbiology*, *149*(Part 9), 2475–2485, doi:10.1099/mic.0.26302-0.

Simpson, J., K. Bland, R. Fetter, and C. Goodman (2000), Short-range and long-range guidance by slit and its Robo receptors: A combinatorial code of Robo receptors controls lateral position, *Cell*, *103*(7), 1019–1032, doi:10.1016/S0092-8674(00)00206-3.

Sparrow, M., S. Warwick, and A. Everett (1995), Innervation and function of the distal airways in the developing bronchial tree of fetal pig lung, *Am. J. Respir. Cell Mol. Biol.*, *13*(5), 518–525.

Sparrow, M. P., M. Weichselbaum, and J. Paul B. McCray (1999), Development of the innervation and airway smooth muscle in human fetal lung, *Am. J. Respir. Cell Mol. Biol.*, *20*, 550–560.

Spindler, S. R., and V. Hartenstein (2010), The *Drosophila* neural lineages: a model system to study brain development and circuitry, *Dev. Genes Evol.*, *220*(1-2), 1–10, doi:10.1007/s00427-010-0323-7.

Strausberg, R. L., et al. (2002), Generation and initial analysis of more than 15,000 full-length human and mouse cDNA sequences, *Proc. Natl. Acad. Sci. USA.*, *99*(26), 16,899–16,903.

Strecker, T., S. McGhee, S. Shih, and D. Ham (1994), Permeablization, staining, and culture of living *Drosophila* embryos, *Biotechnic & Histochemistry*, *69*(1), 25–30, doi:10.3109/10520299409106257.

Sun, Q., S. Bahri, A. Schmid, W. Chia, and K. Zinn (2000), Receptor tyrosine

phosphatases regulate axon guidance across the midline of the Drosophila embryo, *Development*, *127*(4), 801–812.

Sutherland, D., C. Samakovlis, and M. Krasnow (1996), Branchless encodes a *Drosophila* FGF homolog that controls tracheal cell migration and the pattern of branching, *Cell*, *87*(6), 1091–1101, doi:10.1016/S0092-8674(00)81803-6.

Swanson, L. E., M. Yu, K. S. Nelson, P. Laprise, U. Tepass, and G. J. Beitel (2009), *Drosophila convoluted/dALS* is an essential gene required for tracheal tube morphogenesis and apical matrix organization, *Genetics*, *181*(4), 1281–1290, doi: 10.1534/genetics.108.099531.

Takada, A., et al. (2012), Role of ER stress in ventricular contractile dysfunction in type 2 diabetes, *PLOS ONE*, *7*(6), doi:10.1371/journal.pone.0039893.

Tanaka-Matakatsu, M., T. Uemura, H. Oda, M. Takeichi, and S. Hayashi (1996), Cadherin-mediated cell adhesion and cell motility in *Drosophila* trachea regulated by the transcription factor Escargot, *Development*, *122*(12), 3697–3705.

Tanjore, H., T. S. Blackwell, and W. E. Lawson (2012), Emerging evidence for endoplasmic reticulum stress in the pathogenesis of idiopathic pulmonary fibrosis, *Am. J. Physiol. Lung Cell Mol. Physiol.*, *302*(8), 721–729, doi: 10.1152/ajplung.00410.2011.

Tear, G., R. Harris, S. Sutaria, K. Kilomanski, C. Goodman, and M. Seeger (1996), *commissureless* controls growth cone guidance across the CNS midline in

Drosophila and encodes a novel membrane protein, *Neuron*, *16*(3), 501–514, doi: 10.1016/S0896-6273(00)80070-7.

Tefft, D., M. Lee, S. Smith, D. Crowe, S. Bellusci, and D. Warburton (2002), mSprouty2 inhibits FGF10-activated MAP kinase by differentially binding to upstream target proteins, *Am. J. Physiol. Lung Cell Mol. Physiol.*, *283*(4), L700–L706, doi:10.1152/ajplung.00372.2001.

Therianos, S., S. Leuzinger, F. Hirth, C. Goodman, and H. Reichert (1995), Embryonic development of the *Drosophila* brain: formation of commissural and descending pathways, *Development*, *121*(11), 3849–3860.

Thomas, J. (1998), Axon guidance: Crossing the midline, *Curr. Biol.*, *8*(3), R102–R104, doi:10.1016/S0960-9822(98)70058-2.

Thomas, T., and M. Dziadek (1994), Expression of collagen α1(IV), laminin and nidogen genes in the embryonic mouse lung: implications for branching morphogenesis, *Mech. Dev.*, *45*, 193–201.

Tiso, N., A. Filippi, S. Pauls, M. Bortolussi, and F. Argenton (2002), BMP signalling regulates anteroposterior endoderm patterning in zebrafish, *Mech. Dev.*, *118*(1-2), 29–37, doi:10.1016/S0925-4773(02)00252-6.

Tollet, J., A. W. Everett, and M. P. Sparrow (2001), Spatial and temporal distribution of nerves, ganglia, and smooth muscle during the early pseudoglandular stage of fetal mouse lung development, *Dev. Dyn.*, *221*, 48–60.

Tsarouhas, V., K.-A. Senti, S. A. Jayaram, K. Tiklova, J. Hemphala, J. Adler, and C. Samakovlis (2007), Sequential pulses of apical epithelial secretion and endocytosis drive airway maturation in *Drosophila*, *Dev. Cell*, *13*(2), 214–225, doi: 10.1016/j.devcel.2007.06.008.

Tseng, B., S. Cavin, F. Booth, E. Olson, M. Marin, T. McDonnell, and I. Butler (2000), Pulmonary hypoplasia in the myogenin null mouse embryo, *Am. J. Respir. Cell Mol. Biol.*, *22*(3), 304–315.

Tucker, K., M. Meyer, and Y. Barde (2001), Neurotrophins are required for nerve growth during development, *Nat. Neurosci.*, *4*(1), 29–37.

Vincent, S., E. Ruberte, N. Grieder, C. Chen, T. Haerry, R. Schuh, and M. Affolter (1997), DPP controls tracheal cell migration along the dorsoventral body axis of the *Drosophila* embryo, *Development*, *124*(14), 2741–2750.

Virag, A., and A. Griffiths (2004), A mutation in the *Neurospora crassa* actin gene results in multiple defects in tip growth and branching, *Fungal Genet. Biol.*, *41*(2), 213–225, doi:10.1016/j.fgb.2003.10.010.

Wang, S., S. Jayaram, J. Hemphala, K. Senti, V. Tsarouhas, H. Jin, and C. Samakovlis (2006), Septate-junction-dependent luminal deposition of chitin deacetylases restricts tube elongation in the *Drosophila* trachea, *Curr. Biol.*, *16*(2), 180–185, doi:10.1016/j.cub.2005.11.074.

Wappner, P., L. Gabay, and B. Shilo (1997), Interactions between the EGF receptor

and DPP pathways establish distinct cell fates in the tracheal placodes, *Development*, *124*(22), 4707–4716.

Warburton, D., C. Wuenschell, G. Flores-Delgado, and K. Anderson (1998), Commitment and differentiation of lung cell lineages, *Biochem. and Cell Biol.*, *76*, 971–995.

Warburton, D., M. Schwarz, D. Tefft, G. Flores-Delgado, K. Anderson, and W. V. Cardoso (2000), The molecular basis of lung morphogenesis, *Mech. Dev.*, *92*(1), 55–81.

Warburton, D., et al. (2005), Molecular mechanisms of early lung specification and branching morphogenesis, *Pediatr. Res.*, *57*(5, Part 2), 26R–37R.

Warburton, D., J. Zhao, M. Berberich, and M. Bernfield (1999), Molecular embryology of the lung: then, now, and in the future, *Am. J. Physiol. Lung Cell Mol. Physiol.*, *276*(5), L697–L704.

Weinstein, B. (2002), Plumbing the mysteries of vascular development using the zebrafish, *Semin. Cell Dev. Biol.*, *13*(6), 515–522, doi:10.1016/S1084-9521(02)00105-2.

Wessler, I., C. Kirkpatrick, and K. Racke (1999), The cholinergic 'pitfall': Acetylcholine, a universal cell molecule in biological systems, including humans, *Clin. Exp. Pharmacol. Physiol.*, *26*(3), 198–205, doi:10.1046/j.1440-1681.1999.03016.x.

Wessler, I. K., and C. J. Kirkpatrick (2001), The non-neuronal cholinergic system:

an emerging drug target in the airways, *Pulm. Pharmacol. Ther.*, *14*, 423–434, doi:10.1006/pupt.2001.0313.

Wigglesworth, V. (1972), *The Principles of Insect Physiology*, Chapman and Hall, London.

Wilson, J., J. DiFiore, and C. Peters (1993), Experimental fetal tracheal ligation prevents the pulmonary hypoplasia associated with fetal nephrectomy: possible application for congenital diaphragmatic hernia, *J. Pediatr. Surg.*, *28*, 1433–1439.

Wilson, S. M., R. E. Olver, and D. V. Walters (2007), Developmental regulation of lumenal lung fluid and electrolyte transport, *Respir. Physiol. Neurobiol.*, *159*(3), 247–255, doi:10.1016/j.resp.2007.10.004.

Wongtrakool, C., S. Roser-Page, H. N. Rivera, and J. Roman (2007), Nicotine alters lung branching morphogenesis through the $\alpha(7)$ nicotinic acetylcholine receptor, *Am. J. Physiol. Lung Cell Mol. Physiol.*, *293*(3), L611–L618, doi: 10.1152/ajplung.00038.2007.

Yao, K., and K. White (1994), Neural specificity of *elav* expression: Defining a *Drosophila* promoter for directing expression to the nervous system, *J. Neurochem.*, *63*(1), 41–51.

Zhao, J., D. Bu, M. Lee, H. Slavkin, F. Hall, and D. Warburton (1996), Abrogation of transforming growth factor-beta type II receptor stimulates embryonic mouse lung branching morphogenesis in culture, *Dev. Biol.*, *180*(1), 242–257, doi: 10.1006/dbio.1996.0298.

Zherebitskaya, E., J. Schapansky, E. Akude, D. R. Smith, R. Van der Ploeg, N. Solovyova, A. Verkhratsky, and P. Fernyhough (2012), Sensory neurons derived from diabetic rats have diminished internal Ca2+ stores linked to impaired re-uptake by the endoplasmic reticulum, *ASN Neuro*, *4*(1), 1–10, doi: 10.1042/AN20110038.

Zhong, T., S. Childs, J. Leu, and M. Fishman (2001), Gridlock signalling pathway fashions the first embryonic artery, *Nature*, *414*(6860), 216–220, doi: 10.1038/35102599.

Zia, S., A. Ndoye, V. Nguyen, and S. Grando (1997), Nicotine enhances expression of the alpha 3, alpha 4, alpha 5, and alpha 7 nicotinic receptors modulating calcium metabolism and regulating adhesion and motility of respiratory epithelial cells, *Res. Commun. Mol. Pathol. Pharmacol.*, *97*(3), 243–262.